UNCLASSIFIED

AD NUMBER:	AD0475633

LIMITATION CHANGES

TO:

Approved for public release; distribution is unlimited.

FROM:

Distribution authorized to U.S. Gov't. agencies and their contractors; Administrative/Operational Use; 31 OCT 1965. Other requests shall be referred to Office of Naval Research, Arlington, VA 22203.

AUTHORITY

ONR notice dtd 27 Jul 1971

THIS PAGE IS UNCLASSIFIED

Investigations on the Direct Conversion of Nuclear
Fission Energy to Electrical Energy in a Plasma Diode
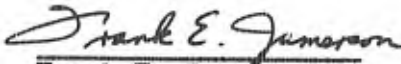
Report No. 6

Authors

Charles B. Leffert

David B. Rees

Fay E. Gifford

Frank E. Jameson
Frank E. Jamerson
Project Supervisor

Report for Period November 1, 1964 to October 31, 1965

Research Laboratories, General Motors Corporation
Warren, Michigan

ABSTRACT

Reaction kinetics and electron transport were studied in noble gas
plasmas generated by fission fragment ionization in order to evaluate these
plasmas for a nuclear thermionic energy converter. The electron density that
would result from fission fragment ionization of Ar-Cs and Ne-Ar gas mix-
tures was predicted from the computed ion generation rate and ion loss pro-
cesses in the plasma. The first experimental verification of the electron
density was made with a resonant microwave cavity operated inpile. For
typical conditions in a research reactor, i.e. a neutron flux of $10^{13} cm^{-2}$
sec^{-1} and an electron temperature of 1300°K, the computed maximum electron
density for neon-argon, viz., $2.4 \times 10^{12} cm^{-3}$ occurs at Ar/Ne=3.4×10^{-4} and
94 torr while for argon-cesium, the maximum electron density is $3.6 \times 10^{12} cm^{-3}$
and occurs at Cs/Ar=1.7×10^{-4} and 94 torr. The favorably-high electron den-
sity in argon seeded with cesium and the fact that argon has the lowest
electron-neutral scattering cross section (Ramsauer) minimum at energies
typical of an operating converter, indicate that this gas mixture is par-
ticularly well-suited for the noble gas converter.

The electron transport properties of these plasmas are being investi-
gated theoretically and a ceramic-metal diode with a nuclear thermionic
emitter ($BaO-UO_2-W$) has been developed for inpile measurement of the elec-
tron transport properties. Analytical solutions have been obtained for the
current-voltage characteristic of a thermionic diode in which the plasma
is generated by uniform fission-fragment ionization and the electron den-
sity is controlled by ambipolar diffusion loss.

i

TABLE OF CONTENTS

INVESTIGATIONS ON THE DIRECT CONVERSION OF
NUCLEAR FISSION ENERGY TO ELECTRICAL ENERGY IN A PLASMA DIODE

INTRODUCTION

The analysis of reaction kinetics and electron transport in a noble-gas plasma generated by fission fragment ionization has been continued. These studies evaluate such a plasma for application to a nuclear thermionic energy converter.

Theoretical calculations and experimental verification have been reported[1] on the rate at which fission fragments produce ions in noble gases. Also, a study of the dominant ion loss processes in the plasma has been reported[1] for the neon-argon system.

In this report we present first the results of reaction kinetic studies on the argon-cesium system. The reaction rate constants are evaluated for argon and cesium, and the results of a detailed study of the factors that influence the electron density in the plasma are presented. The electron density generated in the argon-cesium system is compared to that generated in the neon-argon system.

Theoretical and experimental studies were initiated on the transport of thermionic electrons through a fission fragment plasma. An analytic solution was obtained from the transport equations for the current-voltage characteristic of a plasma diode for the case of electron density controlled by ambipolar diffusion loss. Finally, the development of a nuclear-heated thermionic diode to be operated inpile is described.

OBJECTIVES

The objectives initially set for the current reporting period were:
1. Extend reaction kinetics studies to include the analysis of the electron density generated in an argon-cesium plasma.
2. Perform microwave measurements inpile to determine experimentally the electron density generated by fission fragments in the Ne-Ar and Ar-Cs plasmas.

3. Construct a diode using a nuclear thermionic emitter and operate it inpile in order to determine the electron transport properties of a mixed-gas plasma.

4. Initiate a theoretical analysis on the electron transport properties of mixed-gas plasmas generated by fission fragments.

The reaction kinetics studies are substantially completed except for additional microwave measurements. The thermionic diode for electron transport has been developed and will soon be operated inpile.

CONCLUSIONS

1. Reaction kinetics studies of noble gas plasmas generated by fission fragments indicate that a significantly higher electron density can be maintained in binary, Penning-type gas plasmas than in single-gas plasmas.

2. Calculations show that the electron density in neon-argon and argon-cesium plasmas is a sensitive function of the total gas pressure and the ratio of the constituent gases.

3. For the neon-argon plasma, the computed maximum value of the electron density, viz., $2.4 \times 10^{12} cm^{-3}$, occurs at $Ar/Ne = 3.4 \times 10^{-4}$ and a gas pressure of 94 torr for an electron temperature of 1300°K, a container of diffusion length 1.6 mm and a neutron flux of $10^{13} cm^{-2} sec^{-1}$ (which is about a factor of 10 less than the flux available in a power reactor).

4. For the argon-cesium plasma, the maximum value of the electron density is $3.6 \times 10^{12} cm^{-3}$ and occurs at $Cs/Ar = 1.7 \times 10^{-4}$ and a gas pressure of 94 torr, under the same experimental conditions indicated above for neon-argon.

5. Thus, in both of these Penning-type gas plasmas, the maximum value of the electron density occurs at similar values of trace gas concentration ($\approx .01\%$) and a total pressure of approximately 100 torr, despite the fact that important reaction rates of various species in argon-cesium differ markedly from the corresponding rates in neon-argon.

2

6. At low temperature ($\approx 300°K$), the collisional-radiative recombination process, involving atomic ion — two electron encounters, is a dominant loss process in the neon-argon and argon-cesium plasma. The influence of this loss process diminishes rapidly as the temperature is increased.

7. The favorably-high electron density in argon seeded with cesium, and the fact that argon has the lowest Ramsauer minimum at energies typical of an operating converter, indicate that this gas mixture is particularly well-suited for the noble gas converter.

8. The first measurement of the electron density in the neon-argon plasma, obtained with a resonant microwave cavity operated in the core of the reactor, is in good agreement with the value of electron density predicted by the reaction kinetics studies.

9. Analytical solutions have been obtained for the problem of thermionic electron transport through a fission-fragment-generated plasma in which electron density is controlled by ambipolar diffusion loss. This theory can be used to interpret current-voltage data from thermionic, noble-gas diodes operating in the diffusion mode.

10. Heat transfer tests in the laboratory have shown that the design and construction of the thermionic diode to be used for inpile measurements of electron transport are satisfactory. The laboratory tests of a prototype tube with a BaO-UO_2-W emitter are complete.

FUTURE PLANS

1. Measurements of the electron number density of fission-fragment-generated plasmas in a microwave cavity will be continued for neon-argon and argon-cesium mixtures.

2. The measurements of electron density in neon-argon and argon-cesium plasmas will be compared with the predications of the reaction kinetics analysis under various conditions in order to check the analysis.

3. The thermionic diode incorporating the BaO-UO_2-W emitter will be operated inpile with argon-cesium and neon-argon fillings in order to study the electron transport through the fission-fragment-generated plasma.

3

4. Theoretical work on electron transport through noble-gas plasmas will be extended to include volume loss processes which are both linear and quadratic in electron density. The theory will be used, together with the results of 1, 2 and 3, to determine optimum design parameters for a noble gas thermionic energy converter.

REFERENCES

1. Investigations on the Direct Conversion of Nuclear Fission Energy in a Plasma Diode, 1964 Annual Report No. 5; C. B. Leffert, D. B. Rees and F. E. Jamerson.

ACKNOWLEDGMENTS

SECTION A

REACTION RATES OF IONS, METASTABLE AND EXCITED
STATES IN ARGON-CESIUM PLASMAS

ABSTRACT

The Penning-type argon-cesium plasma is currently of much interest to us
for application in thermionic energy conversion. A study of the ionization
properties of this gas mixture under irradiation by fission fragments requires
knowledge of 30 reaction rates between various excited and ionized states.
These reaction rates are discussed for such processes as diffusion, recombina-
tion, molecular ion formation, charge exchange, volume ionization and destruc-
tion of ionic, excited and metastable states in the multicomponent plasma. Val-
ues for the frequency of these interactions are reported and finally collected
in tabular form suitable for reference. The report is presented in a form sim-
ilar to an earlier report on reaction rates in a neon-argon plasma. In gen-
eral the production, conversion and loss rates of the various species in argon-
cesium are larger than those for neon-argon, due principally to the larger
atomic size of both the major (argon $\gg$ neon) and minor (cesium $\gg$ argon) constit-
uents of the plasma.

i

CONTENTS

OBJECT

The purpose of this work was to make a compilation of the fundamental

reaction rates between ions, excited states and atoms in an argon-cesium plasma.

SUMMARY

Reaction rate coefficients are reported for various interactions between
excited and metastable states of argon and atomic and molecular ions of argon
and cesium. Although much of the data are approximate, particularly for inter-
actions involving cesium, reliable data are available for most of the dominant
processes which determine the electron number density in an argon-cesium plasma
generated by fission fragments. The reaction rates are presented for a tempera-
ture of 300°K. The most temperature-sensitive coefficient is that for colli-
sional-radiative recombination and this temperature dependence is discussed.

I. INTRODUCTION

Theoretical studies of electron number density in binary gas plasmas
require knowledge of a large number of competing diffusion and conversion pro-
cesses for atomic ions, molecular ions and various excited states. The equa-
tions which yield the electron density in Penning-type plasmas were formulated
by Professor D. J. Rose[1] for the case where the plasma is generated by fis-
sion-fragment excitation and ionization of the gas. About 30 rate coefficients
were needed as input data when applied to a neon-argon plasma[2] and these have
been presented in a previous report by Rees.[3] The equations are applicable
to any Penning-type gas mixture. Very recently Leffert used the equations,[4]
with the appropriate rate coefficients, to study the electron density in argon-
cesium plasmas. The rate coefficients required for this study form the subject
of the present report.

A major difference between the present work and the earlier study of neon-
argon coefficients is the emphasis now placed on collisional-radiative recombina-
tion. This loss process for atomic ions is important not only in the argon-cesium

1

system but also in the neon-argon system. A two-body radiative recombination process for atomic ions was considered in the neon-argon work, but this loss was small. Recent work by Bates et al.[5] has shown that radiative recombination in the presence of collisional-de-excitation by electrons is a much more important loss process, particularly at low temperatures.

In general, less is known about the reaction rates of the argon-cesium system than the neon-argon system. Although sufficient data are available for pure argon reactions, much of the available cesium data are approximate. In some instances we have computed rate coefficients from first principles. The dearth of good experimental data for cesium stems from the deleterious effects caused by cesium deposition in much experimental work, and from the difficulty of precisely controlling and determining cesium vapor pressures.

Since the compilation of rate coefficients for argon-cesium is a parallel study to the work reported for neon-argon, we will refer continually to the previous report as $R1^{(3)}$ to avoid unnecessary duplication. Table I is a summary of the reactions that we consider. N_o is the atomic concentration of the major gas argon, and A_o is the atomic concentration of the minor gas cesium.* When we refer to a particular species by its conventional rotation, such as Ar^+ for the atomic argon ion, we will occasionally include in parentheses its actual number density as given in Table I; i.e., we write $Ar^+(N_+)$ for atomic argon ions of number density N_+.

II. GENERATION RATE OF ATOMIC IONS AND EXCITED STATES BY FISSION FRAGMENTS

The fission fragments generate mainly atomic argon ions $Ar^+(N_+)$, metastable argon states $Ar^m(N_m)$, and excited argon states $Ar^x(N_x)$ that are not metastable. The molecular ions $Ar_2^+(N_{2+})$ and $Cs_2^+(A_{2+})$ are not generated directly in the atomic gas mixture. Also, since $A_o \ll N_o$, atomic cesium ions $Cs^+(A_+)$ are not created in appreciable amounts by the fission fragments.

The generation rate S_1 refers to the production of excited argon states which do not decay into metastable states. The only ions that can result from

---

*Table I is a general representation which we adopt for any binary Penning-type system of N-major and A-minor concentrations. In this particular case, A_o is the concentration of neutral cesium atoms per cm^3 and should not be confused with the chemical symbol for argon.

2

TABLE I. Particle density equations for binary gas plasma.

Time Derivative	From Direct Flux	Diffusion	2- and 3-Body Recombination	3-Body Molecular Ion Formation	2-Body Charge Exchange	Metastable-Metastable Collisions	Radiation Molecular Ion Formation Via N_x	Metastable Destruction Via N_o	Penning Ionization	Eq. No.
$\dfrac{\partial N_+}{\partial t} =$	$S_o N_o$	$-\dfrac{K_{1,a} N_o N_+}{\Lambda^2}$	$-[C_1 + C_2 N_o + C_3 n_e] N_+ n_e$	$-C_4 N_+ N_o^2$ $-C_5 N_+ N_o A_o$	$-C_6 N_+ A_o$	$+C_7 N_m^2$				(1)
$\dfrac{\partial N_x}{\partial t} =$	$S_1 N_o$		$+C_8[C_1 + C_2 N_o + C_3 n_e] N_+ n_e$				$-N_x/\tau_x$ $-C_9 N_x N_o$			(2)
$\dfrac{\partial N_m}{\partial t} =$	$S_2 N_o$	$-\dfrac{K_m N_o N_m}{\Lambda^2}$	$+C_{10}[C_1 + C_2 N_o + C_3 n_e] N_+ n_e$ $+C_{11} C_{16} N_{2+} n_e$			$-C_{12} N_m^2$		$-C_{13} N_o N_m$ $-C_{14} N_o N_m^2$	$-C_{15} N_m A_o$	(3)
$\dfrac{\partial N_{2+}}{\partial t} =$		$-\dfrac{K_{2,a} N_o N_{2+}}{\Lambda^2}$	$-C_{16} N_{2+} n_e$	$+C_4 N_+ N_o^2$ $+C_5 N_+ N_o A_o$	$-C_{17} N_{2+} A_o$		$+C_9 N_x N_o$			(4)
$\dfrac{\partial A_+}{\partial t} =$		$-\dfrac{K_{3,a} N_o A_+}{\Lambda^2}$	$+[C_{18} + C_{19} N_o + C_{22} n_e] N_+ n_e$	$-C_{20} A_+ A_o N_o$	$+C_6 N_+ A_o$ $+C_{17} N_{2+} A_o$				$+C_{15} N_m A_o$	(5)
$\dfrac{\partial A_{2+}}{\partial t} =$		$-\dfrac{K_{4,a} N_o A_{2+}}{\Lambda^2}$	$-C_{21} A_{2+} n_e$	$+C_{20} A_+ A_o N_o$						(6)

3

S_1 are molecular ions produced by the Hornbeck-Molnar process (C_9) which involves very highly excited argon states.[6] From the discussion of S_1 presented in R1, we again conclude that $S_2 \gg S_1$ and that the contribution of S_1 to the total ion generation rate can be neglected.

We previously reported detailed computations for the generation rate of atomic argon ions (S_o) and presented experimental verification of the results.[7] The value of S_o evidently depends not only on the gas density but also on the uranium load, neutron flux and tube geometry. For the present study, we compute the argon ion generation rate at the center of a cylindrical microwave cavity of 5 mm height. This cavity is currently being used for inpile measurements of electron density.[8] At a neutron flux of $1 \times 10^{13} cm^{-2} sec^{-1}$, the computed value is[8]

$$S_o(Ar^+) = 3.74 \times 10^{-3} \ sec^{-1} \qquad (1)$$

The argon metastable generation rate (S_2) includes the contribution of excited states which decay into metastable states as the result of excitation transfer and the imprisonment of resonance radiation. In R1, we calculated S_2 for neon from data on ion generation rates in pure neon and in neon-argon mixtures, and we obtained the result that $S_2(Ne^m) = S_o(Ne^+)/2$. We cannot perform a similar calculation for the generation rate of argon metastable states because of the absence of reliable data*on the ion generation rate in argon-cesium mixtures. However, the work of Platzman[9] and Utterback and Miller[10] on α-particle and fission-fragment tracks in noble gases shows that the ratio S_2/S_o is not expected to vary significantly from one noble gas to another. Furthermore, we expect that the relationship $S_2 = S_o/2$ is particularly valid for argon because of the similarity in the structure of the excitation levels in neon and argon. For neon, most of the electrons which are excited into higher levels will eventually fall to the ground state through the $(2p)^5(3s)^1$ excited state which consists again of four levels, two of which are metastable. We

---

* We cannot compute the ion generation rate in argon-cesium mixtures because there are no values available for eV/ion pair. An attempt was made to measure the ion generation rate in argon-cesium using an ion tube operated inpile.[7] However, the data, which were not very reproducible, indicated extremely low values of eV/ion pair (≈ 6) which we cannot accept on physical grounds. It is possible that the work function of uranium was sufficiently lowered by deposited cesium that thermionic emission occurred. This would lead to an apparent ion generation rate greater than the true value from fission fragments.

4

therefore consider that to a good approximation $S_2(Ar^m) = S_o(Ar^+)/2$ for argon excited and ionized by fission fragments. For the microwave cavity, this yields

$$S_2(Ar^m) = 1.87 \times 10^{-3} \text{ sec}^{-1} \tag{2}$$

III. DIFFUSION COEFFICIENTS FOR METASTABLES, ATOMIC AND MOLECULAR IONS

The ambipolar diffusion coefficients D_a for Ar^+, Ar_2^+, Cs^+ and Cs_2^+ in argon at $T°K$ are determined from measurements of ion mobility μ_o^+ (at standard conditions of $273°K$ and 760 torr) by

$$D_a = \frac{2kT}{e} \cdot \mu_o^+.$$

The ambipolar diffusion coefficient K_a at unit atom density (i.e. $D_a/2.69 \times 10^{19}$) and $300°K$ is thus

$$K_a = 1.4 \times 10^{18} \, \mu_o^+ \text{ cm}^{-1} \text{ sec}^{-1}, \tag{3}$$

where μ_o^+ is in units of $\text{cm}^2(\text{volt.sec})^{-1}$.

$K_{1,a}(Ar^+)$ in Argon

We use the experimental value of $\mu_o^+(Ar^+) = 1.6 \text{ cm}^2(\text{V.sec})^{-1}$ obtained recently by Oskam and Mittelstadt.[11] This value is in excellent agreement with the earlier determinations of Hornbeck,[12] Varney,[13] Biondi and Chanin[14] and Holstein.[15] From Eq.(3),

$$K_{1,a}(Ar^+) = 2.2 \times 10^{18} \text{ cm}^{-1} \text{ sec}^{-1}. \tag{4}$$

$K_{2,a}(Ar_2^+)$ in Argon

Oskam and Mittelstadt[11] give a value for $\mu_o^+(Ar_2^+) = 1.9 \text{ cm}^2(\text{V.sec})^{-1}$. This agrees well with Beaty's[16] earlier value of $1.85 \text{ cm}^2(\text{V.sec})^{-1}$. Thus, from (3)

$$K_{2,a}(Ar_2^+) = 2.7 \times 10^{18} \text{ cm}^{-1} \text{ sec}^{-1}. \tag{5}$$

$K_{3,a}(Cs^+)$ in Argon

The mobility of alkali metal ions in noble gases has been studied by Tyndall.[17] In a summary of this work by Dalgarno,[18] Tyndall's values are tabulated in terms of $\mu_o^+\sqrt{m_r}$ where m_r is the reduced mass of the two-body collision

5

system in units of the proton mass. For Cs^+ in argon, $\mu_o^+\sqrt{m_r}=11.5$, and with $\sqrt{m_r}=5.55$, we obtain $\mu_o^+(Cs^+)=2.1cm^2(V.sec)^{-1}$. This value is consistent with the graph of mobility as a function of ion mass in argon given by Chanin and Biondi.[19] From (3)

$$K_{3,a}(Cs^+) = 2.9 \times 10^{18} \text{ cm}^{-1} \text{ sec}^{-1}. \qquad (6)$$

$K_{4,a}(Cs_2^+)$ in Argon

The Langevin curves given by Tyndall[17] and Chanin and Biondi[19] extend as far as an ion mass of 200, (Hg^+). However we continue to use the Langevin formula $\mu_o^+\sqrt{m_r}=11.5$ to calculate the mobility of Cs_2^+ of mass 266 in argon. The point-charge-source theory of scattering should still apply to this ion, even though it is molecular, because resonant charge transfer effects are absent. In addition, the curve of mobility versus ion mass in argon shows that mobility becomes insensitive to ion mass for heavy ions (because of $\sqrt{m_r}$) so that little error will be introduced by extending the curve to mass 266. For Cs_2^+ in argon, $\sqrt{m_r}=5.81$, so that $\mu_o^+(Cs_2^+)=1.98$ cm^2(V.sec)$^{-1}$, $(cf.\mu_o^+(Cs^+)$ above). By relation (3),

$$K_{4,a}(Cs_2^+) = 2.8 \times 10^{18} \text{ cm}^{-1} \text{ sec}^{-1}. \qquad (7)$$

$K_m(Ar^m)$ in Argon

The diffusion coefficient of argon metastables in argon at 1 torr and $300°K$ $(N_o=3.22 \times 10^{16} cm^{-3})$ has been measured by Futch and Grant[20] in two experiments. They quote values for D_m of 54 ± 6 and 48 ± 6 cm^{2}sec^{-1}. For the same experimental conditions, Phelps and Molnar[21] have published $D_m=54$cm^{2}sec^{-1}. We use this value to determine K_m.

$$K_m(Ar^m) = 54 \times 3.22 \times 10^{16} \text{ cm}^{-3} \text{ cm}^2 \text{ sec}^{-1}$$

$$= 1.7 \times 10^{18} \text{ cm}^{-1} \text{ sec}^{-1}. \qquad (8)$$

Diffusion Length

Λ is the characteristic diffusion length of the container,[22] and for a cylindrical vessel of radius R and height H is given by $\Lambda^2 = \dfrac{1}{(\frac{\pi}{H})^2 + (\frac{2.4}{R})^2}$.

For a microwave cavity[8] of H=0.5cm and R=1.14cm,

$$\Lambda^2 = 0.023 \text{ cm}^2 \qquad (9)$$

6

IV. ELECTRON-ION RECOMBINATION COEFFICIENTS FOR
ARGON AND CESIUM ATOMIC AND MOLECULAR IONS

The dominant recombination loss for atomic ions (Ar^+, Cs^+) under the present conditions is three-body collisional-radiative recombination (C_3, C_{22}) involving one ion-two electron collisions. The importance of this loss process was first emphasized by the theoretical work of D'Angelo,[23] Bates and Kingston,[24] and McWhirter[25] for high temperature ($\geqslant 5,000°K$), high electron-density ($> 10^{14} cm^{-3}$) plasmas. Subsequent work by Bates, Kingston and McWhirter[5] has shown that this process of recombination in the presence of collisional de-excitation by electrons is important even in tenuous plasmas if the electron temperature is low.

The theory applies to hydrogen-like transitions among excited states and the continuum so that the results are valid for all hydrogenic ions. Bates et al. considered that an alkali ion such as cesium could be represented approximately by hydrogenic energy levels provided the ground level of the atom was made inaccessible. It was consequently suggested that the coefficients for collisional-radiative recombination are insensitive to the ion species (for singly charged ions), especially at the lower temperatures ($< 1,000°K$). Furthermore, the computations of Bates et al. are in good agreement with the recombination measurements of Aleskovskii[26] for atomic cesium ions over the range $10^{11} < n_e < 10^{14} cm^{-3}$ and $1,000 < T_e < 3,500°K$.

Tables of values for the collisional-radiative coefficient are given by Bates et al. at temperatures of 250, 500, 1000, 2000°K, etc., up to 64,000°K. The recombination rate is expressed in terms of a two-body coefficient $\alpha(n_e, T_e)$ where the recombination loss per cm^3 per sec is $\alpha(n_e, T_e)n_e N_+$. For values of $10^{11} \lesssim n_e \lesssim 10^{13} cm^{-3}$, (expected in the present work) and a temperature of 250°K, α is proportional to n_e, the recombination being collision dominated. For this regime, we can thus write the recombination loss as $C_3(T_e)n_e^2 N_+$ where $C_3 = 2.7 \times 10^{-19}$ $cm^6 sec^{-1}$ at 250°K. However, C_3 is a strong function of temperature and varies as T_e^{-5} around 250°K. For $T_e = 300°K$, we therefore write the collisional-radiative recombination coefficients for Ar^+ and Cs^+ as

$$C_3, C_{22} = 2.7 \times 10^{-19} \left(\frac{250}{300}\right)^5$$

$$= 1.1 \times 10^{-19} cm^6 sec^{-1}. \quad (10)$$

7

Note the marked change in C_3, C_{22} with temperature. This loss process evidently becomes much less significant as the temperature increases. The dependence of C_3, C_{22} on temperature is discussed further in Appendix 2.

The two-body radiative recombination terms, C_1 and C_{18} in Table I represent the lower limit of collisional-radiative recombination, i.e., $C_3 n_e$, $C_{22} n_e$ become equal, respectively, to the constant values C_1, C_{18} in the absence of collisional de-excitation when n_e is small. We include C_1, C_{18} here because the approximation $\alpha(n_e, T_e) = C(T_e) n_e$ is valid only over the restricted range mentioned above. For tenuous plasmas ($n_e \sim 10^5 cm^{-3}$) this approximation is incorrect since $C(T_e) n_e$ becomes too small. Although this regime is not presently of interest to us, we nevertheless can improve the $C(T_e) n_e$ approximation by including the proper lower limits C_1, C_{18}. This will in no way affect the correct collisional-radiative contribution of C_3 and C_{22} for value $10^{11} \lesssim n_e \lesssim 10^{13}$ cm^{-3}, since the contribution from C_1 and C_{18} is negligible under these conditions. The radiative recombination coefficient C_1 for Ar^+ is $3 \times 10^{-12} cm^{-3} sec^{-1}$[27] and C_{18} for C_s^+ is $3.8 \times 10^{-12} cm^3 sec^{-1}$,[5] where both these values are at 250°K. Since C_1, C_{18} vary with temperature[27] as $T_e^{-1/2}$, we obtain at 300°K

$$C_1 = 2.7 \times 10^{-12} \ cm^3 \ sec^{-1} \tag{11}$$

$$C_{18} = 3.5 \times 10^{-12} \ cm^3 \ sec^{-1}. \tag{12}$$

The coefficients C_2, C_{19} are three-body atomic ion-electron recombination coefficients where the third-body is a neutral argon atom. In this radiationless transition the function of the third body is to remove the surplus energy released by recombination, and as shown in R1, only the argon atom need be considered for this purpose when $N_o \gg A_o$. This makes $C_2 = C_{19}$. Values of C_2, C_{19} are obtained from an extension of Thomson's classical theory by Massey and Burhop.[28] The general expression for C_2, C_{19} is

$$C_2, \ C_{19} = \frac{(8kT/\pi m)^{1/2} \ 8\pi r_o^3 m \ q_e}{3M} \tag{13}$$

where m is the electron mass, M is the mass of the gas atom, q_e is the total elastic cross section for electron-atom collisions and r_o is the electron-ion distance within which recombination is assumed to occur. The value of r_o at

8

$300°K$ is given in R1 as 3.71×10^{-6}. With $q_e(Ar) = 4 \times 10^{-17} cm^2$ from the measurements of Ramsauer,[33] we evaluate C_2, C_{19} at $300°K$ as follows:

$$C_2, C_{19} = \frac{(8 \times 1.36 \times 10^{-16} \times 300/3.14 \times 9.11 \times 10^{-28})^{1/2} \cdot 8 \times 3.14 \times (3.71 \times 10^{-6})^3 \times 9.11 \times 10^{-28} \times 4 \times 10^{-17}}{3 \times 40 \times 1.67 \times 10^{-24}}$$

$$C_2, C_{19} = 2.5 \times 10^{-30} \ cm^6 \ sec^{-1}. \tag{14}$$

The coefficients of dissociative recombination, C_{16} and C_{21}, for the molecular ions Ar_2^+ and Cs_2^+ respectively, have been determined experimentally although the data for Cs_2^+ are not precise. The latest published value for C_{16} at $300°K$ given below (Oskam and Mittelstadt[29]) is in good agreement with the value obtained by Biondi.[30]

$$C_{16} = 6.7 \times 10^{-7} \ cm^3 \ sec^{-1}. \tag{15}$$

Dandurand and Holt[31] have reported measurements of recombination in cesium plasmas. At pressures $\lesssim 1$ torr, the value of the recombination coefficient varied with pressure, but for pressures > 1 torr and $T_e \approx 300°K$, the coefficient appeared to saturate at $\approx 1 \times 10^{-6} cm^3 sec^{-1}$. This saturated value is probably the dissociative recombination coefficient C_{21} for Cs_2^+. There is further supporting evidence from the experimental studies of Hammer, Thomas and Aubrey.[32] These workers report an upper bound for C_{21} of $5.4 \times 10^{-7} cm^3 sec^{-1}$ at values of $T_e \approx 1000°K$. Since C_{21} varies with electron temperature[27] as $T_e^{-3/2}$, the upper bound for C_{21} at $300°K$ becomes $3 \times 10^{-6} cm^3 sec^{-1}$. For the present work we selected a value of C_{21} between this upper bound and the result of Dandurand and Holt, i.e.

$$C_{21} \approx 2 \times 10^{-6} \ cm^3 \ sec^{-1} \tag{16}$$

V. PRODUCTION OF EXCITED STATES FROM
RECOMBINATION PROCESSES

It is energetically possible that recombination of argon ions and electrons can lead to the production of excited argon states, and this effect is included in Table I by the dimensionless fractions C_8, C_{10}, C_{11}. Similar fractions for the production of excited cesium states are not considered since such states cannot usefully contribute by any scheme to the ion density.

9

Little is known about the production of excited or metastable states from recombination. In the present study, the dominant recombination loss of argon ions is via dissociative recombination C_{16}, so that the important fractional value is C_{11}, the metastable argon production which results from C_{16}. Values for C_8, C_{10} are unimportant in comparison.

Recent work by Rogers and Biondi[30,34] on the dissociative mechanism in helium and neon has indicated that subsequent to the dissociation of the molecular ions, one of the atoms is in a highly excited state. We assume that this mechanism of dissociative recombination also occurs in argon which has a dissociative recombination rate similar to neon. C_{11} thus becomes the probability that a highly excited argon state decays to a metastable state. Since most of the excited argon states will fall to the ground state through the $(3p)^5(4s)^1$ excited state[35] which consists of four levels, two of which are metastable, we propose that an appropriate value for C_{11} is one-half.

$$C_{11} \approx 0.5 \tag{17}$$

We do not have reliable values for C_8, C_{10} but as mentioned above these are not important values in the present study. In R1, we did present tentative arguments, based on computations by Bates and Dalgerno,[27] which suggested that a value of 0.1 was an upper bound for both C_8 and C_{10}, but much significance should not be attached to this value.

$$C_8, C_{10} \lesssim 0.1 \tag{18}$$

VI. THREE-BODY MOLECULAR ION FORMATION

The conversions of Ar^+ to Ar_2^+, and Cs^+ to Cs_2^+ in three-body collisions are important processes in the argon-cesium plasma. The conversion frequency $(C_4 \times 3.22 \times 10^{16})$ for Ar^+ to Ar_2^+ in three-body collisions involving the argon ion and two argon atoms, has been determined by Loeb[36] as $\nu = 570p^2 sec^{-1}$ where p is in torr. This yields

$$C_4 = 5.5 \times 10^{-31} cm^6 sec^{-1}. \tag{19}$$

The coefficient C_5, representing a collision between an atomic argon ion, an argon atom and a cesium atom, is not known but since the cesium takes no part in the collision except to satisfy conditions for conservation of momentum, C_5 will be approximately equal to C_4. More precise knowledge of C_5 is not required for the present conditions because $N_o \gg A_o$, and thus $C_4 N_o^2 \gg C_5 N_o A_o$.

$$C_5 \approx 5 \times 10^{-31} \, cm^6 \, sec^{-1} \tag{20}$$

Since no value was available for the important production rate (C_{20}) of Cs_2^+ from three-body collisions involving an atomic cesium ion, a cesium atom and an argon atom, we calculated a value for C_{20} from classical collision probability theory. This calculation is discussed in Appendix I. We obtain

$$C_{20} = 4.8 \times 10^{-31} \, cm^6 \, sec^{-1} . \tag{21}$$

VII. TWO-BODY CHARGE EXCHANGE

Two-body charge exchange (C_6, C_{17}) is energetically possible when the potential energy of the incident ion is greater than or equal to the ionization energy of the target atom. The processes considered here are charge exchange between an atomic argon ion $(V_i$ (potential energy)$=15.76$ eV$)$ and a cesium atom to yield an atomic cesium ion $(V_i=3.89eV)$, and the similar exchange collision between a molecular argon ion $(V_i=14.7eV^{[37]})$ and a cesium atom.

As indicated in R1, the cross section Q_{cx} for charge exchange is maximum when the collision time is approximately equal to the time for electronic transition. That is,

$$\bar{v} \approx \frac{10^{-8} \Delta E}{h} \tag{22}$$

where $\bar{v} (= \left[8kT(M_1 + M_2)/\pi M_1 M_2 \right]^{1/2})$ is the average velocity of approach of the two particles of mass M_1 and M_2, ΔE is the difference in ionization energies of the unlike colliding particles, and h is Planck's constant. For the large potential energy differences between argon ions and cesium ions $(\sim 12eV)$, the right hand side of relation (22) becomes $\approx 3 \times 10^8 cm \, sec^{-1}$. However, $\bar{v}$ is only about $5 \times 10^4 cm \, sec^{-1}$ for both charge transfer collisions at 300°K, so that

11

$\bar{V} \ll 10^{-8} \Delta E/h$. C_6 and C_{17} therefore refer to charge exchange rates far from the maximum rates. From the charge transfer data available for other gases,[38] we note that far from maximum, Q_{cx} tends to range from 10^{-16} to 10^{-17} cm^2. We thus make an estimate of C_6, C_{17} by taking Q_{cx} for both processes as $\sim 5 \times 10^{-17}$ cm^2. Such an estimate is sufficient to establish that charge transfer is unimportant under the present conditions. Since C_6, $C_{17} = \bar{V}Q_{cx}$, we obtain

$$C_6, \ C_{17} \sim 3 \times 10^{-12} \ \text{cm}^3 \ \text{sec}^{-1}. \tag{23}$$

VIII. VOLUME DESTRUCTION OF METASTABLE STATES

The predominant loss processes for argon metastables in the volume of the gas are two-body collisions (C_{13}) with argon atoms, three-body collisions (C_{14}) with argon atoms, and two-body ionizing collisions (C_{15}) with cesium atoms (Penning effect). The first two processes for the destruction of argon metastables by argon atoms have been determined by Phelps and Molnar[21] from measurements of the decay constant of the radiation absorbed by the metastable atoms. They give the destruction frequency as $9p^2 + 40p$ sec^{-1} at 300°K where p is in torr. Therefore, $C_{13} = 40/n$ and $C_{14} = 9/n^2$ where $n(=3.22 \times 10^{16} \text{cm}^{-3})$ is the neutral atom density at 1 torr and 300°K.

$$C_{13} = 1.2 \times 10^{-15} \ \text{cm}^3 \ \text{sec}^{-1} \tag{24}$$

$$C_{14} = 8.7 \times 10^{-33} \ \text{cm}^6 \ \text{sec}^{-1}. \tag{25}$$

There is no published data available for the very important Penning ionization (C_{15}) of a cesium atom in collision with an argon metastable state. However, in a private communication,[39] Nolan has offered a preliminary value of $Q_i \approx 1 \times 10^{-14}$ cm^2 for the ionization cross section of this process. This extremely large preliminary value (for atomic collisions) indicates an unusually efficient conversion of metastable energy to ionization energy. The value of Q_i was estimated from Townsend-type measurements on the spatial growth of ionization in an argon-cesium mixture. Since the average velocity of approach for metastable argon-cesium collisions at 300°K is $\bar{V} = 4.55 \times 10^4$ cm sec^{-1},

$$C_{15} \approx 4.6 \times 10^{-10} \ \text{cm}^3 \ \text{sec}^{-1}. \tag{26}$$

12

Collisions between pairs of metastable argon states (C_7, C_{12}) do not appear to have been studied. However, the concentration N_m of argon metastable states in the present study is sufficiently low ($\sim 10^{10} \text{cm}^{-3}$) that collisions between pairs of metastable states will be rare in comparison with collisions between a metastable state and a neutral atom ($N_o \sim 10^{18} \text{cm}^{-3}$). Even so, an order-of-magnitude estimate of the coefficients C_7, C_{12} is useful to establish that the influence of metastable-metastable collisions is negligibly small. The metastable-metastable ionization cross section for helium has been determined by Phelps[40] as $Q_m \approx 10^{-14} \text{cm}^2$ and we assume this value for crude estimates of ion production from metastable-metastable argon collisions. Thus for $\bar{V} = 5.64 \times 10^4 \text{cm sec}^{-1}$ for argon-argon collisions,

$$C_7 \sim 5.6 \times 10^{-10} \text{ cm}^3 \text{ sec}^{-1}. \tag{27}$$

Not all collisions between metastable states lead to atomic ion production so that $C_{12} > C_7$, although not necessarily by a significant amount. However, the above relatively large value of Q_m suggests that almost all metastable-metastable de-excitation collisions lead to ionization. For the present purposes, therefore, it is sufficient to consider

$$C_{12} \sim 5.6 \times 10^{-10} \text{ cm}^3 \text{ sec}^{-1}. \tag{28}$$

IX.   COLLISIONS INVOLVING HIGHLY EXCITED STATES

It is unlikely that there will be a sufficient density N_x of highly excited argon states ($14.7 < V_x < 15.8 \text{eV}$) in the plasma to produce significant molecular ion production via the Hornbeck-Molnar[6] process (C_9). These states tend to decay rapidly to lower excited levels which cannot lead to molecular ion formation. Nevertheless, we report an estimate of C_9 for completeness. From pulsed discharge data, Hornbeck[41] has determined the product τQ_x for argon where Q_x is the cross section for ion formation from N_x and τ is the mean lifetime of N_x. The value of τQ_x is $1 \times 10^{-22} \text{cm}^2$ sec at a value of E/p (E is the uniform electric field) = 30 $V(\text{cm torr})^{-1}$ and a pressure p of 8 torr. Loeb[41] suggests a separation of τQ_x as $\tau \approx 10^{-6}$ sec and $Q_x \approx 10^{-16} \text{cm}^2$. An accurate determination of τ under the present conditions of higher pressure (≈ 100 torr) would require further identification of the high lying excited states and an

13

analysis of the decay and transport of resonance and non-resonance radiation through the gas for our particular tube. However, the above values are adequate for the present purpose.

$$c_9 \sim 5.6 \times 10^{-12} \text{ cm}^3 \text{ sec}^{-1}. \tag{29}$$

$$\tau \sim 10^{-6} \text{ sec}. \tag{30}$$

X. COLLECTION OF DATA

Table II summarizes the production, diffusion and conversion coefficients of ions, excited and metastable states discussed in this report. All the reaction rates refer to a temperature of 300°K.

14

TABLE II. Rate coefficients for Ar-Cs plasma at 300°K

Process	Symbol	Value
Production Ar^+ by fission fragments	S_o	3.74×10^{-3} sec^{-1}
Diffusion Ar^+ in Ar	$K_{1,a}$	2.2×10^{18} cm^{-1} sec^{-1}
2-body radiative recombination Ar^+	C_1	2.7×10^{-12} cm^3 sec^{-1}
3-body Thomson recombination Ar^+	C_2	2.5×10^{-30} cm^6 sec^{-1}
Collisional-radiative recombination Ar^+	C_3	1.1×10^{-19} cm^6 sec^{-1}
3-body $Ar^+ \longrightarrow Ar_2^+$ with Ar, Ar	C_4	5.5×10^{-31} cm^6 sec^{-1}
3-body $Ar^+ \longrightarrow Ar_2^+$ with Ne, Ar	C_5	$\approx 5 \times 10^{-31}$ cm^6 sec^{-1}
2-body $Ar^+ \longrightarrow Cs^+$	C_6	$\sim 3 \times 10^{-12}$ cm^3 sec^{-1}
Metastable-metastable $Ar^m \longrightarrow Ar^+$	C_7	$\sim 5.6 \times 10^{-10}$ cm^3 sec^{-1}
Production Ar^x by fission fragments	S_1	$\ll S_2$ sec^{-1}
Production Ar^x by atomic recombination	C_8	$\lesssim 0.1$
Mean lifetime Ar^x	τ	$\sim 10^{-6}$ sec
2-body ion formation $Ar^x \longrightarrow Ar_2^+$	C_9	$\sim 5.6 \times 10^{-12}$ cm^3 sec^{-1}
Production Ar^m by fission fragments	S_2	1.87×10^{-3} sec^{-1}
Diffusion Ar^m in Ar	K_m	1.7×10^{18} cm^{-1} sec^{-1}
Production Ar^m by recombination of Ar^+	C_{10}	$\lesssim 0.1$
Production Ar^m by recombination of Ar_2^+	C_{11}	≈ 0.5
Metastable-metastable Ar^m destruction	C_{12}	$\sim 5.6 \times 10^{-10}$ cm^3 sec^{-1}
Destruction Ar^m via Ar	C_{13}	1.2×10^{-15} cm^3 sec^{-1}
Destruction Ar^m via Ar, Ar	C_{14}	8.7×10^{-33} cm^6 sec^{-1}
Penning ionization $Ar^m + Cs \longrightarrow Cs^+$	C_{15}	$\approx 4.6 \times 10^{-10}$ cm^3 sec^{-1}
Diffusion Ar_2^+ in Ar	$K_{2,a}$	2.7×10^{18} cm^{-1} sec^{-1}
2-body dissociative recombination of Ar_2^+	C_{16}	6.7×10^{-7} cm^3 sec^{-1}
2-body $Ar_2^+ \longrightarrow Cs^+$	C_{17}	$\sim 3 \times 10^{-12}$ cm^3 sec^{-1}
Diffusion Cs^+ in Ar	$K_{3,a}$	2.9×10^{18} cm^{-1} sec^{-1}
2-body radiative recombination Cs^+	C_{18}	3.5×10^{-12} cm^3 sec^{-1}
3-body Thomson recombination Cs^+	C_{19}	2.5×10^{-30} cm^6 sec^{-1}
3-body $Cs^+ + Cs + Ar \longrightarrow Cs_2^+$	C_{20}	4.8×10^{-31} cm^6 sec^{-1}
Diffusion Cs_2^+ in Ar	$K_{4,a}$	2.8×10^{18} cm^{-1} sec^{-1}
2-body dissociative recombination Cs_2^+	C_{21}	$\approx 2 \times 10^{-6}$ cm^3 sec^{-1}
Collisional-radiative recombination Cs^+	C_{22}	1.1×10^{-19} cm^6 sec^{-1}
Characteristic diffusion length	Λ^2	0.023 cm^2

APPENDIX A

PRODUCTION OF MOLECULAR CESIUM ION FROM COLLISION OF
ATOMIC CESIUM ION, CESIUM ATOM AND ARGON ATOM

The reaction rate C_{20} for

$$Cs^+ + Cs + Ar \longrightarrow Cs_2^+ + Ar$$
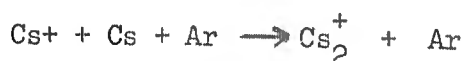
is determined from an application of some of the classical collision theories of Langevin[42] and Thomson.[43] We consider the argon atom only as a kinetic energy sink for Cs^+ or Cs and we do not take into account the binding energy of the Cs_2^+ ion. The result is therefore considered a first approximation only.*

If K is the dielectric constant of argon at pressure p containing N_o atoms per cm^{-3}, the attractive force on an atom by an ion of charge e at distance r is

$$f = \frac{K - 1}{2\pi N_o} \frac{e^2}{r^5} , \qquad (1)$$

which corresponds to a potential energy

$$V = - \frac{K - 1}{8\pi N_o} \frac{e^2}{r^4} . \qquad (2)$$

We postulate that Cs_2^+ will be produced when either Cs^+ or Cs lose sufficient energy in collision with Ar for Cs^+ or Cs to describe a closed orbit relative to the other. If Cs^+ and Cs possess an average energy $\frac{3}{2}kT$ at temperature T, a closed orbit will be formed if

$$\frac{3}{2} kT = \frac{K - 1}{8\pi N_o} \frac{e^2}{r^4} . \qquad (3)$$

---

* Two analogous reactions have been studied by Oskam.[52] We show the following comparison between Oskam's measured values and the values we calculate using this theory:

	Measured	Calculated
$Ar^+ + Ar + Ne \longrightarrow Ar_2^+ + Ne$	2.5×10^{-31} cm^6 sec^{-1}	1.3×10^{-31} cm^6 sec^{-1}
$Ar^+ + Ar + He \longrightarrow Ar_2^+ + He$	1.1×10^{-31} cm^6 sec^{-1}	0.92×10^{-31} cm^6 sec^{-1}

16

That is, Cs^+ and Cs must approach each other within r_o defined by

$$r_o^4 = \frac{K-1}{12\pi N_o} \frac{e^2}{kT} .$$

(4)

We now assume that if either Cs^+ or Cs loses an amount of energy of order kT when within a distance r_o of the other, Cs_2^+ will be formed. The number of times per sec that one Cs^+ approaches Cs atoms within r_o is $\pi r_o^2 (V_+^2 + V^2)^{1/2} A_o$ where V_+, V are respectively the average velocities of Cs^+ and Cs, and A_o is the concentration of Cs. The chance that in such an encounter formation of Cs_2^+ will occur is $(P_+ + P)$ times this, where P_+ is the probability that Cs^+ makes a collision involving $\gtrsim kT$ energy loss with Ar when within r_o from Cs, and P is similarly defined for Cs. With a Cs^+ number density of A_+, the number of events $\nu \sec^{-1}$ leading to Cs_2^+ formation becomes

$$\nu = \pi r_o^2 (V_+^2 + V^2)^{1/2} (P_+ + P) A_o A_+ .$$

(5)

For P_+ and P, we take the classical sphere collision probability given by

$$P_+ = 1 + 2 \left\{ \frac{e^{-g_+}}{g_+^2} + \frac{e^{-g_+}}{g_+} - \frac{1}{g_+^2} \right\}$$

(6)

where $g_+ = \dfrac{2r_o}{L_+}$ and L_+ is the mean free path for Cs^+ in Ar. P is this expression with $g = \dfrac{2r_o}{L}$ and L the mean free path for Cs in Ar. Under the present conditions we simplify (6) by noting that $r_o \approx 10^{-8}$ cm, $L_+ \approx 10^{-4}$ cm and thus $g \ll L$. This yields

$$P_+ = \frac{r_o}{L_+} = N_o Q_+ r_o ,$$

(7a)

where Q_+ is the elastic cross section for Cs^+-Ar collisions. Also

$$P = N_o Q r_o .$$

(7b)

We now express the dielectric term $(K-1)$ for argon at any pressure $P < 760$ torr and temperature $300°K$ as [44]

$$(K-1)_P = (K-1)_{760} \left(\frac{P}{760} \right) = \frac{(K-1)_{760} N_o}{2.46 \times 10^{19}} .$$

(8)

17

Expression (4) for r_o^4 then becomes independent of N_o:

$$r_o^4 = \frac{(K-1)_{760}}{12\pi \times 2.46 \times 10^{19}} \frac{e^2}{kT} \tag{9}$$

Thus from Eqs. (5), (7) and (9) we obtain $\nu = C_{20}N_oA_oA_+$ where

$$C_{20} = \pi \left[\frac{(K-1)_{760}}{12\pi \times 2.46 \times 10^{19}} \frac{e^2}{kT} \right]^{1/2} (v_+^2 + v^2)^{1/2} (Q_+ + Q) \tag{10}$$

$(K-1)_{760} = 5.17 \times 10^{-4}$ for argon,[44] so evaluating Eq.(10) yields

$$C_{20} = \pi (4.2)^3 10^{-24} (v_+^2 + v^2)^{1/2} (Q_+ + Q). \tag{11}$$

Q for Cs (of concentration A_o cm^{-3}) in Ar (of concentration N_o cm^{-3}) is given by[45]

$$Q = \sqrt{2}\, \pi \frac{A_o}{N_o} d(Cs) + \frac{\pi}{4} \left[d(Cs) + d(Ar) \right]^2 \left[1 + \frac{M(Cs)}{M(Ar)} \right]^{1/2} \tag{12}$$

where d is the atomic diameter and M the atomic weight. The first term on the right hand side of (12) can be ignored for $N_o \gg A_o$. The second term yields

$$Q = 1.2 \times 10^{-14} \text{ cm}^2. \tag{13}$$

We determine Q_+ from Q by including the effect that an ion polarizes a neutral atom producing mutual attraction which results in a large value of Q. The relation is[43]

$$Q_+ = Q \frac{\left[8 \cdot 8 \left(\frac{2\alpha\, e^2}{\frac{3}{2}\, kT} \right)^{1/2} \right]}{\left[d(Cs) + d(Ar) \right]^2},$$

where $\alpha = \frac{K-1}{4\pi N_o}$ is the polarizability of argon. Thus at 300°K

$$Q_+ = 4.65\, Q = 5.5 \times 10^{-14} \text{ cm}^2. \tag{15}$$

Finally we obtain $(v_+^2 + v^2)^{1/2} = 3.07 \times 10^4$ cm sec^{-1} at 300°K and therefore from Eqs. (11), (13) and (15),

$$C_{20} = 4.8 \times 10^{-31} \text{ cm}^6 \text{ sec}^{-1}.$$

18

COLLISIONAL-RADIATIVE RECOMBINATION AND ITS
DEPENDENCE ON TEMPERATURE

Recent work on recombination loss in plasmas has emphasized the importance of the collisional-radiative process. This work was initiated by D'Angelo,[23] Bates and Kingston,[24] and McWhirter,[25] subsequently studied in considerable detail by Bates, Kingston and McWhirter,[5] and further applied and in some cases experimentally verified by Hinnov and Hirschberg,[46] Aleskovskii,[26] Wada and Knechtli,[47] Stabler,[48] and Cooper and Kunkel.[49] What follows here is a brief physical description of the process and its dependence on temperature particularly as used in the reaction kinetics study.

We represent the three-body collisional-radiative recombination of an atomic ion $(e.g. \ Cs^+)$ and two electrons as

$$Cs^+ + e + e \longrightarrow Cs^{**} + e;$$

$$Cs^{**} + e \longrightarrow Cs^* + e; \quad or \ Cs^{**} \longrightarrow Cs^* + h\nu, \ etc.$$
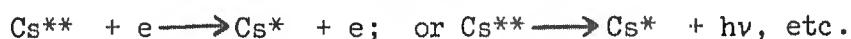
The recombination process is one in which an electron, as a result of a collision with another electron, loses enough energy* to be captured into one of the more highly excited electronic states (Cs^{**}) of the ion. Since electrons capture is proportional to n^4 where n is the principal quantum number, electron capture into highly excited states is most probable. That is, much larger energy exchanges between the colliding electrons are required for electron capture into low lying levels.

The formation of the highly excited state is followed by bound-bound radiative transitions and electron-induced collisional transitions to the ground state via many other states if necessary. Recombination is complete when an excited state finally decays to the ground state. The total rate of populating the ground state is the sum of (1) direct three-body recombination, (2) direct radiative recombination, (3) collisional transitions from all excited states, (4) spontaneous decay from all excited states. This rate therefore depends on the instantaneous populations of all excited states.

---

* An electron-electron collision is much more efficient than an electron-atom collision for degrading electron energy because the masses of the colliding particles are the same.

Solutions to the equations expressing the population and de-population rate of excited states in an optically-thin hydrogen plasma have been given by Bates, Kingston and McWhirter.[5] The results show that atomic recombination rates from this process are several orders of magnitude larger than the pure radiative recombination process considered previously,[27] particularly at the lower temperatures. Although the calculations of Bates et al. were performed for hydrogen ions, they may be expected to apply reasonably well to other singly-ionized atoms, especially at lower temperatures where the important processes which lead to recombination occur at highly-excited hydrogen-like (hydrogenic) states.*

In a subsequent paper, Bates, Kingston and McWhirter[50] discuss the case of an optically thick hydrogen plasma. For example, if the Lyman lines $\left(\nu = R \left\{ \frac{1}{1^2} - \frac{1}{n^2} \right\} \right)$ are completely absorbed, downward radiative transitions from any level n to 1 are balanced by the reverse upward transitions and it is necessary to remove all terms expressing downward Lyman transitions from the equations. In most laboratory plasmas, self-absorption of the Lyman lines does occur with a subsequent reduction in the value of α, the collisional-radiative coefficient. However, for the cool dense plasma generated by fission fragments† the recombination process is dominated by collisional processes; Bates and co-workers show that it then makes little difference whether the plasma is optically thin or optically thick since the value of α remains unchanged. A recent paper by Bates and Kingston[51] emphasizes that even when n_e is as low as $1 \times 10^3 \text{cm}^{-3}$, collisional effects are still important if the plasma is cold (25°K).

Bates, Kingston and McWhirter[5] express the collisional-radiative recombination rate as $\alpha(n_e,T)n_e N_+$ where $\alpha(n_e,T)$ is the recombination coefficient. Since the initial recombination into highly excited levels involves a 2 electron-one ion collision and moreover since the collisional de-excitation of this level involves further electron impacts, $\alpha(n_e,T)$ is evidently a strong function of both temperature and electron concentration. The tabulated values of $\alpha(n_e,T)$ given by Bates et al. for various values of n_e and T show this. When collisional de-excitation dominates α is proportional to n_e, and for the lower temperatures around 300°K, α varies as T^{-5}.

---

* Those states having energy $E_n = -R/n^2$ and multiplicity $\omega_n = 2n^2$.

†For most plasmas, high electron density is synonymous with high temperature.

Note that α is an effective two-body rate coefficient. The above work-
ers emphasize that the decision to express the results in terms of a two-body
coefficient does not imply that two-body processes predominate; the decision
is purely a matter of convenience. However, for the reaction kinetic equa-
tions shown previously in the text (Table I), it is necessary to express this
recombination by a three-body rate coefficient, i.e. to express $\alpha(n_e, T)n_e N_+$ as
$C(T)n_e n_e N_+$. This approximation, which is appropriate for collision-dominated
de-excitation processes, is a reasonable approximation for the high density
$(\gtrsim 10^{12} \text{cm}^{-3})$ relatively cool $(\lesssim 1300°K)$ plasmas of interest to us.

Figure 1 shows the dependence of C on T for different values of n_e where
we have used the values of $\alpha(n_e, T)$ calculated by Bates, Kingston and McWhirter.
It is seen that for $n_e \gtrsim 10^{12} \text{cm}^{-3}$ and $T \lesssim 1300°K$, C is essentially a function of
T only. The effect of the temperature variation of C on the electron number
density as determined from the reaction kinetic analysis, was studied[4] by
selecting a temperature and reading off from Fig. 1 the appropriate value of
C to be used in the collisional-radiative term $C N_+ n_e^2, (C=C_3=C_{22})$. For
example:

C $(\text{cm}^{-6}\text{sec}^{-1})$	T°K
1.08×10^{-19}	300
1.0×10^{-20}	500
1.0×10^{-21}	870
1.0×10^{-22}	1300
1.0×10^{-23}	≈ 2400

As the temperature increases much beyond 1300°K, the recombination process is
no longer collision-dominated even for values of $n_e > 10^{12} \text{cm}^{-3}$. Thus we see
from Fig. 1 that for a selected value of $C=1.0 \times 10^{-23} \text{cm}^{-3}\text{sec}^{-1}$, a precise plasma
temperature cannot be specified unless n_e is known. That is, C is no longer a
function of T only (for $n_e \gtrsim 10^{12} \text{cm}^{-3}$) and the approximation $\alpha(n_e, T)n_e N_+ =$
$C(T)n_e^2 N_+$ is no longer valid.

THREE - BODY COLLISIONAL - RADIATIVE RECOMBINATION COEFFICIENT
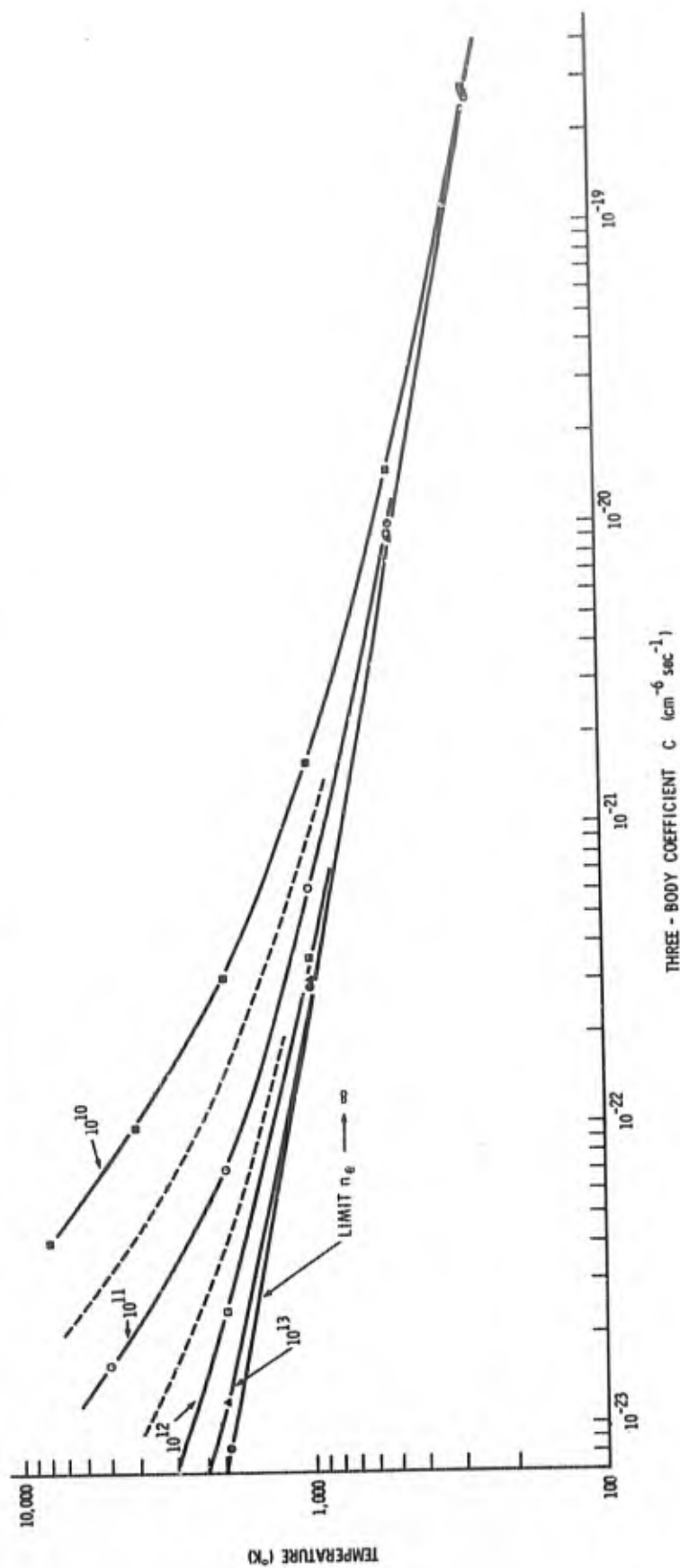
Fig. 1. The variation of the three-body collisional radiative recombination coefficient C with temperature T and electron number density n_e. $C = \alpha(n_e,T)/n_e$ is taken from the data of Bates, Kingston and McWhirter (Proc.Roy.Soc.A267,297,1962) for an optically-thin hydrogen plasma where α is a two-body collisional-radiative recombination coefficient. Over the range of parameters shown here, C is essentially unchanged for (1) pseudo-alkali ion and (2) plasma optically thick toward lines of Lyman series.

22

REFERENCES

1. D. J. Rose, "Reaction Kinetics of the Fission Fragment Plasma", See ONR Annual Report No. 5, Contract Nonr-3109(00), AD 609 177, Oct. 1964, Section B.

2. C. B. Leffert, "Computer Solutions to the Reactor Kinetics Equations", ibid., Section C.

3. D. B. Rees, "Production, Diffusion and Conversion Rates of Ions, Metastable and Excited States in Penning-Type Neon-Argon Plasmas", ibid., Section D.

4. C. B. Leffert, "Electron Density in Ar-Cs and Ne-Ar Plasmas - a Theoretical Study", Section B of this report.

5. D. R. Bates, A. E. Kingston and R.W.P.McWhirter, Proc. Roy. Soc. A267, 297, 1962.

6. J. A. Hornbeck and J.P. Molnar, Phys. Rev., 84, 621, 1951.

7. C. B. Leffert, D. B. Rees and F. E. Jamerson, ONR Annual Report No. 5, AD609177, Contract Nonr-3109(00), Oct. 1964; J. Appl. Phys. to be published Dec.,1965.

8. C. B. Leffert, "Theory and Experimental Results for First Inpile Microwave Measurement of Electron Density", Section C of this report.

9. R. L. Platzman, Int. J.Appl. Radiation and Isotopes, 10, 116 , 1961.

10. N. G. Utterback and G. H. Miller, Phys. Rev., 116, 976, 1959.

11. H. J. Oskam and V. R. Mittelstadt, Phys. Rev., 132,1435, 1963.

12. J. A. Hornbeck, Phys. Rev., 84, 615, 1951.

13. R. N. Varney, Phys. Rev., 88, 362, 1952.

14. M. A. Biondi and L. M. Chanin, Phys. Rev., 94, 910, 1954; Phys. Rev., 106, 473, 1957.

15. T. Holstein, J. Phys. Chem., 56, 832, 1952.

16. E. C. Beaty, Proc. Fifth Inter. Conf. on Ionization Phenomena, (Munich), Vol. I, 183, 1962.

17. A. M. Tyndall, The Mobility of Positive Ions in Gases, (Cambridge), 1938.

18. A. Dalgarno, "Diffusion and Mobilities", p.643 of Atomic and Molecular Processes, (Edited by D. R. Bates), (Academic), 1962.

19. L. M. Chanin and M. A. Biondi, Phys. Rev., 107, 1219, 1957.

20. A. H. Futch and F. A. Grant, Phys. Rev., 104, 356, 1956.

21. A. V. Phelps and J. P. Molnar, Phys. Rev., 89, 1202, 1953.

22. S. C. Brown, Basic Data of Plasma Physics, (Wiley), p.47, 1959.

23. N. D'Angelo, Phys. Rev., 121, 505, 1961.

24. D. R. Bates and A. E. Kingston, Nature, 189, 652, 1961.

25. R. W. P. McWhirter, Nature, 190, 902, 1961.

26. Yu M. Aleskovskii, Soviet Physics JETP, 17, 570, 1963.

27. D. R. Bates and A. Dalgarno, "Electronic Recombination", p.245 of Atomic and Molecular Processes, (Edited by D. R. Bates), (Academic), 1962.

28. H. S. W. Massey and E. H. S. Burhop, *Electronic and Ionic Impact Phenomena*, (Oxford), p.618, 1951.

29. H. J. Oskam and V. R. Mittelstadt, Phys. Rev., 132, 1445, 1963.

30. M. A. Biondi, Phys. Rev. 129, 1181, 1963.

31. P. Dandurand and R. B. Holt, Phys. Rev. 82, 868, 1951.

32. J. M. Hammer, J. J. Thomas, and B. B. Aubrey, RCA Princeton, DDC Report No. AD 427812, 1963.

33. C. Ramsauer, 1930-1932 Ann. Physik; see R. B. Brode, Rev. Modern Physics, 5, 257, 1933.

34. W. A. Rogers and M. A. Biondi, Phys. Rev. 134, A1215, 1964.

35. T. Tsukishima, J. Phys. Soc. Japan, 18, 558, 1963.

36. L. B. Loeb, *Basic Processes of Gaseous Electronics*, (California), p.477, 1955.

37. M. S. B. Munson, J. L. Franklin and F. H. Field, J.Chem.Phys. 67, 1542, 1963.

38. E.W. McDaniel, *Collision Phenomena in Ionized Gases*, (Wiley), p.240, 1964.

39. J. Nolan, Westinghouse Corp., Private communication, 1964.

40. A. V. Phelps, Communication to M. A. Biondi, Phys. Rev., 88, 660, 1952.

41. J. A. Hornbeck, in *Basic Processes of Gaseous Electronics* (California) by L. B. Loeb, p. 701, 1955.

42. P. Langevin, in *Collision Phenomena in Ionized Gases*, by E. W. McDaniel, p. 701, 1964.

43. J. J. Thomson, Phil. Mag., 47, 337, 1924.

44. L. Essen, in *Handbook of Chemistry and Physics*, 40th Ed, (Chemical Rubber Publishing Company) p. 2522, 1959.

45. E. W. McDaniel, *Collision Phenomena in Ionized Gases*, p. 39, 1964.

46. E. Hinnov and J. G. Hirschberg, Phys. Rev., 125, 795, 1962.

47. J. Y. Wada and R. C. Knechtli, Phys. Rev. Letters, 10, 513, 1964.

48. R. C. Stabler, *Sixth Inter. Conf. on Ionization Phenomena*, (Paris), Vol.I, 449, 1963.

49. W. S. Cooper and W. B. Kunkel, Phys. Rev., 138, A1022, 1965.

50. D. R. Bates, A. E. Kingston and R. W. P. McWhirter, Proc. Roy. Soc., A270, 155, 1962.

51. D. R. Bates and A. E. Kingston, Proc. Phys. Soc., 83, 43, 1964.

52. H. J. Oskam, Philips Res. Repts., 13, 401, 1958.

SECTION B

ELECTRON DENSITY IN Ar-Cs AND Ne-Ar PLASMAS - A THEORETICAL STUDY

CONTENTS

SECTION B

ELECTRON DENSITY IN Ar-Cs AND Ne-Ar PLASMAS -
A THEORETICAL STUDY

ABSTRACT

The low electron-atom scattering cross section for argon and the low
ionization potential of cesium make a plasma generated from an argon-cesium
gas mixture by fission-fragment ionization a potentially good candidate for a
thermionic energy converter. The reaction kinetics have been investigated for
various mixtures of these gases to study the influence of reaction coefficients,
total pressure and partial pressure of the gas constituents on electron density.
The curves of electron density versus gas composition and total pressure were
similar in shape to those for the neon-argon system but the electron density
was about 1.5 times greater.

OBJECT

Analyze the important parameters which determine the electron density for
plasmas generated in argon-cesium and neon-argon mixtures.

CONCLUSIONS

1. The electron density generated by fission-fragment ionization in argon-
   cesium is about 1.5 times greater than in neon-argon under the same
   conditions.
2. The dependence of electron density on electron temperature, total and
   partial pressure of the gas constituents is similar in both mixtures.
3. For the gas at the operating temperature of a thermionic energy converter
   ($1300°K$) and a gap spacing of 0.5 cm, the conditions for maximum electron

1

density exist at a pressure of 100 torr and Ar/Ne=3.4×10^{-4} for Ne-Ar, and Cs/Ar=1.7×10^{-4} for Ar-Cs.

4. For a fully enriched uranium fission source in a neutron flux of 1.0×10^{13} $sec^{-1} cm^{-2}$, a maximum electron density of $3.8 \times 10^{12} cm^{-3}$ was calculated for Ar-Cs at 1300°K.

INTRODUCTION

The reaction kinetics equations that control the electron number density in a mixed-gas plasma ionized by fission fragments were formulated by Rose[1] and the reaction rate coefficients were evaluated by Rees[2] for the neon-argon system. The reaction kinetics equations for the neon-argon system were solved on the IBM 7094 computer and a parametric study of the effect of the gas pressure and the ratio of Ar/Ne were reported by Leffert.[3] In these first studies the collisional-radiative recombination loss of the argon ion (Ar^+) was neglected. A study of this recombination loss made by Rees indicated that for the conditions of low electron temperature and medium electron density ($\sim 10^{12} cm^{-3}$), the collisional-radiative loss could be large. The computer code was modified to include the collisional-radiative loss term. A parametric code study[4] showed that by including this term the enhanced electron density that resulted from the mixed gas was lost at low electron temperature ($\sim 300°K$). At the gas temperature expected for our thermionic diode ($\sim 1300°K$), however, most of the enhanced electron density still remained. Measurements of electron density in neon-argon with a microwave resonant cavity technique are reported elsewhere.[5] The gap in the microwave cavity was 0.5 cm and the calculations in this report are based on that gap dimension.

Another plasma of interest to thermionic energy conversion is the argon-cesium system ionized by fission fragments. Of the noble gases, argon has the lowest electron-atom cross section at energies typical of diode operation and should therefore offer the minimum plasma resistance to electron transport across the diode. Cesium has the lowest ionization potential (3.89 eV) and thus the $^3P_2$(11.53 eV) and the $^3P_0$(11.72 eV) metastable levels of argon have more than sufficient energy to ionize the cesium. Argon has a greater stopping power for fission fragments than neon and thus should give a higher ion generation rate. Also cesium should deposit on the cool collector surface, lower its work function and therefore increase the power output of the thermionic converter. These arguments favor the argon-cesium system over the neon-

2

argon system. The conductivity of the plasma is fixed largely by the electron density which is dependent on the rates of many reactions that occur within the plasma.

The reaction kinetics code was used to calculate electron density in the argon-cesium mixture and to analyze the influence of pressure, ratio of Cs/Ar, collisional-radiative recombination, Penning ionization coefficient and ion diffusion. The Ar-Cs system is also compared to the Ne-Ar system. The influence of pressure and the ratio of gas constituents was determined at 1300°K for both the Ar-Cs and Ne-Ar systems so that these two gas mixtures could be compared at temperatures typical of an operating thermionic energy converter. The study of the influence of collisional-radiative recombinations at lower temperatures ($\sim$ 500°K) will aid in the analysis of the forthcoming inpile microwave experiments on Ar-Cs.

REACTION KINETICS

Equations for Particle Densities

The general equations which describe the reaction kinetics for a binary gas mixture have been described in detail previously.[1,3] The equations contained in the computer program are listed in Table I where all time derivatives were set equal to zero for the steady state case. The collisional-radiative term ($C_{22}n_e^2 A_+$) is now included in the code.[4]

Rate Coefficients for an Argon-Cesium Plasma

The reaction rate coefficients for an argon-cesium plasma have been determined [6] and these are listed in Table II. The explanation of the various coefficients will be aided by reference to the equations in Table I.

Generation Rate for Argon Ions and Argon Metastables

The generation rate for argon ions in the argon-cesium mixture (S_+) was scaled from previous calculations using the ion generation rate code.[9] The pertinent data are shown in Table III.

TABLE I. Particle density equations for binary gas plasma.

Time Derivative	From Direct Flux	Diffusion	2- and 3-Body Recombination	3-Body Molecular Ion Formation	2-Body Charge Exchange	Metastable-Metastable Collisions	Radiation Via N_x	Molecular Ion Formation Via N_x	Metastable Destruction Via N_o	Penning Ionization	Eq. No.
$\dfrac{\partial N_+}{\partial t} =$	$S_o N_o$	$-\dfrac{K_{1,a} N_o N_+}{\Lambda^2}$	$-\left[C_1 + C_2 N_o + C_3 n_e\right] N_+ n_e$	$-C_4 N_+ N_o^2$ $-C_5 N_+ N_o A_o$	$-C_6 N_+ A_o$	$+C_7 N_m^2$					(1)
$\dfrac{\partial N_x}{\partial t} =$	$S_1 N_o$	$-\dfrac{K_m N_o N_m}{\Lambda^2}$	$+C_8\left[C_1 + C_2 N_o + C_3 n_e\right] N_+ n_e$				$-N_x/\tau_x$	$-C_9 N_x N_o$			(2)
$\dfrac{\partial N_m}{\partial t} =$	$S_2 N_o$	$-\dfrac{K_m N_o N_m}{\Lambda^2}$	$+C_{10}\left[C_1 + C_2 N_o + C_3 n_e\right] N_+ n_e$ $+C_{11} C_{16} N_{2+} e$			$-C_{12} N_m^2$			$-C_{13} N_o N_m$ $-C_{14} N_o^2 N_m$	$-C_{15} N_m A_o$	(3)
$\dfrac{\partial N_{2+}}{\partial t} =$		$\dfrac{K_{2,a} N_o N_{2+}}{\Lambda^2}$	$-C_{16} N_{2+} n_e$	$+C_4 N_+ N_o^2$ $+C_5 N_+ N_o A_o$	$-C_{17} N_{2+} A_o$			$+C_9 N_x N_o$			(4)
$\dfrac{\partial A_+}{\partial t} =$		$\dfrac{K_{3,a} N_o A_+}{\Lambda^2}$	$+\left[C_{18} + C_{19} N_o + C_{22} n_e\right] N_+ n_e$	$-C_{20} A_+ A_o N_o$	$+C_6 N_+ A_o$ $+C_{17} N_{2+} A_o$					$+C_{15} N_m A_o$	(5)
$\dfrac{\partial A_{2+}}{\partial t} =$		$\dfrac{K_{4,a} N_o A_{2+}}{\Lambda^2}$	$-C_{21} A_{2+} n_e$	$+C_{20} A_+ A_o N_o$							(6)

Equation for charge neutrality: $n_e = N_+ + N_{2+} + A_+ + A_{2+}$ (7)

4

TABLE II. Rate coefficients for Ar-Cs plasma at $300°K$

Process	Symbol	Value
Production Ar^+ by fission fragments	S_o	3.74×10^{-3} sec^{-1}
Diffusion Ar^+ in Ar	$K_{1,a}$	2.2×10^{18} cm^{-1} sec^{-1}
2-body radiative recombination Ar^+	C_1	2.7×10^{-12} cm^3 sec^{-1}
3-body Thomson recombination Ar^+	C_2	2.5×10^{-30} cm^6 sec^{-1}
Collisional-radiative recombination Ar^+	C_3	1.1×10^{-19} cm^6 sec^{-1}
3-body $Ar^+ \longrightarrow Ar_2^+$ with Ar, Ar	C_4	$5.5 \times 10^{-31} cm^6$ sec^{-1}
3-body $Ar^+ \longrightarrow Ar_2^+$ with Ne, Ar	C_5	$\approx 5 \times 10^{-31}$ cm^6 sec^{-1}
2-body $Ar^+ \longrightarrow Cs^+$	C_6	$\sim 3 \times 10^{-12}$ cm^3 sec^{-1}
Metastable-metastable $Ar^m \longrightarrow Ar^+$	C_7	$\sim 5.6 \times 10^{-10}$ cm^3 sec^{-1}
Production Ar^x by fission fragments	S_1	$\lll S_2$ sec^{-1}
Production Ar^x by atomic recombination	C_8	$\lesssim 0.1$
Mean lifetime Ar^x	τ	$\sim 10^{-6}$ sec
2-body ion formation $Ar^x \longrightarrow Ar_2^+$	C_9	$\sim 5.6 \times 10^{-12}$ cm^3 sec^{-1}
Production Ar^m by fission fragments	S_2	1.87×10^{-3} sec^{-1}
Diffusion Ar^m in Ar	K_m	1.7×10^{18} cm^{-1} sec^{-1}
Production Ar^m by recombination of Ar^+	C_{10}	$\lesssim 0.1$
Production Ar^m by recombination of Ar_2^+	C_{11}	≈ 0.5
Metastable-metastable Ar^m destruction	C_{12}	$\sim 5.6 \times 10^{-10}$ cm^3 sec^{-1}
Destruction Ar^m via Ar	C_{13}	1.2×10^{-15} cm^3 sec^{-1}
Destruction Ar^m via Ar, Ar	C_{14}	8.7×10^{-33} cm^6 sec^{-1}
Penning ionization $Ar^m + Cs \longrightarrow Cs^+$	C_{15}	$\approx 4.6 \times 10^{-10}$ cm^3 sec^{-1}
Diffusion Ar_2^+ in Ar	$K_{2,a}$	2.7×10^{18} cm^{-1} sec^{-1}
2-body dissociative recombination of Ar_2^+	C_{16}	6.7×10^{-7} cm^3 sec^{-1}
2-body $Ar_2^+ \longrightarrow Cs^+$	C_{17}	$\sim 3 \times 10^{-12}$ cm^3 sec^{-1}
Diffusion Cs^+ in Ar	$K_{3,a}$	2.9×10^{18} cm^{-1} sec^{-1}
2-body radiative recombination Cs^+	C_{18}	3.5×10^{-12} cm^3 sec^{-1}
3-body Thomson recombination Cs^+	C_{19}	2.5×10^{-30} cm^6 sec^{-1}
3-body $Cs^+ + Cs + Ar \longrightarrow Cs_2^+$	C_{20}	4.8×10^{-31} cm^6 sec^{-1}
Diffusion Cs_2^+ in Ar	$K_{4,a}$	2.8×10^{18} cm^{-1} sec^{-1}
2-body dissociative recombination Cs_2^+	C_{21}	$\approx 2 \times 10^{-6}$ cm^3 sec^{-1}
Collisional-radiative recombination Cs^+	C_{22}	1.1×10^{-19} cm^6 sec^{-1}

TABLE III. Code calculations for ion generation rate (S) at midpoint of tube.

$$\phi = 1.0 \times 10^{13} \; cm^{-2} \; sec^{-1}$$
$$\rho = 240 \; torr$$
$$N_o = 8.5 \times 10^{18} \; cm^{-3}$$

Ionization Tube (d=0.3 cm)
$$S_{Total} \; (Ne^+ + Ar^+ \; in \; Ne\text{-}Ar) = 2.57 \times 10^{16} \; cm^{-3} \; sec^{-1}$$
$$S \; (Ar^+ \; in \; Ar) = 3.645 \times 10^{16} \; cm^{-3} \; sec^{-1}$$

Microwave Tube (d=0.5cm)
$$S_{Total} \; (Ne^+ + Ar^+ \; in \; Ne\text{-}Ar) = 2.258 \times 10^{16} \; cm^{-3} \; sec^{-1}$$

From these values the ion generation rate $S(Ar^+ \; in \; Ar)$ for the microwave tube was

$$S(Ar^+ in \; Ar) = S_o N_o = \frac{2.258}{2.57} \times 3.645 \times 10^{16} = 3.20 \times 10^{16} \; cm^{-3} \; sec^{-1}$$

and

$$S_o(Ar^+) = 3.20 \times 10^{16} / \; 8.5 \times 10^{18} = 3.74 \times 10^{-3} \; sec^{-1}$$

Following the calculations for the production of neon metastables in Ne-Ar,[2] the production rate of argon metastables by the fission fragments was taken as

$$S_2(Ar^m) = 0.5 \; S_o(Ar^+) = 1.87 \times 10^{-3} \; sec^{-1}.$$

PARAMETER STUDIES

One objective of this study was to compare the electron density generated by fission-fragment ionization in an argon-cesium gas mixture to that generated in a neon-argon mixture under comparable operating conditions. For the argon-cesium system, the operating conditions (See Table IV) were set equal to those for the previous kinetic study on the neon-argon system.[4]

TABLE IV. Operating conditions.

Neutron flux	$\phi = 1.0 \times 10^{13} \; cm^{-2} \; sec^{-1}$
Spacing	$d = 0.5 \; cm$
Characteristic diffusion length	$\Lambda = 0.1592 \; cm$
Gas filling	argon-cesium

The spacing corresponds to that of the microwave cavity used in earlier inpile experiments.[5] The optimum electrode spacing for a thermionic converter is not yet known but a value of 0.5 cm is reasonable for comparison of the Ar-Cs and Ne-Ar gas mixtures. For the detailed study of the influence of pressure and ratio of gas constituents for the Ar-Cs and Ne-Ar mixtures, the gas temperature was set to 1300°K. In the study of the influence of collisional-radiative recombination the gas temperature was varied.

Effect of Total Pressure and Partial Pressure of Gas Constituents

The effect of pressure and cesium-to-argon ratio (Cs/Ar) on the electron number density were obtained in one series of computations. The results of these calculations are shown in Figs. A-1 and A-2 of the Appendix where the electron number density (n_e,cm^{-3}) is plotted as a function of the atom number density (N_o,cm^{-3}) for various constant values of Cs/Ar from 0 to 10^{-2}. These data are also presented in a three-dimensional plot in Fig. 1 where the total gas pressure $p=N_o \times (3.22 \times 10^{16})^{-1}$ is substituted for N_o.

The electron number density is strongly dependent upon the collisional-radiative loss (see later section) of the atomic cesium ion, Cs$^+$, (via C_{22}) which in turn is dependent upon the electron temperature. For this study, the electron temperature was set equal to 1300°K ($C_{22}=1.0 \times 10^{-22}$) which was considered to be representative of the gas temperature in our thermionic diode.

The curves of n_e vs N_o at constant Cs/Ar exhibit a maximum in n_e similar to that found for the neon-argon system[3,4] (Fig.2). At low pressure (≤ 10 torr) the ion production rate is small and the Cs$^+$ ion diffuses out of the plasma. Both of these factors cause n_e to decrease with decreasing pressure. At high pressure (≥ 300 torr) the 3-body conversion (C_{20}) of Cs$^+$ to Cs$_2^+$ (which promptly loses its charge via recombination) becomes rapid and n_e decreases with increasing pressure.

The curves for various Cs/Ar ratios show a strong dependence of n_e on the Cs/Ar ratio. If the ratio Cs/Ar is too small ($\leq 10^{-6}$) the cesium atoms are not in sufficient abundance to produce cesium ions (Cs$^+$) from the argon metastable states (C_{15}). On the other hand, if the ratio Cs/Ar is too large, the Cs$^+$ ions are rapidly converted to Cs$_2^+$ via the 3-body conversion C_{20}. In the cross plot of n_e vs Cs/Ar at constant pressure in Fig. 3, a maximum in n_e occurs at the value of Cs/Ar where the production and loss of Cs$^+$ are optimum.

7

TABLE V.   Comparison of dominant reaction kinetics coefficients for Ne-Ar and Ar-Cs systems

Neutron flux	$\phi = 1.0 \times 10^{13}$ cm^{-2} sec^{-1}
Electrode spacing	$d = 0.5$ cm
Characteristic diffusion length	$\Lambda = 0.1592$ cm
Emitter temperature	$T_E = 1700°K$
Collector temperature	$T_C = 900°K$
Gas temperature	$T_G = 1300°K$

Process	Symbol	Dimension	Value Ne-Ar	Value Ar-Cs
Production of N_+ by fission fragments	S_o	sec^{-1}	1.93×10^{-3}	3.74×10^{-3}
Production of N_m by fission fragments	S_2	sec^{-1}	0.879×10^{-3}	1.87×10^{-3}
Penning ionization $N_m + A \longrightarrow A_+ + N_o$	C_{15}	cm^3 sec^{-1}	1.8×10^{-11}	4.6×10^{-10}
Diffusion of N_m	K_m	cm^{-1} sec^{-1}	5.5×10^{18}	1.7×10^{18}
N_+	K_1	cm^{-1} sec^{-1}	5.7×10^{18}	2.2×10^{18}
N_{2+}	K_2	cm^{-1} sec^{-1}	9.1×10^{18}	2.7×10^{18}
A_+	K_3	cm^{-1} sec^{-1}	1.0×10^{19}	2.9×10^{18}
A_{2+}	K_4	cm^{-1} sec^{-1}	9.5×10^{18}	2.8×10^{18}
3-body $N_+ + 2N_o \longrightarrow N_{2+} + N_o$	C_4	cm^6 sec^{-1}	5.8×10^{-32}	5.5×10^{-31}
3-body $A_+ + A_o + N_o \longrightarrow A_{2+} + N_o$	C_{20}	cm^6 sec^{-1}	2.5×10^{-31}	4.8×10^{-31}
Production of N_m by recombination of N_{2+}	C_{11}	—	0.5	0.5
2-body destruction of N_m via N_o	C_{13}	cm^3 sec^{-1}	1.84×10^{-15}	1.2×10^{-15}
3-body destruction of N_m via $2N_o$	C_{14}	cm^6 sec^{-1}	5.0×10^{-34}	8.7×10^{-33}
2-body dissociative recombination of N_{2+}	C_{16}	cm^3 sec^{-1}	2.2×10^{-7}	6.7×10^{-7}
2-body dissociative recombination of A_{2+}	C_{21}	cm^3 sec^{-1}	6.7×10^{-7}	2.0×10^{-6}
Collisional radiative recombination of N_+	C_3	cm^6 sec^{-1}	1.00×10^{-22}	1.00×10^{-22}
Collisional radiative recombination of A_+	C_{22}	cm^6 sec^{-1}	1.00×10^{-22}	1.00×10^{-22}

8
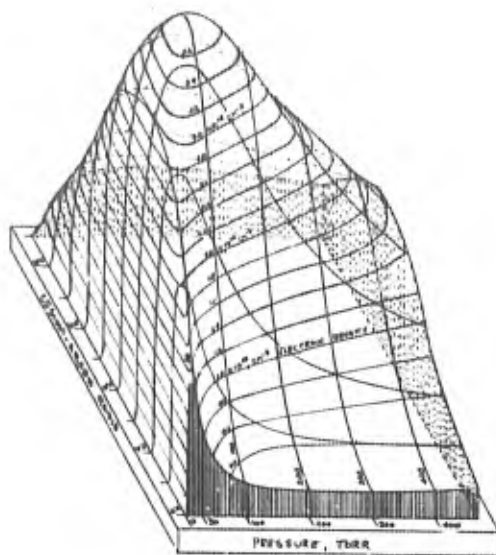
Fig. 1. Contour map showing the singular electron number density maximum in a fission-fragment-generated plasma of argon-cesium at the critical Cs/Ar ratio and total gas pressure.
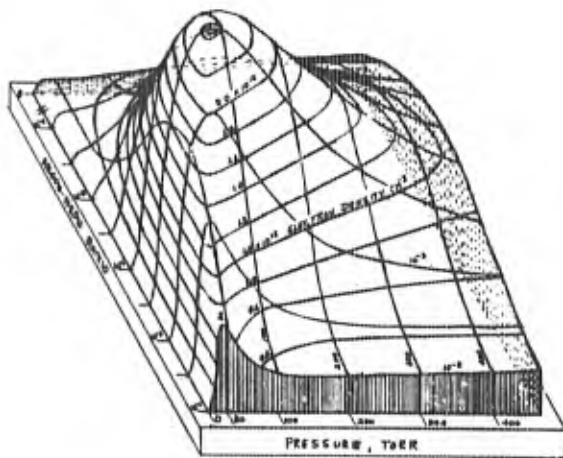
Fig. 2. Contour map showing the singular electron number density maximum in a fission-fragment-generated plasma of neon-argon at the critical Ar/Ne ratio and total gas pressure.

9
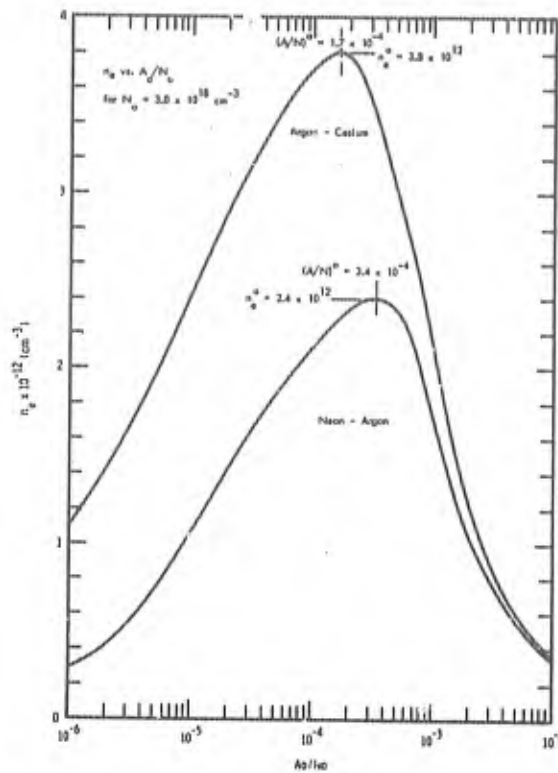
Fig. 3. Electron number density (n_e) as a function of the ratio of the gas constituents (A_o/N_o) for $N_o = 3.0 \times 10^{18} cm^{-3}$.

Comparison with Neon-Argon System. The previous computations on the neon-argon system[4] were extended to cover the same operating conditions and range of A_o/N_o as for argon-cesium. These results are shown in 2-dimensional plots in Figs. A-2 and A-3 in the Appendix and in a 3-dimensional plot in Fig. 2. The 3-dimensional contour maps (Figs. 1 and 2) are similar in shape but the electron number density for the argon-cesium system is about 1.5 greater than that of the neon-argon system. The increased electron density of Ar-Cs over Ne-Ar is a consequence of the higher ion-generation rate coefficients for the Ar-Cs system. The reaction rate coefficients for both systems are compared in Table V. The production rate of N_+ and N_m by fission fragments for Ar is about twice as great as that for Ne and the Penning ionization coefficient (C_{15}) is about 25 times larger. On the other hand, the 3-body conversion of the atomic to the molecular ion of the parent gas (C_4) is about 10 times greater for argon than for neon but this has little influence since the predominant ion is that of the minor gas species. The 3-body conversion of the atomic to the molecular ion of the neon gas species (C_{20}) is a factor of only 1.9 greater for Cs_+ than for Ar_+. The 3-body

10

destruction of $N_m(C_{14})$ for Ar_m is about 17 times that for Ne_m but is apparently overridden by the increased production rate terms.

Conditions for Maximum n_e - The electron density maxima for Ar-Cs and Ne-Ar in Figs. 1 and 2 both occur at $N_o \simeq 3.0 \times 10^{18} \text{cm}^{-3}$ but at somewhat different values of A_o/N_o. A cross-plot of n_e vs A_o/N_o is shown in Fig. 3 for both Ar-Cs and Ne-Ar at $N_o = 3.0 \times 10^{18} \text{cm}^{-3}$. The dimensions of the maximum electron density, n_e^o, are:

TABLE VI. Maximum n_e for Figure Nos. 1 and 2

	Neon-Argon	Argon-Cesium
$n_e^o = n_e^{max}$, cm^{-3}	2.4×10^{12}	3.8×10^{12}
$N_o^o = N_o$ at n_e^o, cm^{-3}	3.0×10^{18}	3.0×10^{18}
$(A_o/N_o)^o = A_o/N_o$ at n_e^o	3.4×10^{-4}	1.7×10^{-4}
n_e at N_o^o for pure N_o	0.17×10^{12}	0.13×10^{12}
Electron enhancement = $n_e^o/(n_e$ for pure $N_o^o)$	14	29

The enhancement of the electron density that results from the small addition of A_o was obtained by comparing n_e^o to the value of n_e for the pure gas, N_o at N_o^o. The addition of argon to neon increased the electron density by a factor of 14 and the addition of cesium to argon increased the electron density by a factor of 29.

Effect of Collisional-Radiative Recombination (C_{22}) and Electron Temperature

The importance of the volume recombination loss involving 3-body collisions of an atomic ion and two electrons has been discussed elsewhere.[6] In a study of the influence of this reaction on the electron density in neon-argon using the reaction kinetics code,[4] the collisional-radiative recombination loss (C_{22}) was found to greatly influence the electron density, particularly as a function of the electron temperature. The curves for $Ar/Ne = 1.0 \times 10^{-4}$ are reproduced in Fig. 4. A similar study was made for the argon-cesium system and the results are shown in Fig. 5. The influence of the collisional-radiative loss is even more striking for the case of Ar-Cs. Comparing the ratio of the maximum n_e (in the curve n_e vs N_o) at $Te = 1300°K$ to that for $C_{22} = 0$ $(T_e \longrightarrow \infty)$, i.e. $n_e^{max}(T_e = 1300°K)/n_e^{max}(C_{22} = 0)$, this ratio was about 1/2 for the Ne-Ar system while it is about 1/4 for the Ar-Cs system.

11
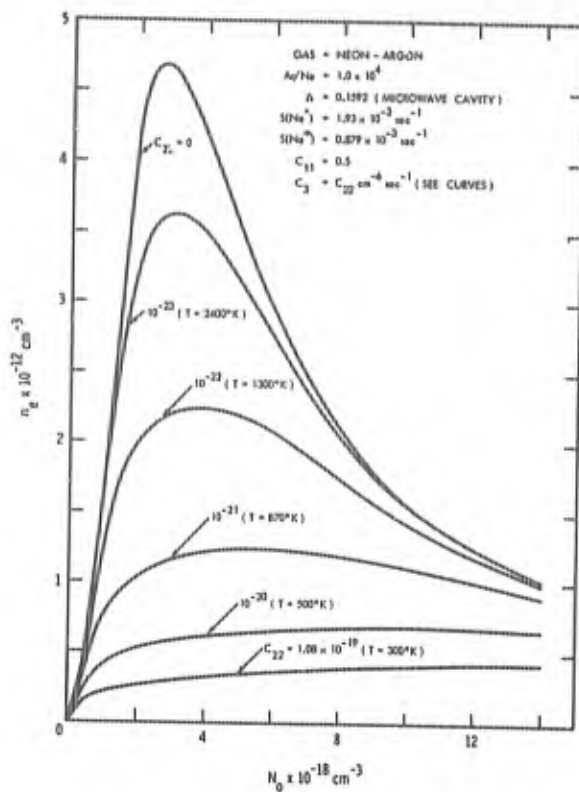
Fig. 4. Effect of collisional-radiative recombination $(C_{22}A^+n_e^2)$ on electron number density at $\Phi=1.0 \times 10^{13}$ neutrons $cm^{-3}sec^{-1}$.
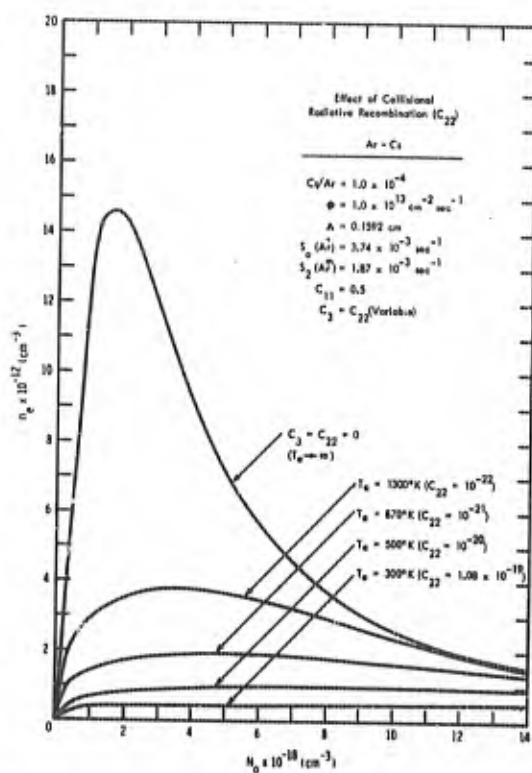
Fig. 5. Effect of collisional-radiative recombination (C_3, C_{22}) on electron number density.

12

In the proposed inpile microwave experiment on Ar-Cs, the influence of gas temperature on electron density will be investigated by varying the temperature of the resonant cavity with a flow of cool gas against the outside walls of the cavity. The Cs/Ar ratio will be varied by a seperate gas coolant flow against the cesium reservoir.

Effect of Penning Ionization Coefficient (C_{15})

One of the argon-cesium reactions about which little is known is the ionization of cesium by argon metastables (C_{15})

$$Ar^m + Cs \longrightarrow Cs^+ + Ar \tag{8}$$

Measurements of the Townsend α coefficient in argon-cesium have been made by Nolan[8] and from these data an estimate of the cross section for reaction (8) was obtained. These measurements did not distinguish between the ion species produced nor the specific reaction that produced them, nevertheless, using information on the other possible reactions, the cross section for reaction (8) was estimated to be $q_i = 1 \times 10^{-14} cm^{-2}$.

The accuracy of this cross section was estimated to be within an order of magnitude so it was important to investigate the influence of this cross section on the reaction kinetics. The product of q_i and the average velocity $\bar{V}(Ar^m,Cs)$ gives the reaction coefficient C_{15}.

$$C_{15} = 1 \times 10^{-14} \ cm^{-2} \times 4.6 \times 10^4 \ cm/sec = 4.6 \times 10^{-10} \ cm^3 \ sec^{-1}. \tag{9}$$

To find the influence of this rate on n_e a code run was made with 1/3 the value of C_{15} computed in (9), i.e. $C_{15} = 1.53 \times 10^{-10} cm^3 sec^{-1}$. The effect on n_e is shown in Fig. 6 where the curves of n_e vs N_o are plotted for both values of C_{15}. The factor of 3 change in C_{15} changes n_e as much as a factor of about 2 so it will be important to establish this reaction rate more precisely if the information becomes available.

Effect of Ion Diffusion

The ion loss to the emitter electrode depends upon the sheath potential. If the emitter sheath is electron rich (as we expect), the ion flow from the plasma to the emitter will be retarded. In this case the diffusion loss as computed in the above kinetics studies ($-D_i A_{i+}/\Lambda^2$) would be too high and the electron density too low. To evaluate the influence of the ion diffusion loss on n_e, a series of computations were made in which the total ion diffusion

13
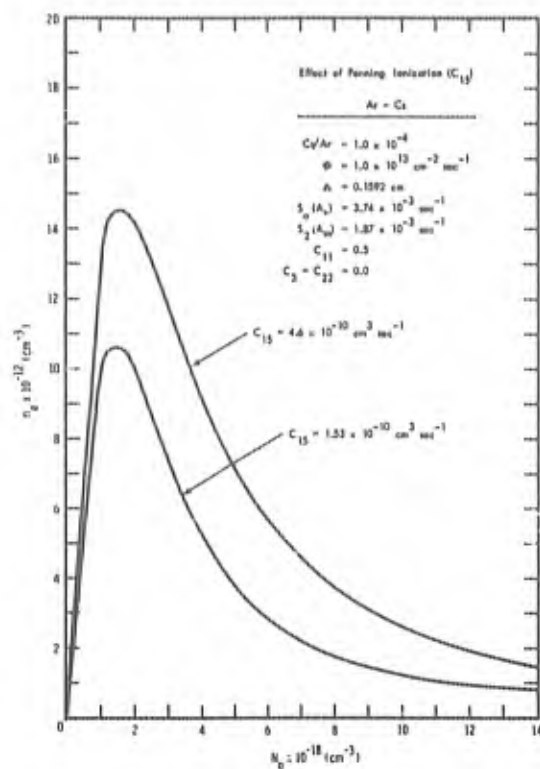
Fig. 6. Effect of Penning ionization coefficient (C_{15}) on the electron number density in Ar-Cs.
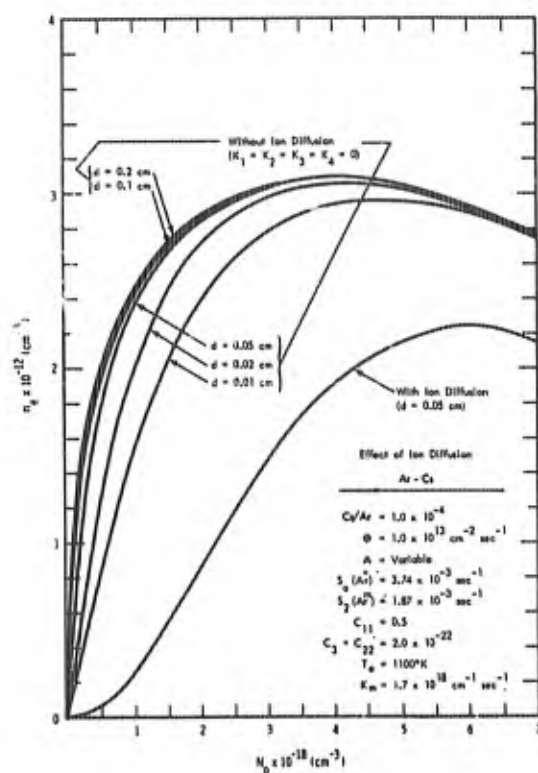
Fig. 7. Effect of ion diffusion and electrode spacing (with no ion diffusion) on electron number density.

14

loss was set to zero $(D_i = 0)$. Only the diffusion of the metastables $(-D_m N_m / \Lambda^2)$ remained unchanged and the influence of the metastable diffusion was found by varying the electrode spacing d $(\Lambda = d/2\pi)$. The results of this study are shown graphically in Fig. 7.

As seen from Fig. 7 the reduction of ion loss to the electrodes can significantly increase the electron density. At pressures around 30 torr $(N_o \simeq 1 \times 10^{18} \, cm^{-3})$, n_e is increased about an order of magnitude while at pressures around 150 torr $(N_o \simeq 5 \times 10^{18} \, cm^{-3})$, n_e is increased about 50%.

The influence of the electrode spacing on n_e is small except for the very small spacings $(d < 0.01 \, cm)$.

The influence of fission-fragment ion generation rate on n_e is also evident in Fig. 7. At low pressures $(N_o < 1 \times 10^{18} \, cm^{-3})$ the ion generation rate is proportional to N_o and this is evident for the curves with no ion diffusion loss where n_e rapidly approaches zero as N_o approaches zero. Ion diffusion loss shifts the maximum in the curve of n_e vs N_o to higher values of N_o.

REFERENCES

1. C. B. Leffert, D. B. Rees and F. E. Jamerson, ONR Annual Report No. 5, Contract Nonr-3109(00), (Oct.1964). Section B of this report is a collection of notes of D. J. Rose titled, "Reaction Kinetics of the Fission Fragment Plasma".

2. D. B. Rees, "Production, Diffusion and Conversion Rates of Ions, Metastable and Excited States in Penning-Type Neon-Argon Plasmas", ONR Annual Report No. 5, Section D, loc. cit.

3. C. B. Leffert, "Computer Solutions to the Reaction Kinetics Equations", ONR Annual Report No. 5, Section C, loc. cit.

4. C. B. Leffert, "Code Study of the Effect of Collisional-Radiative Recombination on the Electron Density in Neon-Argon", General Motors internal report.

5. See Section C of this report.

6. See Section A of this report.

7. C. B. Leffert, "Ion Generation Rate Theory and Analysis of Experimental Current-Voltage Data", ONR Annual Report No. 5, Section A, loc. cit.

8. J. Nolan, Westinghouse Corporation, private communication (7/18/64).

APPENDIX A
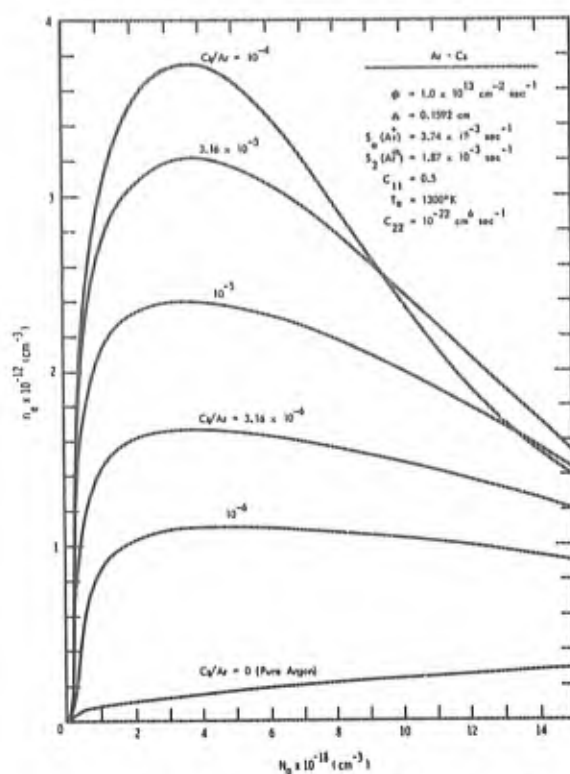
Fig. A-1. Electron number density (n_e) as a function of the argon density (N_O) and the ratio of the gas constituents (Cs/Ar) for Cs/Ar = 0 to 10^{-4}.
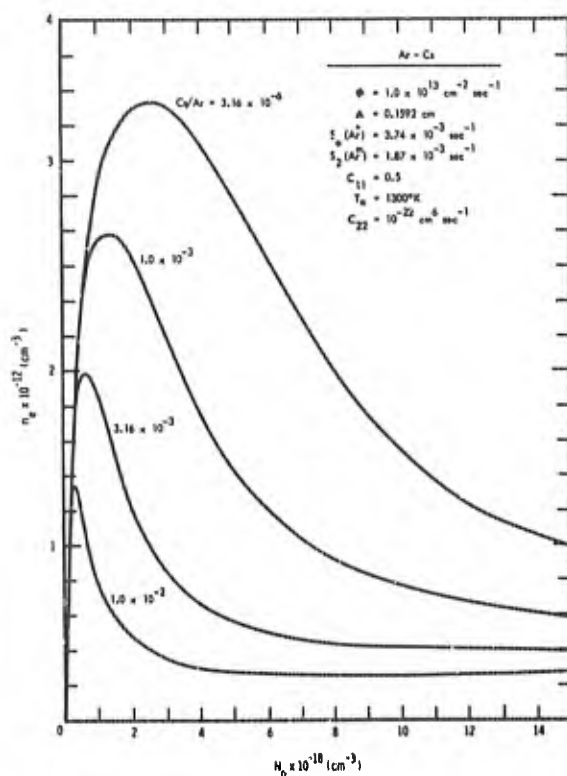
Fig. A-2. Electron number density (n_e) as a function of the argon density (N_O) and the ratio of the gas constituents (Cs/Ar) for Cs/Ar = 3.16 x 10^{-4} to 10^{-2}.

17
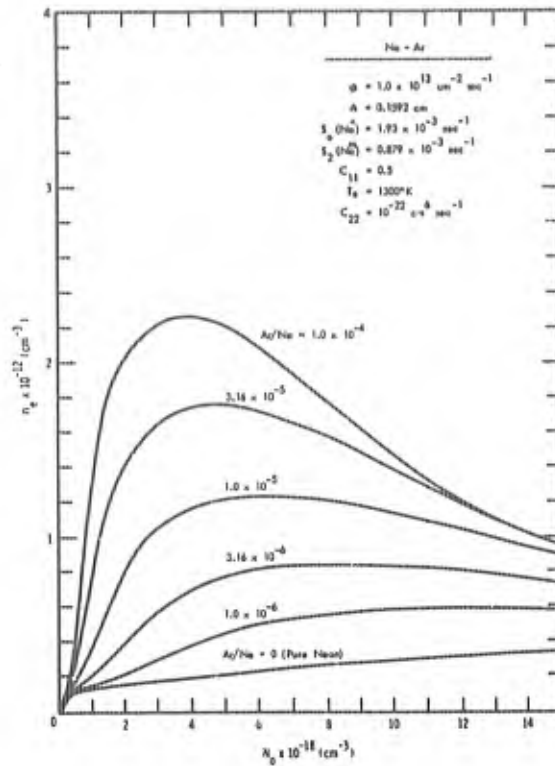
Fig. A-3. Electron number density (n_e) as a function of the neon density (N_O) and the ratio of the gas constituents (Ar/Ne) for $Ar/Ne = 0$ to 10^{-4}.
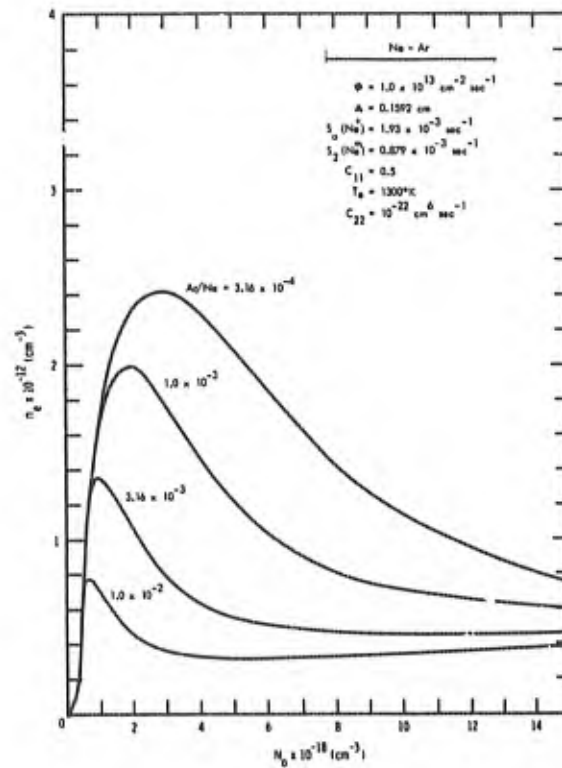
Fig. A-4. Electron number density (n_e) as a function of the neon density (N_O) and the ratio of the gas constituents (Ar/Ne) for $Ar/Ne = 3.16 \times 10^{-4}$ to 10^{-2}.

18

SECTION C

THEORY AND EXPERIMENTAL RESULTS FOR FIRST INPILE MICROWAVE MEASUREMENT OF ELECTRON DENSITY

ABSTRACT

The electron number density in a fission-fragment-generated plasma has been measured inpile with microwave techniques. The results of the first inpile run with microwaves are summarized. The fit between the measured electron density and that predicted from the reaction kinetics theory was good. The elements of microwave theory which pertain to the measurement of the electron density in a resonant cavity are reviewed. The design and development of a resonant microwave cavity with a fission fragment source are described.

CONTENTS

OBJECT

The objectives of this study were to (1) measure the electron density in a fission-fragment-generated plasma using a resonant microwave cavity and (2) compare the measured electron density to that predicted by our reaction kinetics theory.

CONCLUSIONS

1. It has been demonstrated that the electron number density in plasmas generated by fission-fragment ionization of a noble-gas mixture can be measured by the microwave frequency-shift method.
2. The stringent design requirements imposed by both the nuclear and microwave environments resulted in a resonant cavity with a relatively low microwave quality factor $(Q \sim 1500)$.
3. The limited frequency sweep of the microwave generator plus the low Q for the cavity used in the first inpile run necessitated the use of a dynamic method to measure the frequency shift.
4. A frequency shift of 1 Gc was observed for a neon-argon mixture at a pressure of 140 torr and operated in a neutron flux of $4 \times 10^{12} \text{cm}^{-2} \text{sec}^{-1}$. The electron number density calculated for a 1 Gc frequency shift agreed well with that computed from the reaction-kinetics analysis. Nevertheless verification of the reaction-kinetics theory is still considered tentative.

I. INTRODUCTION

The output power of a thermionic energy converter is strongly dependent on the electron number density of the interelectrode plasma. Our studies on fission-fragment-generated plasmas to date have been directed towards establishing how the electron number density depends upon such variables as the composition and pressure of the gas, the neutron flux and dimensions of the tube. The manner in which the electron number density varies with these parameters has been calculated in recent studies for both the neon-argon and argon-cesium gas mixtures.[1,2,3,4]

1

The reaction kinetics study[1,2] requires knowledge of 23 reaction coefficients. Though not all are important for the calculation of the electron density, some are not well established and an experimental verification of the calculation was sought.

Microwave methods have been developed for obtaining information on electron density, conductivity and collision-frequency for a cavity filled with a plasma.[5] These methods can be applied to a cavity filled with a fission-fragment-generated plasma and the analysis is somewhat simplified since such a plasma is of relatively uniform density.

This report summarizes the microwave theory applicable to measurement of the resonant frequency of a cavity, describes the apparatus assembled for inpile measurements and finally presents the results of the first inpile run on a neon-argon plasma.

II. MICROWAVE THEORY

High-frequency electromagnetic waves interact strongly with ionized gases and thus provide a powerful tool for measuring plasma properties. The microwave techniques developed to measure plasma properties such as electron particle density and temperature have been reported in detail by a number of authors.[5,6] The literature is quite extensive so in this section only those formulas will be reproduced which are pertinent to the design of the microwave components and to the analysis of the data. The basic elements of microwave theory that lead to the derivation of these formulas are reviewed in another report.[11]

Effect of Plasma on Cavity Resonance

The change in the resonance properties of a microwave cavity with the introduction of a plasma are given by[9]

$$\left(\frac{1}{Q_1} - \frac{1}{Q_0}\right) - 2j\frac{\Delta\omega}{\omega_o} = \frac{1}{\epsilon_o\omega_o}\frac{\int_V \sigma(r)\ E^2(r)\ dV}{\int_V E^2(r)\ dV}, \ (\Delta\omega << \omega_o). \qquad (1)$$

ω is the resonant angular frequency of the cavity with plasma inside; ω_o is the resonant frequency of the cavity in the absence of the plasma and $\Delta\omega = \omega - \omega_o$ is the change in the resonant angular frequency due to the perturbation by the plasma. Q_0 and Q_1 are the "unperturbed" and "plasma" values,

2

respectively, of the cavity characteristic, Q, which is defined by

$$Q = \frac{\omega_o \text{ (energy stored)}}{\text{average power loss}} = \frac{2\pi \text{ (energy stored)}}{\text{energy loss per cycle}} \quad (2)$$

In Eq.(1), E is the electric field in the cavity, σ is the complex conductivity of the plasma, ϵ_o is the permittivity of free space and $j = \sqrt{-1}$. For the noble gas plasmas of interest in these studies the complex conductivity is related to the electron number density (n) by

$$\sigma = \sigma_r + j\,\sigma_i = \frac{ne^2}{m\,(\nu + j\omega)} = \frac{\omega_p^2 \,\epsilon_o}{\omega} \left(\frac{\nu/\omega - j}{1 + \nu^2/\omega^2} \right) \quad (3)$$

where e and m are the charge and mass of the electron and ν is the collision frequency between electrons and neutral atoms and is assumed independent of the electron velocity. The last relation in Eq.(3) is obtained by substituting for n the angular plasma frequency, ω_p, where

$$\omega_p = \left(\frac{ne^2}{\epsilon_o m} \right)^{1/2} \quad (4)$$

or numerically $f_p = \omega_p/2\pi \text{(cps)} = 8979 \left[n(cm^{-3}) \right]^{1/2}$.

The change in the cavity Q and the change in resonant angular frequency in Eq.(1) can be separately expressed after substituting Eq.(3) for the complex conductivity. The imaginary parts of the right and left hand sides are then equated to give the change in resonant angular frequency

$$\frac{\Delta\omega}{\omega_o} = \frac{1}{2} \left[\frac{1}{1 + (\nu/\omega)^2} \right] \frac{\int_V \left(\frac{\omega_p}{\omega} \right)^2 E_o^2 \, dV}{\int_V E_o^2 \, dV} \quad (5)$$

and the real parts of the right and left hand sides are equated to give the change in the cavity Q

$$\frac{1}{Q_1} - \frac{1}{Q_2} = \Delta\left(\frac{1}{Q}\right) \simeq \left[\frac{\nu/\omega}{1 + (\nu/\omega)^2} \right] \frac{\int_V \left(\frac{\omega_p}{\omega} \right)^2 E_o^2 \, dV}{\int_V E_o^2 \, dV} \quad (6)$$

3

From Eqs. (5) and (6) it also follows that

$$\frac{1}{Q_1} - \frac{1}{Q_2} = 2\left(\frac{\nu}{\omega}\right)\left(\frac{\Delta\omega}{\omega_o}\right). \tag{7}$$

The electron number density is related to the shift in the resonant angular
frequency of the cavity by Eq.(5) and the collision frequency (ν) is related
by Eq.(7) to the change in the cavity Q and the shift in resonant frequency
$(\Delta\omega)$. The intrinsic or unloaded Q, Q_U, is not measurable, however, since the
cavity must be coupled to the transmission line through some kind of impedance.
A quantity known as the loaded Q, Q_L, can be obtained from measurements of the
voltage standing wave ratio (VSWR) in the transmission line and Q_U is then
calculated from Q_L. (5)
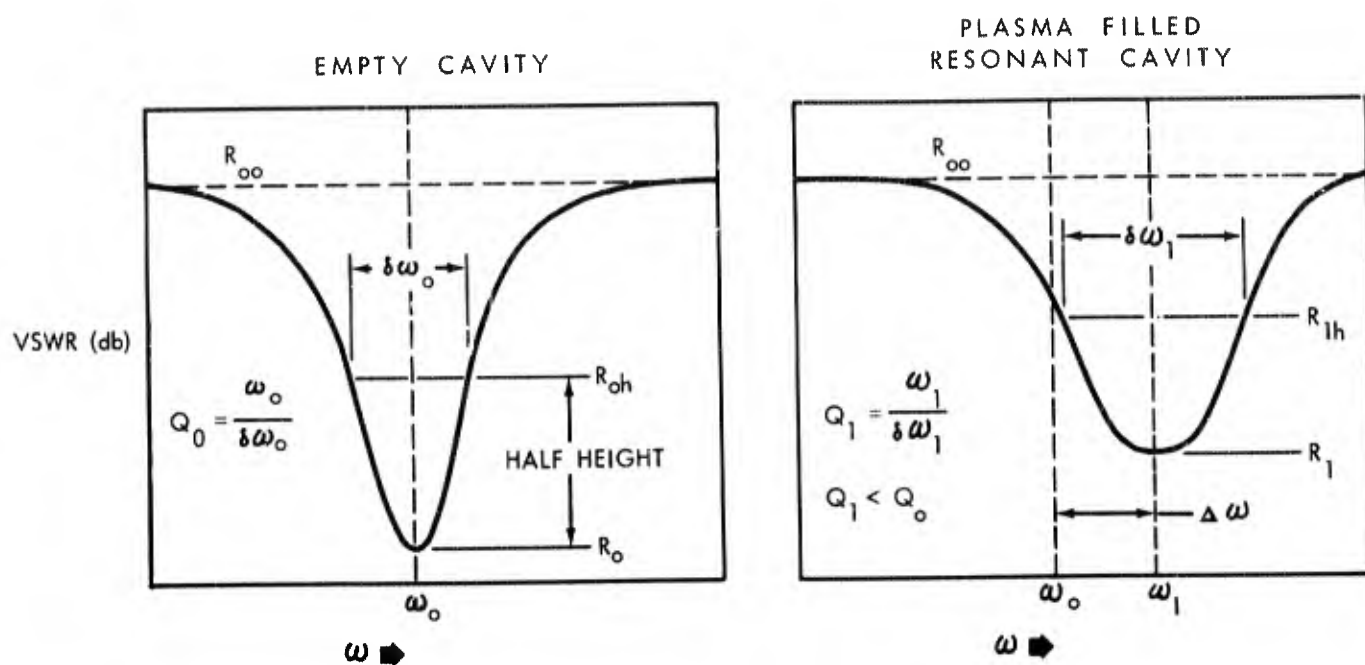
Fig. 1.   Effect of plasma on cavity resonance.

4

Selection of Microwave Probing Frequency

Using Eq.(4) and assuming the electron number density to be uniform over the volume of the cavity, the integrals cancel in Eq.(5) and since $f = \omega/2\pi$, we get

$$\Delta f \, f_o = \frac{4.03 \times 10^7 \, n}{1 + (\nu/\omega)^2} \simeq 4 \times 10^7 \, n. \tag{8}$$

We can now use Eq.(8) to find the proper microwave frequency for probing the resonant cavity. We select $\Delta f \sim 1$ Gc as a shift in frequency that can be readily measured and $n \sim 5 \times 10^{11} \, cm^{-3}$ as typical of the plasmas to be generated in the research reactor. Substitution in (8) yields $f \sim 20$ Gc (which falls in the K-band). The collision frequency is $\nu = 6 \times 10^9 sec^{-1}$ for 140 torr neon so $(\nu/\omega) = (\nu/2\pi f_o) = 0.04$ and the factor $\left[1 + (\nu/\omega)^2\right]^{-1}$ can be neglected in (8).

We had available a Model 150 K-band microwave generator manufactured by Strand Labs., Inc. with a frequency range of 23-25 Gc. This instrument has a narrow frequency sweep (100 Mc) over a klystron mode and the output is not constant but sinusoidal over the sweep. Also the output signal cannot be modulated, which is necessary to drive meters which display the VSWR directly. Therefore the initial inpile experiment was limited to a frequency-shift measurement since the circuit was not appropriate for a point-by-point measurement of VSWR.

The type of signals expected from this instrument are depicted in Fig.2(b) along with signals which would be obtained if the input were constant with frequency (as from a backward-wave oscillator).

Sweep frequency oscillator   Klystron-mode oscillator
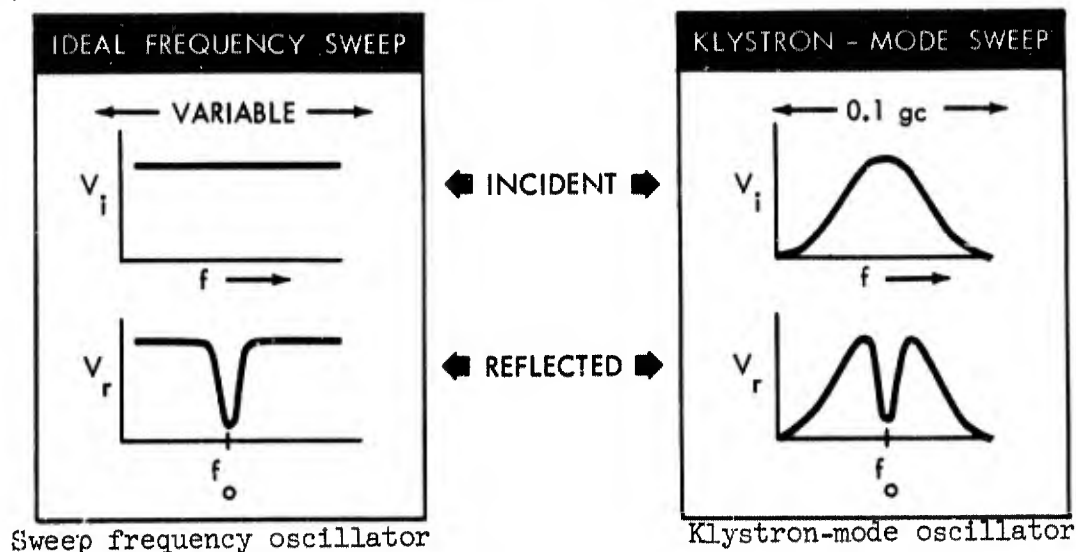
Fig. 2. Incident and reflected signals from a resonant cavity (see Fig. 7 for the circuit).

5

Dimensions of Cavity

The wavelength of the resonance frequency for TM (labeled, T_{MNS}) modes for a right circular cylinder is[6]

$$\lambda_o = \frac{2h}{\left[s^2 + (h/a)^2 (P_{mn}/\pi)^2\right]^{1/2}} \tag{9}$$

where h is the height, a the radius, s is the integral number of modes along h, P_{mn} is the rth root of $J_m(P)=0$, m is the number of circumferential maxima, and n is the number of radial maxima.

To obtain the 1 Gc frequency shift from the klystron generator, f_o was set to 23.2 Gc ($\lambda_o = c/f_o = 1.293$cm) near the lower end of the frequency range. A cavity of inside diameter about 1 inch was desirable so in Eq.(9) we chose the TM_{020} mode and obtained for the diameter, $D=2a=2.272$cm=0.8945 in. For this mode the resonant frequency is independent of the height h, so we chose h=0.5cm, as near the height of the ionization tube (0.3cm) as the dimensions of the wave guide would permit.

The orientation of the field lines for this mode are shown in Fig. 3.

↑ = $\vec{E}$
−− = $\vec{H}$
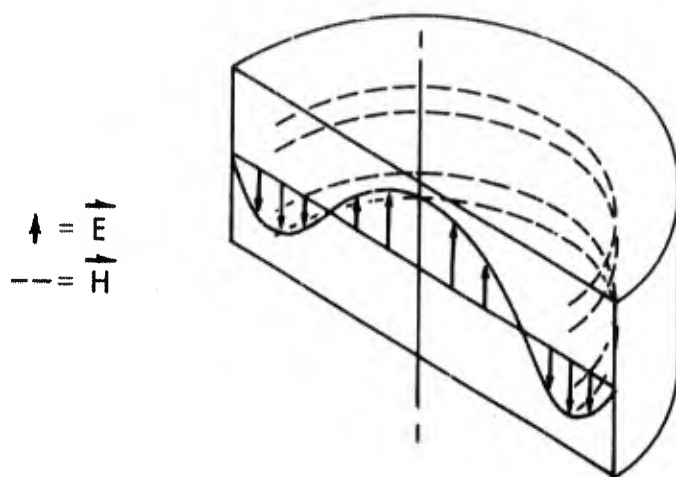
Fig. 3. Orientation of field lines in the TM_{020} mode of a right circular sylinder.

Electron Number Density from Resonant Frequency Shift

Equation (8) can now be solved to find the electron number density from the shift in the resonant frequency of this particular cavity. Substituting f_o=23.2 Gc in (8) gives

$$n = 5.75 \times 10^2 \, \Delta f. \tag{10}$$

6

Change in the Cavity Q and Measurement of Collision Frequency

For this estimate of the magnitude of the Q of the cavity, we ignore the series losses in the coupling circuit between the cavity and the transmission line and use Eq.(7) to estimate $\Delta\left(\frac{1}{Q_U}\right) \approx \left(\frac{1}{Q_1} - \frac{1}{Q_0}\right)$. For this cavity ($\omega_0 = 2\pi f_0 = 146 \times 10^9 \text{sec}^{-1}$) and for 140 torr neon ($\nu/\omega \sim 0.84$) we estimate $\Delta(1/Q) = 3.6 \times 10^{-3}$ from Eq.(7) for a frequency shift of $\Delta f = 1$ Gc. The measured unperturbed Q_0 for the inpile cavity was 1500 so that for the cavity with the plasma $Q_1 = 230$ from Eq.(7) which is very low and makes the cavity resonance difficult (but possible) to find on the signal output. Nevertheless, it should be possible to measure both Q_1 and Q_0 as well as $\Delta\omega$. From the computed values of Q_U[5] the collision frequency, ν, can be calculated for the plasma using Eq.(7). This was not contemplated for the first run since a determination of $\Delta\omega$ was considered all that could be obtained with the klystron mode oscillator.

III. DESIGN OF CAVITY AND CIRCUIT

Having fixed the diameter and height of the resonant cavity it was necessary to design a vacuum-tight tube that could be operated at elevated temperatures (up to 500°C) and in a nuclear environment. One objective of the inpile experiment was to measure the electron density in the plasma as a function of the plasma temperature in order to check the dependence of the collisional radiative loss process.[2] The fissioning uranium serves as a heat source so it was decided to obtain the plasma temperature variation by suspending the cavity in a gas environment and regulating the heat loss rate. A U-235 foil bonded to one end of the cavity, similar to the ionization tube design,[1] was chosen as the source of the fission fragments. The losses of the cavity depend on the conductivity of the inside walls of the cavity so it was evident that the uranium would certainly lower the Q from that of our all copper-plated cavity. Electroplating of the uranium surface, with Cu, for example, was not desirable since it would seriously reduce the flux of fission fragments.

Design and Construction of the Cavity: The mechanical design of this cavity is shown in Fig. 4.
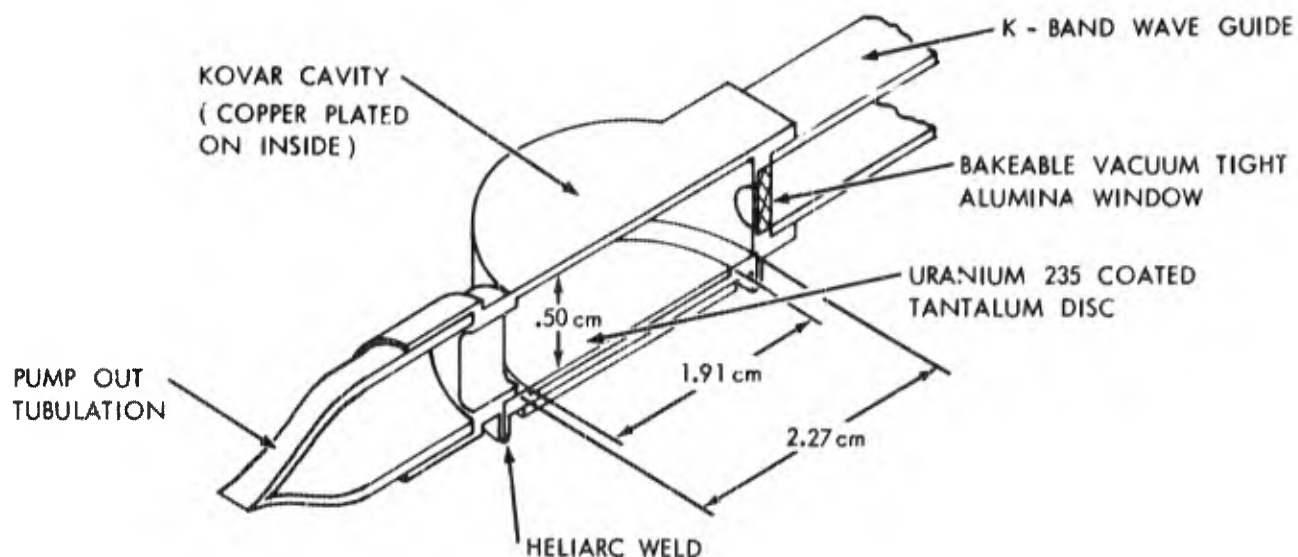
Fig. 4. Microwave cavity for inpile studies.

The body of the cavity was made of Kovar. The window was made of high-density alumina and after coating with molybdenum-manganese it was brazed to the Kovar with copper. A short section (2-1/4 in.) of stainless steel wave guide was brazed to the Kovar at the same time the ceramic window was brazed in place. The inside of the cavity (less the Kovar cap) was electroplated with copper (∼ 0.004 in.) after which glass-Kovar-copper pump-out tubulation was attached.

Two tantalum discs (0.010 in.) were brazed to the Kovar cap with copper and the U-235 foil was bonded to the top tantalum disc with nickel.[1]

Photographs of the cavity before and after insertion of the uranium cap are shown in Figs. 5 and 6, respectively. The ceramic window can be seen in Fig. 5. A special electrode was made to spot weld this cap assembly to the Kovar cavity at the seating surface. The lips of the Kovar cap and cavity were then heliarc-welded to complete the tube. To obtain a reasonably high Q, good electrical contact is needed at the seating surface between the cap and cavity and it was found that the spot welding step was necessary to prevent the cap from lifting off this seating surface during the heliarc weld.

8

Fig. 5. Microwave cavity before insertion of uranium cap. Note ceramic window to K-band wave guide.
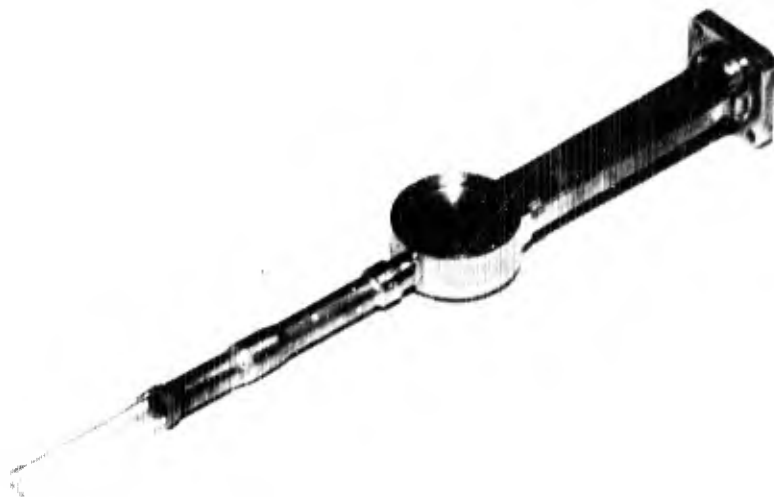
Fig. 6. Microwave cavity ready for heliarc welding.

9

The coupling between the wave guide and the cavity depends critically on the dimensions of the iris or hole in the cavity wall. It is known that the addition of a plasma to a resonant cavity tends to undercouple the cavity to the wave guide so it is helpful to overcouple the cavity by making the hole somewhat oversize. It was found by varying the hole size in experimental cavities that the hole diameter should be about 1/8 in. This dimension is nearly the   height of the wave guide (see Table II).

Considerable trouble was experienced in obtaining a leak-tight bond between the ceramic window and the Kovar cavity. In the first design the ceramic was in the shape of a flat plate(0.170 in.x 0.420 in.x 0.035 in.) which was brazed in a rectangular recess on the cavity. The microwaves were coupled through a hole (0.100 in. to 0.125 in. diam.) in the Kovar wall. This design could not be made completely leak tight so in the second design the ceramic was made circular (~ 0.100 in. diam.x 0.060 in. thick) and brazed in a circular recess in the cavity wall. This design could be made tight initially but leaks developed after subsequent heating because of the different expansion rates of Kovar and the ceramic. In the third design (see Fig. 7) the circular ceramic button was brazed with copper to a thin-walled Kovar tube connected to a flat Kovar plate and this assembly was brazed (80 Au-20 Cu) to the Kovar cavity. The thin wall Kovar was able to yield slightly with heating and thus maintain the bond with the ceramic.
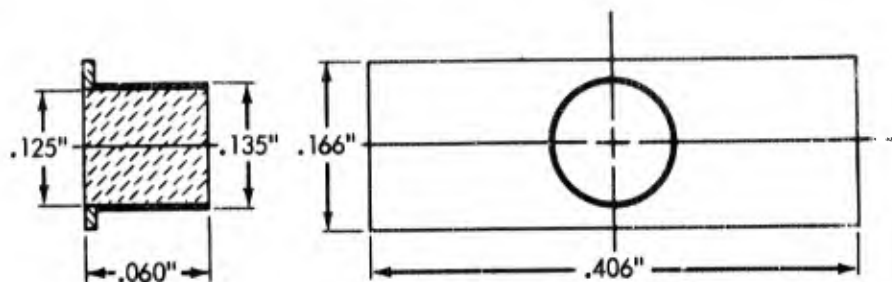
Fig. 7 . Ceramic window assembly of third design.

After heliarc welding the cap to the body a 38-1/2 in. length of copper wave guide was silver-soldered to the stainless steel wave guide (see Fig. 8) and the cavity plus wave guide were connected to the glass vacuum station for processing. A separate mechanical pump kept the wave guide evacuated during processing.

After the cavity was backfilled with gas (neon-argon at 140 torr and Ar/Ne of 10^{-4}) and the copper tubulation pinched off, the cavity was tested preliminary to mounting for the inpile experiment.

10

Microwave Test Circuit: The circuit for the measurement of the cavity
resonant frequenty is shown in Fig. 8. The microwave components in Fig. 8
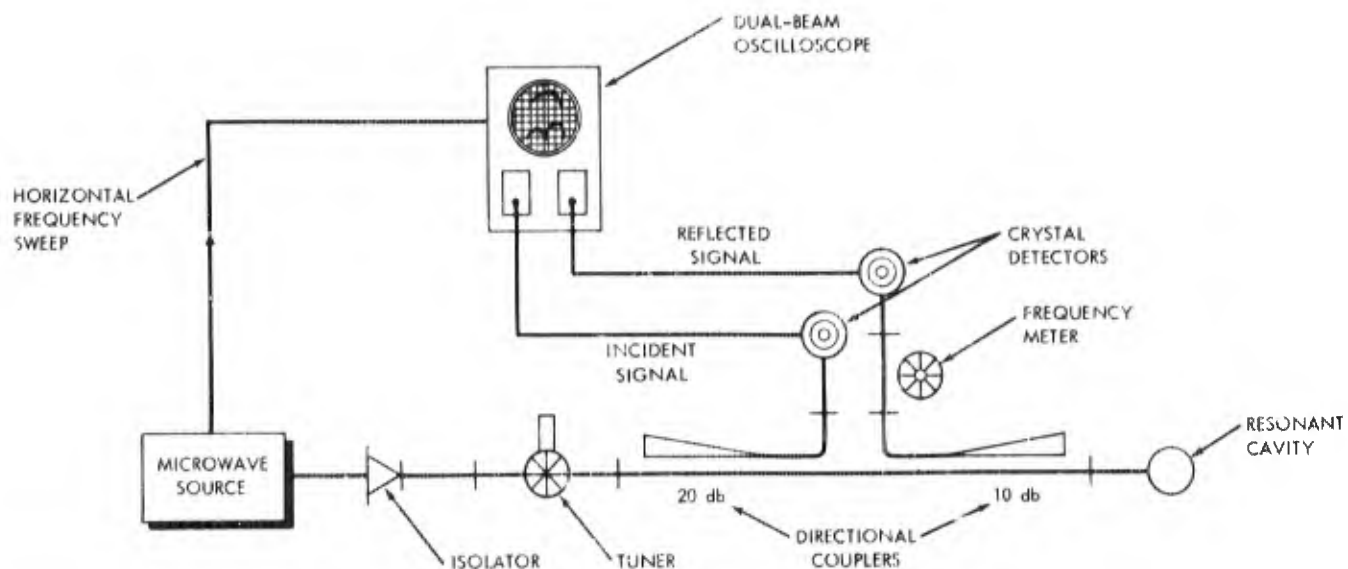
Fig. 8. Microwave circuit for measurement of cavity
resonant frequency.

were on hand for K-band and the circuit was set up and successfully tested.
For the inpile experiment, however, the cavity must be placed in the core
which is about 20 ft below the water level. When an additional 20 ft of wave
guide was placed between the 10 db coupler and the cavity in the circuit of
Fig. 8, the cavity resonance could not be found in the many reflections intro-
duced by the additional wave guide. The problem was solved by moving the 10 db
coupler down to the cavity and then returning the reflected signal back through
a separate 20 ft length of wave guide. The wave guide was evacuated to elim-
inate any influence on the microwave signal of gamma ionization of gas.
The directional coupler was made vacuum tight with epoxy cement.

Microwave Circuit and Support Structure for Inpile Experiment:
To vary the cavity temperature it was decided to suspend the cavity in the 4 ft
long aluminum containment can as shown in Fig. 8. With the cavity mounted in
this fashion and the 4 ft tube filled with gas, the temperature could be varied
by varying the gas pressure in a static system*or the gas could be circulated
at a varying flow rate. In the latter case the gas could be directed against
the uranium cap.

* In the first reactor run reported here the 1/4 in. aluminum gas cooling tube
was not attached and the static cooling method was used.

11

Chromel-alumel thermocouple wires were attached to each end of the cavity and these were returned to the surface of the pool through 1/4 in. Polyflo tubing.
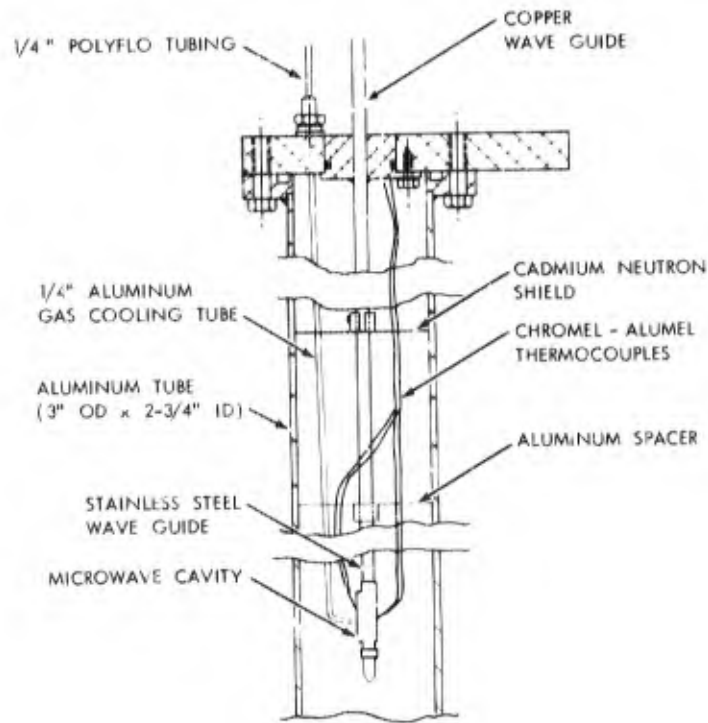
Fig. 9. Microwave resonant cavity mounted in the 4 ft aluminum secondary containment can (see footnote p. 18).

Except for the first day of the week, the University of Michigan reactor operates at full power of 2 mW. In order to be able to vary the neutron flux at full power, it was decided to mount the entire microwave circuit including the microwave generator on one support structure which was attached to a screw jack and then move the assembly vertically to obtain the desired flux.

This assembly is sketched in Fig. 10.

GENERATOR

CRYSTAL DETECTOR
WAVE METER
PHASE SHIFTER
DIRECTIONAL COUPLER (20 db)
VACUUM WINDOW
TUNER

90° TWIST
ISOLATOR

PUMP - OUT CONNECTOR
VACUUM WINDOW

CRYSTAL DETECTOR
SCREW JACK
THERMOCOUPLE WIRES
1/4" POLYFLO TUBING

ALUMINUM SUPPORT TUBE
(2" OD x 20' LONG)

DIRECTIONAL COUPLER (10 db)

RESONANT CAVITY
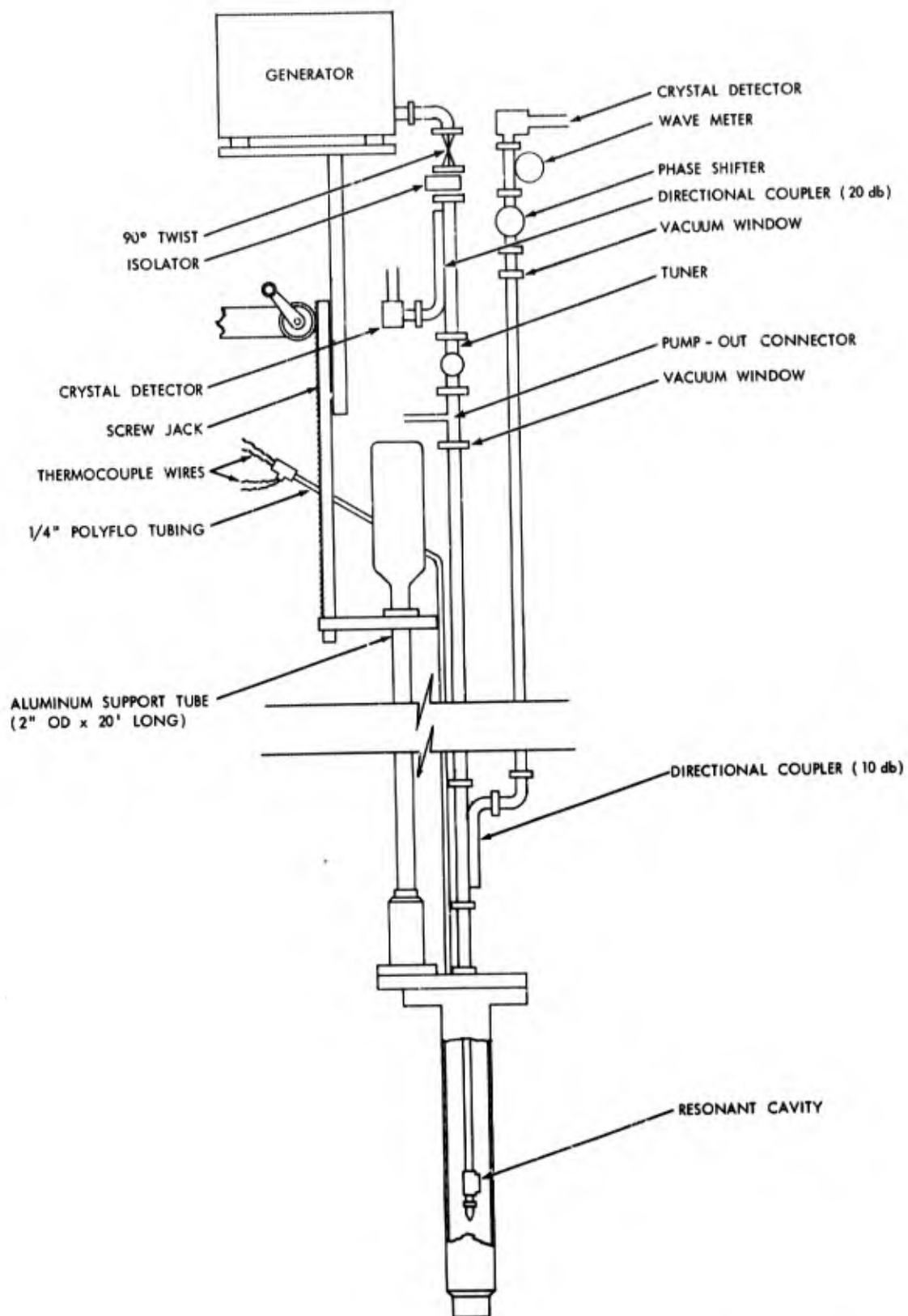
Fig. 10. Microwave circuit and support structure for inpile
experiments at University of Michigan.

13

IV. EXPERIMENTAL RESULTS

After the heliarc weld of the first cavity containing uranium (Cavity 9), it was found that a very small leak had developed from the cavity to the wave guide past the ceramic window (1st design). This leak was repaired with an epoxy cement (GE-SR82) and it was decided to proceed with the construction and testing of this cavity provided it survived the bakeout in the processing step. The seal was good and the cavity was backfilled to 140 torr pressure of a neon-argon mixture with $Ar/Ne=10^{-4}$. The mass spectrometer analysis of this gas showed 109 ppm argon with the balance neon; no other impurities were detectable.

The entire assembly shown in Fig.10 was tested with a cavity(No..9) at General Motors Research Laboratories before shipment to the University of Michigan reactor. One of the tests involved heating the cavity in an oven to find the resonant frequency shift due to just the thermal expansion of the cavity. The cavity was operated in the University of Michigan reactor and some experimental data were obtained. Subsequent operation indicated that the cavity seal had apparently failed. These initial results are discussed and a comparison to our calculated values is shown.

Frequency Shift with Thermal Expansion of the Cavity: The equipment shown in Fig.10 was assembled horizontally in the laboratory area and a small oven was placed over the cavity in place of the 4 ft aluminum containment can. As heat was applied, the temperature of the cavity was monitored with the thermocouples spot welded to each face of the cavity. The shift in the resonant frequency was monitored with the oscilloscope. The data obtained from this test are plotted in Fig. 11.

The predicted thermal coefficient of frequency for a homogeneous cavity is $(\Delta f/f)/\Delta T = -\alpha$ [10] where α is the linear coefficient of expansion for the material. For Kovar $\alpha = 5 \times 10^{-6} (°C)^{-1}$ which is in good agreement with the value of $(\Delta f/f)/\Delta T$ in Fig.14. Such non-homogeneities as solder and varying materials can decrease the actual value of $(\Delta f/f)/\Delta T$ by a factor of 2 or 3.

14

THEORY
$$\left(\frac{\Delta f/f}{\Delta T}\right) = -\alpha$$
$$\alpha_{KOVAR} \cong 5 \times 10^{-6} \, (^\circ C)^{-1}$$

FROM CURVE
$$\left(\frac{\Delta f/f}{\Delta T}\right) = \frac{-46 \times 10^6 \times 1.8}{23 \times 10^9 \times 500} = -7.2 \times 10^{-6} (^\circ C)^{-1}$$
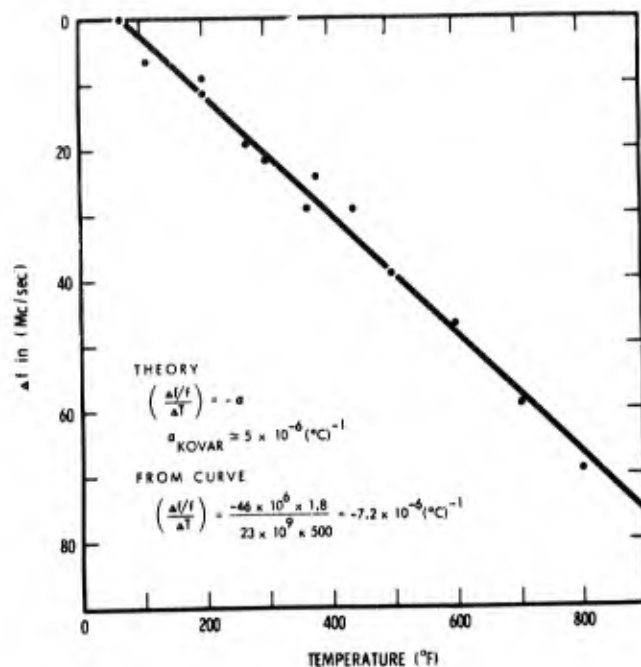
Fig. 11. Frequency shift vs temperature of Cavity No. 9
(due to thermal expansion).

A typical oscilloscope trace is shown in Fig. 12 for the cavity at room
temperature. The horizontal sweep is over a frequency range from about 23.05
to 23.15 Gc. The upper trace is the incident signal (see Fig. 8) and the
lower trace is the reflected signal. The double traces result from the sinu-
soidal input sweep to the klystron. The minimum in the reflected signal repre-
sents the resonant frequency. At this position the wave meter micrometer read
70.20 which from the calibration chart (Fig. 13) gives f_o=23.080 Gc.

The loaded Q of the cavity can be approximated from this oscilloscope
trace. To calculate Q_L accurately one needs a plot of VSWR versus f and then
the frequency difference between the two half-power points is given by[5]

$$\frac{\Delta \omega}{\omega} = \frac{1}{Q_L} . \tag{11}$$

When meter readings were taken at the estimated half-amplitude points on either
side of the resonant peak in Fig. 12 and the results were as follows: Left
side, WM=70.1 or f_2=23.085 Gc; Right side, WM=70.4 or f_R=23.070 Gc. From
these measurements and Eq.(11)

$$Q_L = \frac{f}{\Delta f} \simeq \frac{23.080}{.015} = 1540. \tag{12}$$

15
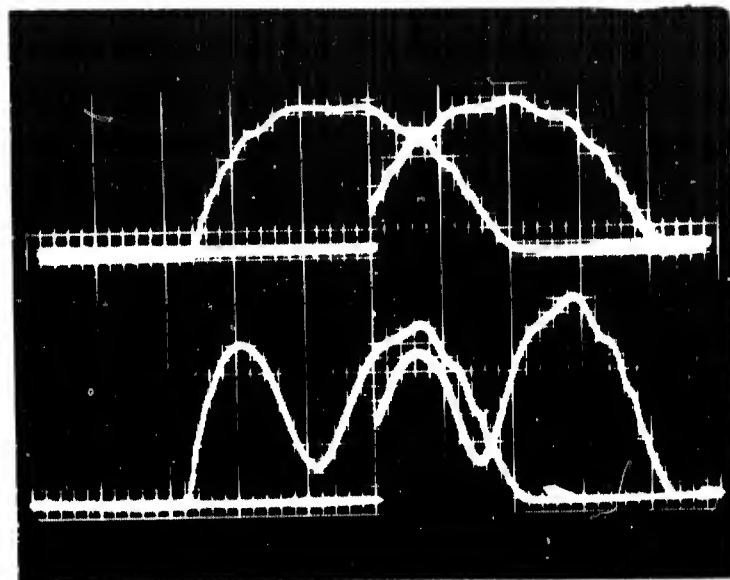
Fig. 12. Oscilloscope traces for Cavity No. 9 at room temperature. The vertical sweep is voltage ($\sim$.05V/cm) and the horizontal sweep is frequency ($\sim$ 20 Mc sec^{-1}cm^{-1}). The resonant frequency (23.08 Gc) is at the minimum in the reflected signal (lower trace). The upper trace is the incident signal.
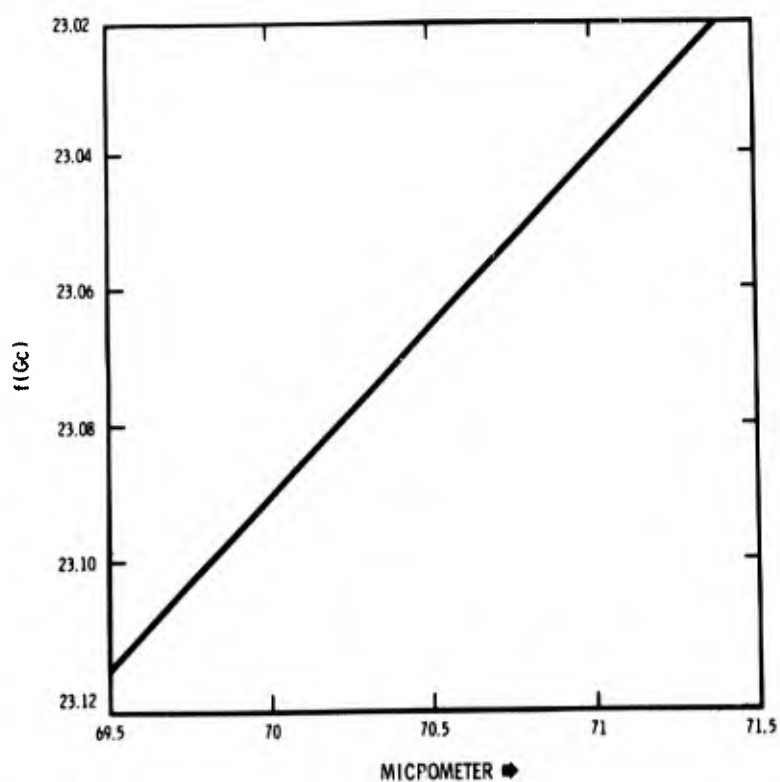
Fig. 13. Wave meter calibration.

Inpile Run

The equipment shown in Fig. 10 was shipped to the University of Michigan reactor and assembled for testing. It had been planned to assemble the apparatus on a Friday at an elevated position in the core where the neutron flux was considerably reduced, take enough data to check out the system, and then on the following Monday to fully insert the cavity in the core and raise the reactor power incrementally.

On Friday with the reactor at full power the cavity was placed at an elevated height in position 60 which is in the outside row of the core facing south (see Fig. 14). The microwave equipment was connected but the resonant frequency could not be found. The thermocouples were connected and showed the surprisingly high temperature of 800 and 1000°F. The 4 ft tube was immediately swung free of the core to reduce the flux and therefore the temperature. During this operation it was observed that a small perturbation traversed the oscilloscope trace as the tube was swung free of the core.

Subsequent investigation showed that the cavity was 1 ft lower in the core than had been intended and therefore at a much higher flux. Apparently the electron number density was sufficiently high that the Q and/or coupling were spoiled to the extent that the shifted resonant frequency could not be found with the existing microwave equipment.

The perturbation of the oscilloscope trace with changing neutron flux suggested a different method for obtaining the resonant frequency shift as follows: (1) with the cavity suspended in the pool but displaced horizontally to a position of low neutron flux, the oscillator frequency is advanced; (2) the cavity is then swung into position in the core and the oscilloscope observed to see if the perturbation crosses the trace; (3) if the perturbation is seen the procedure is repeated with the oscillator further advanced; (4) finally, the shifted resonant frequency is taken as the highest frequency at which the perturbation was seen.

This procedure was used to obtain the shift in the resonant frequency of the cavity for a number of locations near position 60 (Fig. 14). The cavity was swung in and out of position by a long aluminum rod which was hooked onto the wave guide at the top of the 4 ft tube and then manipulated from the "island" in the center of the reactor pool. The locations tested are listed in Table I and reference should be made to Fig. 14.

17.

CORE CONFIGURATION FOR RUN NO. 46
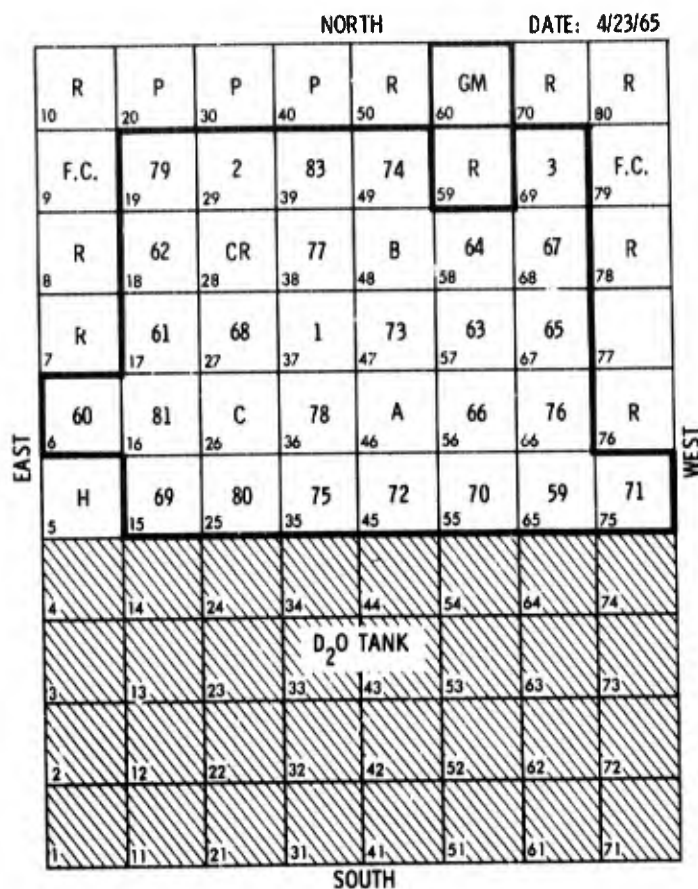
Fig. 14. Core configuration for reactor run 46.

TABLE I.   Core locations tested for frequency shift.

Location	Description
I	2 in. into position 60
II	Resting outside core on No. 50 reflector
III	Tangent to outside boundary of position 60
IV	Resting outside core on No. 70 reflector
V	12 in. outside position 60

The data obtained for these locations are presented in Table II.

18

TABLE II. Frequency shift data for Run 46.

Core Location	Temp.(°C) U-Cap	Body	Wave Meter	f_1 (Gc)	Δf (cps)	n (cm^{-3})
I	316	266	527	24.040	9.60×10^8	5.51×10^{11}
	304	254	550	23.908	8.28×10^8	4.76×10^{11}
	293	238	520	24.080	1.00×10^9	5.74×10^{11}
II	232	204	608	23.580	5.00×10^8	2.87×10^{11}
III	227	177	620	23.516	4.36×10^8	2.50×10^{11}
IV	260	216	600	23.624	5.44×10^8	3.10×10^{11}
V	121	110	686	23.162	0.82×10^8	4.71×10^{10}

In this table $\Delta f = f_1 - f_0$ where $f_0 = 23.080$ Gc and n was obtained from Δf using Eq.(8).

In order to calculate the electron number density for these conditions from our ion generation rate theory and the reaction kinetics theory, it is necessary to know the neutron flux. To obtain these values we used the ionization-tube flux-probe described in Appendix A. The results are listed in Table III.

TABLE III. Neutron flux values measured with ionization tube.

Core Location	ϕ cm^{-2}sec^{-1}	Temp, °K U-Cap	Body	n cm^{-3}
I	4.0×10^{12}	589	539	5.51×10^{11}
		577	527	4.76×10^{11}
		566	511	5.74×10^{11}
II	4.1×10^{12}	505	477	2.87×10^{11}
III	3.3×10^{12}	500	450	2.50×10^{11}
IV	2.8×10^{12}	533	489	3.1×10^{11}
V	1.4×10^{11}	394	383	4.71×10^{10}

V. ANALYSIS OF DATA

The reaction kinetics of the neon-argon system have been reported in detail.[1,2] Additional computer runs were made on the neon-argon system for the conditions of the microwave experiments. These data are reported in this section and the experimental results are compared with theory.

19

Reaction Kinetics for Neon-Argon System

In order to compare the experimental results to theory, the reaction kinetics code was used to compute the electron density for the microwave cavity for the conditions of 140 torr neon-argon ($Ar/Ne=10^{-4}$) at a neutron flux of $4 \times 10^{12} cm^{-2} sec^{-1}$. This corresponds to the neutron flux for core locations I and II in Table III. The results of these computer runs are shown in Fig. 15 where the electron number density is plotted versus the gas pressure for various gas temperatures. This plot shows the strong dependence of the electron density on the gas temperature via the collisional radiative recombination loss term ($C_{22}A_+n_e^2$).

The computed values for n_e for a neutral gas density of $4.95 \times 10^{18} cm^{-3}$ (=140 torr at R.T.) are replotted versus the inverse gas temperature in Fig. 16.

Comparison of Theory to Experiment: Also included in the Figs are the two experimental points. For core location I, the data of Table III were averaged and this point is plotted on Fig. 15. The agreement is considered good in view of the complexity of the reaction kinetics and the dynamical character of the measurements.
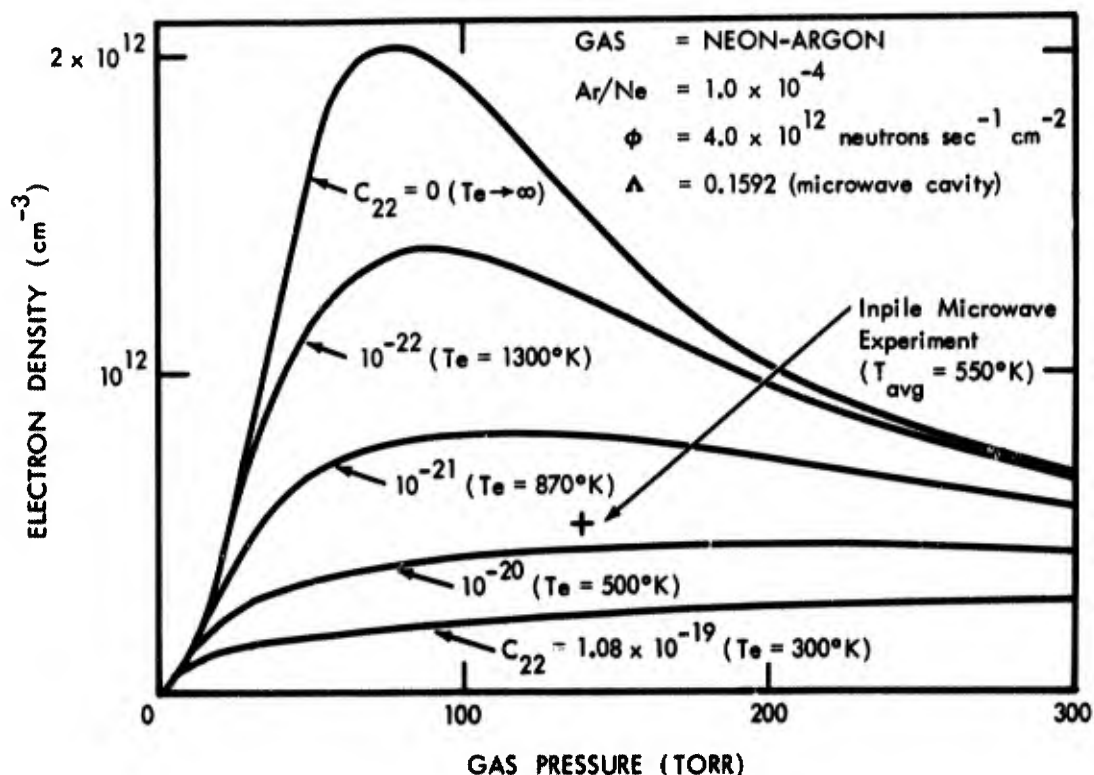
Fig. 15. Effect of collisional-radiative recombination $C_{22}A_+n_e^2$ on electron number density for neon-argon.

20
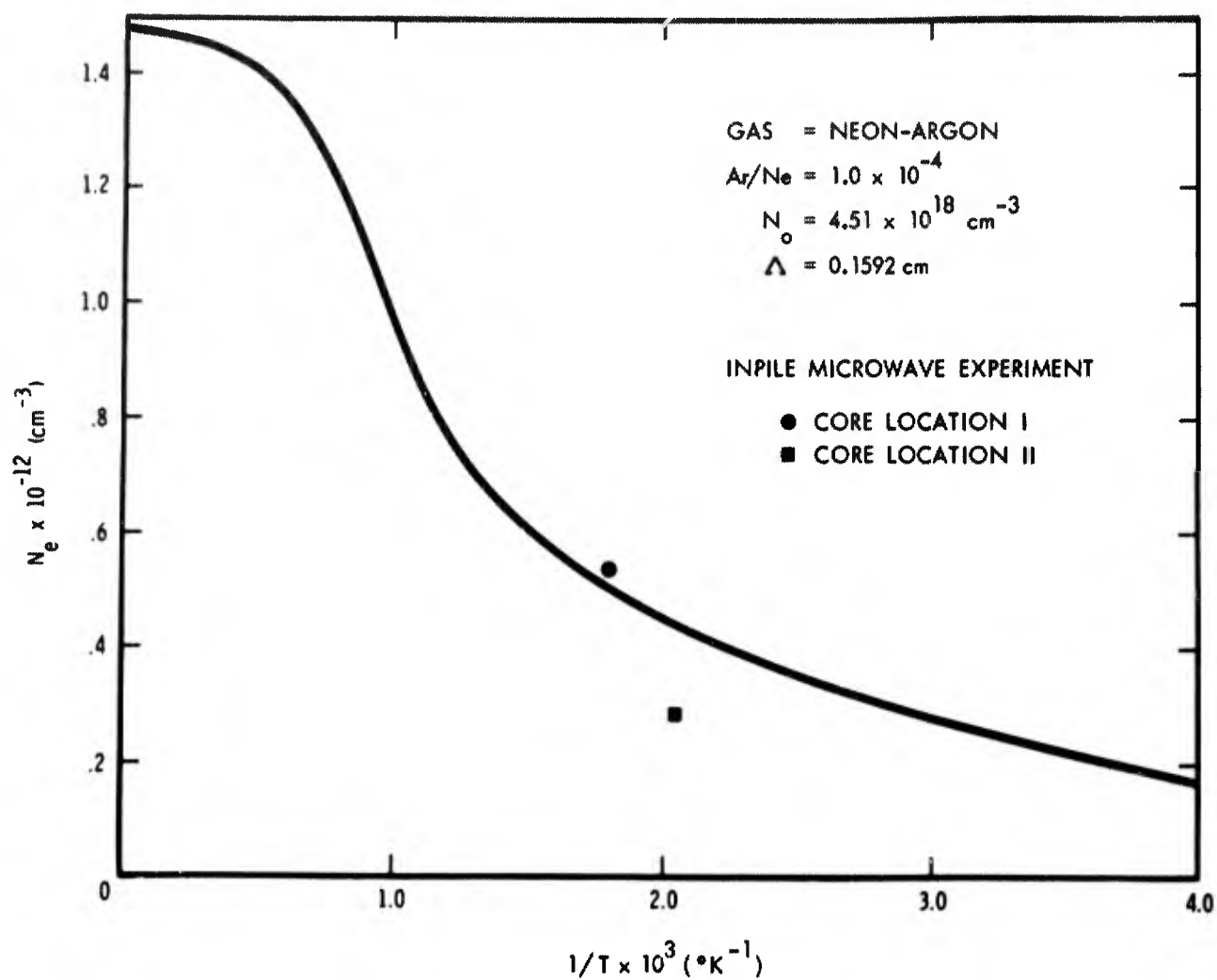
Fig.16. Electron number density versus gas temperature^{-1} for $\phi=4\times10^{12}cm^{-2}sec^{-1}$.

21

VI. REFERENCES

1. C. B. Leffert, D. B. Rees, and F. E. Jamerson, ONR Annual Report No. 5, Contract Nonr-3109(00), AD 609 177, (Oct. 1964).

2. C. B. Leffert, "Code Study of the Effect of Collisional-Radiative Recombination on the Electron Density in Neon-Argon", General Motors internal report.

3. C. B. Leffert, "Ion Generation Rate Theory and Analysis of Experimental Current-Voltage Data", ONR Annual Report No. 5, loc. cit.

4. C. B. Leffert, D. B. Rees, and F. E. Jamerson, "Noble Gas Plasma Produced by Fission Fragments", (to be published in December, 1965, J.A.P.)

5. D. J. Rose and S. C. Brown, "Methods of Measuring the Properties of Ionized Gases at High Frequencies I. Measurement of Q; II. Measurement of Electric Field; III. Measurement of Discharge Admittance and Electron Density", J.A.P. 23 711 (1952); J.A.P. 23 719 (1952); J.A.P. 23 1027 (1952).

6. M. A. Heald and C. B. Wharton, Plasma Diagnostics with Microwaves, (Wiley) (1965).

7. L. Tonks and I. Langmuir, Phys. Rev. 33, 195, 990 (1929).

8. C. L. Chen, Phys. Rev. 135, A627 (1964).

9. J. C. Slater, Revs. Modern Phys. 18, 441 (1946).

10. C. B. Montgomery, Technique of Microwave Measurements, (McGraw-Hill), (1947).

11. C. B. Leffert, "Microwave Theory for Resonant Cavity Measurements of Plasma Parameters", General Motors internal report.

VII . APPENDIX A - IONIZATION-TUBE FLUX-PROBE

After completion of the ion generation rate studies we built a flux-probe for measuring the thermal neutron flux level in a reactor. This flux-probe has been used by the reactor staff for monitoring the neutron flux. The probe consists of an ionization tube filled to 240 torr argon which is mounted in a small aluminum cavity (see Fig. A-1) at the end of a lightweight 20 ft aluminum support tube. The aluminum cavity was filled with monoisopropylbiphenyl to facilitate cooling of the ionization-tube. From our theory and the experimental data for 240 torr argon, the thermal neutron flux, $\emptyset$, can be expressed in terms of the measured ion current at -20 volts as

$$\emptyset = (5.45 \times 10^{13})(I_{ma})^{4/3} \tag{A-1}$$

The thermal flux values obtained using this probe during full reactor power at the locations listed in Table I are shown in Table III together with the temperature in °K for the microwave cavity and the values of n calculated from Eq.(8).
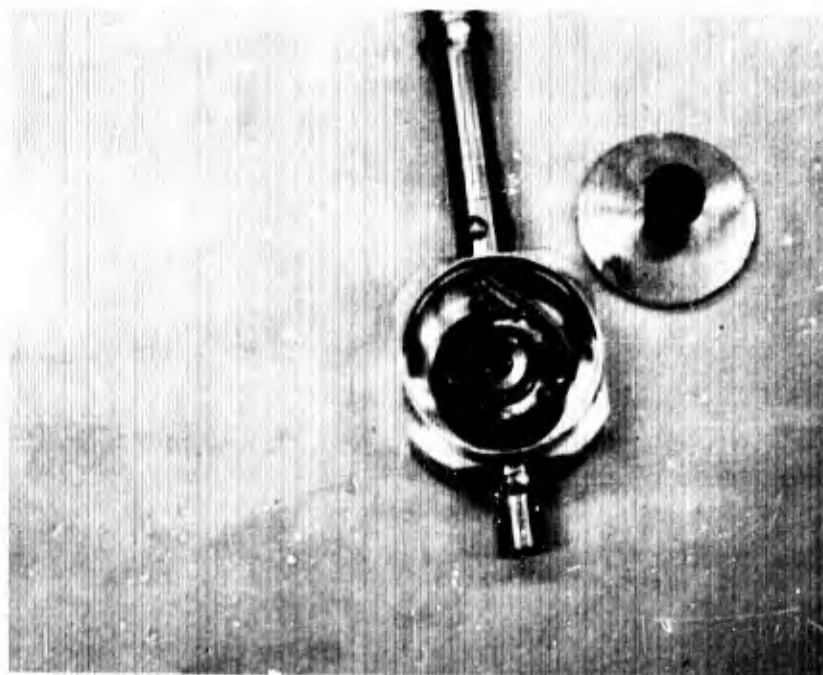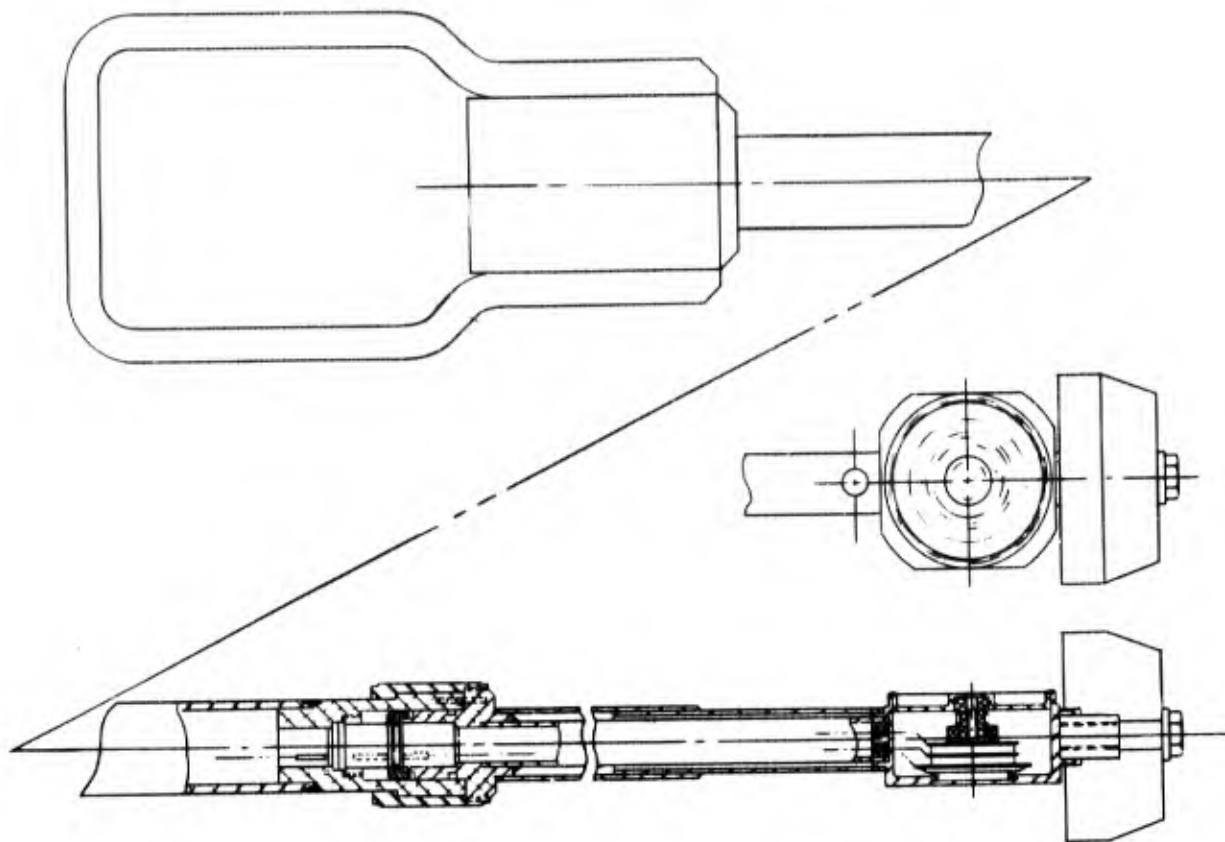
Fig.A-1. Neutron flux probe. A GMRL ionization chamber filled to 240 torr pressure of argon was mounted in an oil-filled aluminum cavity at the end of a 20 ft. aluminum support tube. This device is now used to measure the neutron flux at the University of Michigan reactor.

SECTION D

THEORY FOR THERMIONIC ELECTRON TRANSPORT THROUGH A PLASMA WITH UNIFORM VOLUME PRODUCTION AND AMBIPOLAR DIFFUSION LOSS

ABSTRACT

The design of a thermionic energy converter for optimum performance requires detailed knowledge of the dependence of output current on voltage and the manner in which this relationship changes with various plasma parameters. A theory is presented for the transport of thermionic electrons through a plasma diode, and the current-voltage relationship is derived for a plasma which is generated by fission fragments and which decays by ambipolar diffusion to the walls of the diode. Volume charge loss is not included. The model is thus applicable to the lower values of pressure and gap separation. The calculated curve of current density versus voltage agrees qualitatively with available experimental results.

i

CONTENTS

OBJECT

A theoretical model was desired for the transport of thermionic elec-
trons through a fission-fragment-generated plasma.

SUMMARY

A thermionic electron transport theory appropriate for a uniform volume
source of ionization, and where charge is lost by diffusion and mobility currents
in the plasma, has been developed. Analytic solutions are presented
which are based on the following model of the interelectrode region:
1. The plasma is quasi-neutral and collision-dominated.
2. The plasma is coupled to the electrodes via small collisionless sheaths.
3. The sheath adjacent to the emitter is electron-rich; the collector sheath
   is ion-rich for low currents, but electron-rich at the higher currents.
4. The electron and ion temperatures are constant throughout the plasma.
5. Volume charge loss is negligibly small.
Available experimental data are in qualitative agreement with the theoretical
curve of current density versus voltage.

I. INTRODUCTION

In our previous studies,[1] much quantitative data have been obtained
on the ion production rates and reaction kinetics of single and mixed-gas
plasmas generated by fission-fragment-impact-ionization. These investiga-
tions were directed towards elucidating the fundamental physical processes
which occur in mixed noble gas and noble gas-cesium plasmas, and were not
complicated by the presence of thermionic electrons.

The next phase in our program is to study the transport of thermionic
electrons through the plasma and therefrom attempt to establish optimum con-
ditions of electrode separation, electrode temperatures and partial pressures
of constituent gases that will yield maximum power output in a practical con-
verter. For this purpose a generalized plasma transport theory is required
which must include mobility and diffusion currents, and volume production and
loss processes such as fission-fragment ionization, charge exchange and recom-
bination. Such a theory for the noble gas diode is still lacking at the
present time.

1

For the unignited mode of the cesium converter, where ionization occurs predominantly by contact of cesium vapor with the hot emitter, Hansen and Warner[2] have shown that volume ionization and loss effects can often be neglected, thereby considerably simplifying the transport analysis. In an earlier attempt at a transport theory for the noble gas converter with volume ionization, Leffert[3] computed current-voltage characteristics from studies of the random ion and electron currents at the plasma edge-sheath regions but did not consider the transport properties of the plasma. In addition, the electron density in the plasma was assumed to be uniform.

The present analysis, while still restrictive in approach, takes into account the mobility and diffusion currents in the plasma and determines the electron density distribution across the plasma when coupled with collisionless sheaths at the emitter and collector. Such a theory should predict satisfactorily the transport of thermionic electrons in fission-fragment-generated plasmas for the lower regimes of pressure and gap separation.

II. PHYSICAL MODEL

The model is that for a "high-pressure" thermionic plasma diode wherein collisions occur among the atoms, ions and electrons; that is, the mean free paths of the particles are much less than the interelectrode spacing d. Consider typical values of λ_D, the Debye length for electrons, and λ_e, the electron-neutral atom mean free path, at the emitter temperature of $T_E \approx 1700°K$.[4] Using the results of previous studies[1] for a Ne-Ar mixture (Ar/Ne $\sim 10^{-4}$), where electron densities were $\gtrsim 10^{12} cm^{-3}$ at a neutral gas density $N_o \approx 3 \times 10^{18} cm^{-3}$, we obtain $\lambda_D \lesssim 10^{-4} cm$ and $\lambda_e \approx 10^{-3} cm$, so that $\lambda_D < \lambda_e \ll d$ for electrode separations of order 10^{-1} cm. Under these conditions, we approximate the interelectrode region by a quasi-neutral plasma which is coupled to the electrodes through small collisionless sheaths. The thickness of these sheaths can be neglected for distances of the order of the electrode separation.

Figure 1 is a schematic representation of the potential distribution across the gas-filled diode. We consider plane-parallel symmetry where the properties of the plasma depend only on the variable x. V_E is the negative potential drop across the electron-rich sheath adjacent to the emitter, V_p is

the positive change in potential traversing the plasma from x=o to x=d and V_c is the negative potential drop between the plasma and the collector across the ion-rich collector sheath. For the purposes of this transport study, the
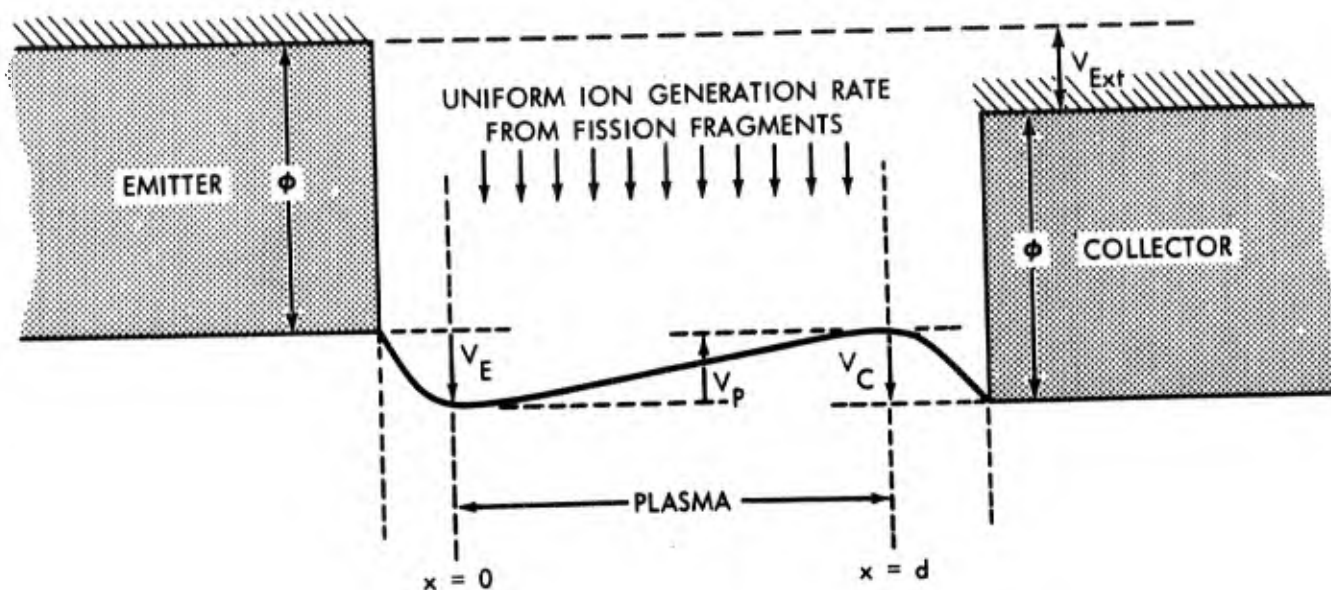
Fig. 1. Schematic representation of potential distribution across thermionic plasma diode.

work function of the emitter is taken to be equal to the work function of the collector.* The external potential drop (V_{Ext}) is thus equal to $V_p - (V_E + V_c)$. For net current densities through the tube in excess of the order of 20 mA cm^{-2}, it will be shown that the polarity of the collector sheath changes from that given in Fig. 1, so that numerically V_{Ext} then becomes equal to $V_p + V_c - V_E$. The polarity of V_E, however, remains unchanged in this electron-rich model.

Computations have been reported previously[1] of the dependence of the ion generation rate in a diode on such parameters as gas species, gas pressure, tube geometry, neutron flux and the uranium load on the surface of one electrode. This work indicates that, to a reasonable approximation, the ion generation rate by fission fragments can be regarded to have a spatially constant

---

*Unequal work functions are immediately included by shifting the I-V curve along the V axis by an amount equal to the work function difference.

3

average value when the electrodes are plane parallel and the product of pressure and gap separation is relatively low. This is the regime where the ambipolar diffusion mode dominates. The ion generation rate S is therefore taken to be independent of the variable x in the present study.

We assume that the electrons and ions have Boltzmann distributions in the plasma region with constant temperatures T_- and T_+ respectively. This considerable simplification is discussed further in Section V. Finally, we note that the temperature of the collector ($\approx 900°K$) is sufficiently low that thermionic electron emission (back emission) can be neglected.

III. MATHEMATICAL ANALYSIS

(1) Electron Density Distrubition Across Plasma

The basic transport equations for the quasi-neutral plasma ($n^+ \approx n^- = n$) are:

$$\Gamma^- = - D^- \frac{dn}{dx} - \mu^- n E, \tag{1}$$

$$\Gamma^+ = - D^+ \frac{dn}{dx} + \mu^+ n E, \tag{2}$$

and

$$\frac{d\Gamma^-}{dx} = \frac{d\Gamma^+}{dx} = S \tag{3), (4}$$

where

$$\Gamma_{net} = \Gamma^- - \Gamma^+. \tag{5}$$

Γ^- and Γ^+ are the particle current densities ($J(A \cdot cm^{-2})/e$) of electrons and positive ions respectively where both these currents are positive for particle flow from the emitter to the collector. Γ_{net} is the total resultant current. The coefficients of diffusion (D) and mobility (μ) are constants in these equations for the constant electron and ion temperatures assumed. $E(x)$ is the electric field distribution across the plasma.

We simplify Eqs.(1)-(5) by integrating Eqs.(3) and (4) and combining the results with Eqs.(1) and (2).

$$Sx + K_1 = - D^- \frac{dn}{dx} - \mu^- n E, \tag{6}$$

$$Sx + K_2 = - D^+ \frac{dn}{dx} + \mu^+ n E. \tag{7}$$

4

K_1, K_2 are constants which can be determined from the boundary conditions of the plasma and the relation

$$\Gamma_{net} = K_1 - K_2 . \tag{5a}$$

The electric field in Eqs.(6), (7) is eliminated by multiplying Eq.(6) by μ^+, Eq.(7) by μ^-, and adding the two equations. Using Eq.(5a) also, we obtain

$$Sx \ (\mu^+ + \mu^-) + \mu^+ \ \Gamma_{net} + (\mu^+ + \mu^-)K_2 = - \ \frac{dn}{dx} \cdot (\mu^+ D^- + D^+ \mu^-),$$

or, in terms of the ambipolar diffusion coefficient D_a,

$$\frac{dn}{dx} = - \left(\frac{S}{D_a}\right) x - \frac{1}{D_a} \left[K_2 + \left(\frac{\mu^+}{\mu^+ + \mu^-}\right) \Gamma_{net} \right]. \tag{6}$$

Integration of this equation yields the electron density distribution across the plasma:

$$n(x) = n_o - \left(\frac{S}{2D_a}\right) x^2 - \frac{x}{D_a} \left[K_2 + \left(\frac{\mu^+}{\mu^- + \mu^+}\right) \Gamma_{net} \right]. \tag{8}$$

The term n_o is the electron density at the plasma-emitter sheath boundary $x=o$.

Equation (8) is used in conjunction with the appropriate sheath equations in order to determine n_o and K_2.

(2) Boundary Equations for Electron-Rich Emitter Sheath

The two equations for the electron and ion currents at $x=o$ are

$$\Gamma^-_{x=o} = K_1 = \nu_E e^{-\eta_E} - \frac{n_o \ v_E^-}{4} , \tag{9}$$

$$\Gamma^+_{x=o} = K_2 = - \frac{n_o \ v_E^+}{4} e^{-\eta_E} . \tag{10}$$

$e^{-\eta_E}$ is the Boltzmann attenuation factor for a potential barrier and $\eta_E = \frac{e \ V_E}{kT_E}$, where e is the electronic charge, V_E the sheath potential, k is Boltzmann's constant and T_E is the temperature of the emitter. The thermionic current density is ν_E, and v_E^- and v_E^+ represent respectively the random electron and ion currents $\left[\sqrt{\frac{8kT_E}{\pi \ M_{\mp}}} \right]$ in the plasma at $x=o$. Because of the proximity of

5

the plasma-emitter sheath boundary to the emitter, we associate these currents with the temperature T_E. Note however that the random currents vary with T_E only as $\sqrt{T_E}$.

(3) Boundary Equations for Ion-Rich Collector Sheath

The equations for the electron and ion currents at $x=d$ are

$$\Gamma^-_{x=d} = Sd + K_1 = \frac{n_d v^-_c}{4} e^{-\eta_c}, \tag{11}$$

$$\Gamma^+_{x=d} = Sd + K_2 = \frac{n_d v^+_c}{4}, \tag{12}$$

where the various terms are defined in a manner exactly analogous to those discussed in Section III.2 above.

Several linear combinations of Eqs.(9), (10), (11), (12) will be useful to us in the analysis, such as the net currents at $x=0$ and $x=d$, and also the particle conservation equations. We list these here.

$$\Gamma_{net}_{x=0} = \nu_E e^{-\eta_E} - \frac{n_o v^-_E}{4} + \frac{n_o v^+_E}{4} e^{-\eta_E}, \tag{13}$$

$$\Gamma_{net}_{x=d} = \frac{n_d v^-_c}{4} e^{-\eta_c} - \frac{n_d v^+_c}{4}, \tag{14}$$

$$Sd = \frac{n_d v^+_c}{4} + \frac{n_o v^+_E}{4} e^{-\eta_E}, \tag{15}$$

$$\nu_E e^{-\eta_E} + Sd = \frac{n_o v^-_E}{4} + \frac{n_d v^-_c}{4} e^{-\eta_c}. \tag{16}$$

(4) Solutions for n_o, n_d, V_E, V_c, for Ion-Rich Collector Sheath

The constant input parameters for determining a single current-voltage curve are ν_E, v^-_E, v^+_E, D_a, d, μ^+, μ^-, and S. The overall procedure adopted is to select a net current and then compute n_o, n_d which in turn enable V_E and V_c to be calculated. Finally V_E and V_c, together with V_p, the potential drop across the plasma (Section III.5), determine the external diode potential for the current selected.

6

We first use Eq.(8) where for $x=d$, K_2 can be replaced by $\left(\frac{n_d v_c^+}{4} - Sd\right)$ from Eq.(12). Simplifying, we obtain

$$n_o = n_d - \left(\frac{S}{2D_a}\right)d^2 + \frac{d}{D_a}\left[\frac{n_d v_c^+}{4} - \left(\frac{\mu^+}{\mu^- + \mu^+}\right)\Gamma_{net}\right] \tag{17}$$

which gives n_o as a linear function of n_d only η_E

Equation (13) yields an expression for $e^{-\eta_E}$ as a function of n_o, viz.,

$$e^{-\eta_E} = \frac{\Gamma_{net} + \frac{n_o v_E^-}{4}}{v_E + \frac{n_o v_E^+}{4}}, \tag{18}$$

and from the conservation Eq.(16), $\frac{n_d v_c^-}{4} e^{-\eta_c}$ can then also be expressed in terms of n_o only. Equation (14) can now be rewritten:

$$\Gamma_{net} = v_E\left(\frac{\Gamma_{net} + \frac{n_o v_E^-}{4}}{v_E + \frac{n_o v_E^-}{4}}\right) + Sd - \frac{n_o v_E^-}{4} - \frac{n_d v_c^+}{4}. \tag{19}$$

Expressions (17) and (19) are the two equations for the two unknowns n_o, n_d. Substitution of the right hand side of Eq.(17) for n_o in (Eq.19) yields a quadratic for n_d. Only one solution exists for real values of n_o, n_d. Knowing n_o and n_d, we determine V_E at temperature T_E from Eq.(18) and V_c at temperature T_c from Eq.(14).

(5) Potential Drop V_p Across Plasma

It is convenient to write the derivative of Eq.(8) as

$$\frac{dn}{dx} = -A_1 x + A_2 \tag{20}$$

where A_1 and A_2 are positive definite given by

$$A_1 = \frac{S}{D_a}. \tag{21}$$

$$A_2 = \frac{1}{D_a}\left[\frac{n_o v_E^+}{4} e^{-\eta_E} - \left(\frac{\mu^+}{\mu^- + \mu^+}\right)\Gamma_{net}\right]. \tag{22}$$

7

We combine Eqs. (7) and (20) in order to express the electric field as

$$E = \frac{S \cdot x}{2\mu^+ n} - \frac{\left\{ D^+ A_2 + \left(\frac{\mu^+}{\mu^+ + \mu^-}\right) \Gamma_{net} \right\}}{\mu^+ n} \qquad (23)$$

where we have also approximated D_a by $2 D^+$, ($T_- \approx T_+$, Section V). Substitution of $n(x)$ from Eq.(8) leads to the following expression

$$\frac{dV}{dx} = -\frac{2D^+ \cdot x}{\mu^+(c + bx - x^2)} + \frac{D^+ A_2 + \left(\frac{\mu^+}{\mu^+ + \mu^-}\right) \Gamma_{net}}{\frac{\mu^+ A_1}{2}(c + bx - x^2)} \qquad (24)$$

where $c = 2n_o/A_1$ and $b = 2A_2/A_1$. This can be immediately integrated between $x=o$ and $x=d$ to give the potential drop across the plasma:

$$V_p = \left(\frac{kT^+}{e}\right) \log_e\left\{1 + \left(\frac{b}{c}\right)d - \left(\frac{1}{c}\right)d^2\right\} + \frac{4D^+ \Gamma_{net}}{(\mu^+ + \mu^-)S} \frac{1}{\sqrt{b^2 + 4c}} \left\{\log_e\left(\frac{d+P}{Q-d}\right) - \log_e \frac{P}{Q}\right\} \qquad (25)$$

where $P = (\sqrt{b^2 + 4c} - b)/2$ and $Q = (\sqrt{b^2 + 4c} + b)/2$.

Thus, for the selected value of Γ_{net}, the external potential drop across the diode for the situation shown in Fig. 1 is

$$V_{Ext} = V_p - V_E - V_c.$$

(6) Current at Which Polarity of Collector Sheath Potential Reverses

In the preceding sections we have considered only an ion-rich sheath at the collector. However, in any numerical substitution of current to determine the diode potential, it is necessary to know whether the collector sheath is ion-rich or electron-rich. The first procedure, therefore, is to compute the net current Γ_{Nvo} at which $V_c=0$. We use the following equations.

Since $e^{-\eta_c} = 1$ for $V_c=0$, Eq.(14) becomes

$$n_d = \frac{4 \Gamma_{Nvo}}{v_c^- - v_c^+}. \qquad (26)$$

8

We substitute this value of n_d into Eq.(17) to obtain

$$n_o = \frac{4 \; \Gamma_{Nvo}}{v_E^- - v_c^+} \left\{ 1 + \frac{v_c^+ d}{4 \; D_a} \right\} - \frac{Sd^2}{2 \; D_a} + \left(\frac{\mu^+}{\mu^+ + \mu^-} \right) \frac{\Gamma_{Nvo} \; d}{D_a} \quad , \qquad (27)$$

which shows n_o as a linear function of Γ_{Nvo} only.

A second n_o, Γ_{Nvo} relationship can be obtained from Eq.(16) where we substitute for $e^{-\eta_e}$ the expression shown in Eq.(18), and also use Eq.(26). We get

$$v_E \left(\frac{\Gamma_{Nvo} + \frac{n_o v_E^-}{4}}{v_E + \frac{n_o v_E^+}{4}} \right) + Sd - \frac{n_o v_E^-}{4} = \frac{v_c^-}{4} \left(\frac{4 \; \Gamma_{Nvo}}{v_c^- - v_c^+} \right) . \qquad (28)$$

Equations (27) and (28) are used to eliminate n_o. The resulting quadratic in Γ_{Nvo} has only one real root.

For values of $\Gamma_{net} < \Gamma_{Nvo}$, the equations of Section III.3 are valid. When $\Gamma_{net} = \Gamma_{Nvo}$ we use the above Eqs. (26), (27), (28). For $\Gamma_{net} > \Gamma_{Nvo}$, the procedures discussed so far are modified as outlined below.

(7) Boundary Equations for Electron-Rich Collector Sheath

When there exists an electron-rich collector sheath, the positive ions are retarded in their motion from the plasma to the collector. Equations (11) and (12) then become

$$\Gamma_{x=d}^- = Sd + K_1 = \frac{n_d v_c^-}{4} \qquad (11a)$$

$$\Gamma_{x=d}^+ = Sd + K_2 = \frac{n_d v_c^+}{4} \; e^{-\eta_c} \qquad (12a)$$

The boundary equations for the electron-rich emitter sheath(Eqs. (9), (10), (13)) remain unchanged, but Eqs.(14), (15), (16) become changed to Eqs. (14a), (15a), (16a) (unwritten) by obvious analogy with the two equations written above.

(8) Solutions for n_o, n_d, v_E, v_c for Electron-Rich Collector Sheath

We write Eq.(8) in terms of K_1 instead of K_2, and then substitute

9

$\left(\dfrac{n_d v_c^-}{4} - Sd\right)$ for K_1 from Eq.(11a). This yields

$$n_o = n_d - \frac{Sd^2}{2\,D_a} + \frac{d}{D_a}\left[\frac{n_d v_c^-}{4} - \left(\frac{\mu^-}{\mu^+ + \mu^-}\right)\Gamma_{net}\right].\tag{29}$$

In a manner similar to that adopted previously (Section III.4), $\dfrac{n_d v_c^+}{4}\,e^{-\eta_c}$ is now written in terms of n_o only, by using the ion conservation Eq.(15a) and expression (18) which is still valid. The resulting terms are substituted into Eq.(14a) to give

$$\Gamma_{net} = \frac{n_d v_c^-}{4} + \frac{n_o v_E^-}{4}\left(\frac{\Gamma_{net} + \dfrac{n_o v_E^-}{4}}{v_E + \dfrac{n_o v}{4}}\right) - Sd.\tag{30}$$

We now have the two Eqs.(29) and (30) for the two unknowns n_o, n_d. With n_o known, V_E is determined from Eq.(18). Similarly, V_c is calculated from Eq.(14a), i.e.

$$e^{-\frac{eV_c}{kT_c}} = \left(\frac{v_c^-}{4} - \frac{\Gamma_{net}}{n_d}\right)\Big/\frac{v_c^+}{4}.$$

Equation (25) for the potential drop across the plasma is unaffected by the change in polarity of the collector sheath potential. Therefore, the potential drop across the diode under these conditions is

$$V_{Ext} = V_p - V_E + V_c.$$

(9) Saturation Current

We consider that the net current through the thermionic diode will saturate when there exists an electron-rich collector sheath of sufficient potential that all the ions are repelled and lost only via the emitter sheath. This leads to the maximum degree of electron space-charge neutralization at the emitter for the present model.

Under these conditions the saturation current is evidently

$$\Gamma_{Sat} = \frac{n_d v_c^-}{4},\tag{31}$$

10

and we determine Γ_{Sat} from this relationship by first computing n_d in the following manner.

Equation (9) for x=d becomes

$$n_d = n_o + \frac{Sd^2}{2 D_a} - \frac{d}{D_a} \left(\frac{\mu^+}{\mu^+ + \mu^-} \right) \Gamma_{Sat}, \tag{32}$$

when we use

$$\Gamma^+ \Big|_{x=0} = -Sd = K_2. \tag{33}$$

Combining Eqs.(31) and (32),

$$n_d = \left\{ n_o + \frac{Sd^2}{2 D_a} \right\} \Big/ \left\{ 1 + \frac{d}{D_a} \left(\frac{\mu^+}{\mu^+ + \mu^-} \right) \frac{v_c^-}{4} \right\}. \tag{34}$$

From Eqs.(16a), (18) and (31), we derive a second n_d-n_o relation:

$$Sd \left(v_E + \frac{n_o v_E^+}{4} \right) = \left(\frac{n_o v_E^-}{4} + \frac{n_d v_c^-}{4} \right) \left(\frac{n_o v_E^+}{4} \right). \tag{35}$$

We use Eqs.(34) and (35) to eliminate n_o; the subsequent quadratic for n_d has only one value of n_d which can give a real value of n_o. This value of n_d yields Γ_{Sat} in Eq.(31).

IV. EXAMPLE OF COMPUTED I-V CHARACTERISTIC

An example of an I-V characteristic computed from the present transport theory is shown in Fig. 2. The purpose of presenting the curve here is to indicate its general shape and not to emphasize the actual currents obtained. The input numbers were chosen merely to test the solutions.

We selected a Ne-Ar mixture (Ar/Ne=10^{-3}) at 100 torr total pressure with a value of S=1.1×10^{16}cm^{-3}sec^{-1}[1] at a neutron flux of 1.0×10^{13}cm^{-2}sec^{-1}. Also, we chose d=0.1cm, v_E=2.0A.cm^{-2}, T_E=1700°K, T_c=900°K and T_p(the mean plasma temperature)=1300°K. Values used for the random electron and ion speeds, in cm sec^{-1} are: v_E^-=2.6x10^7, v_c^-=1.9x10^7, v_E^+=9.5x10^4, v_c^+=6.9x10^4. At a pressure of 100 torr, $\mu^- \approx 5$x10^4cm^2(V.sec)$^{-1}$[5], and $\mu^+ \approx 53$ cm^2(V.sec)$^{-1}$. This single value of ion mobility is considered a satisfactory approximation to make,

11
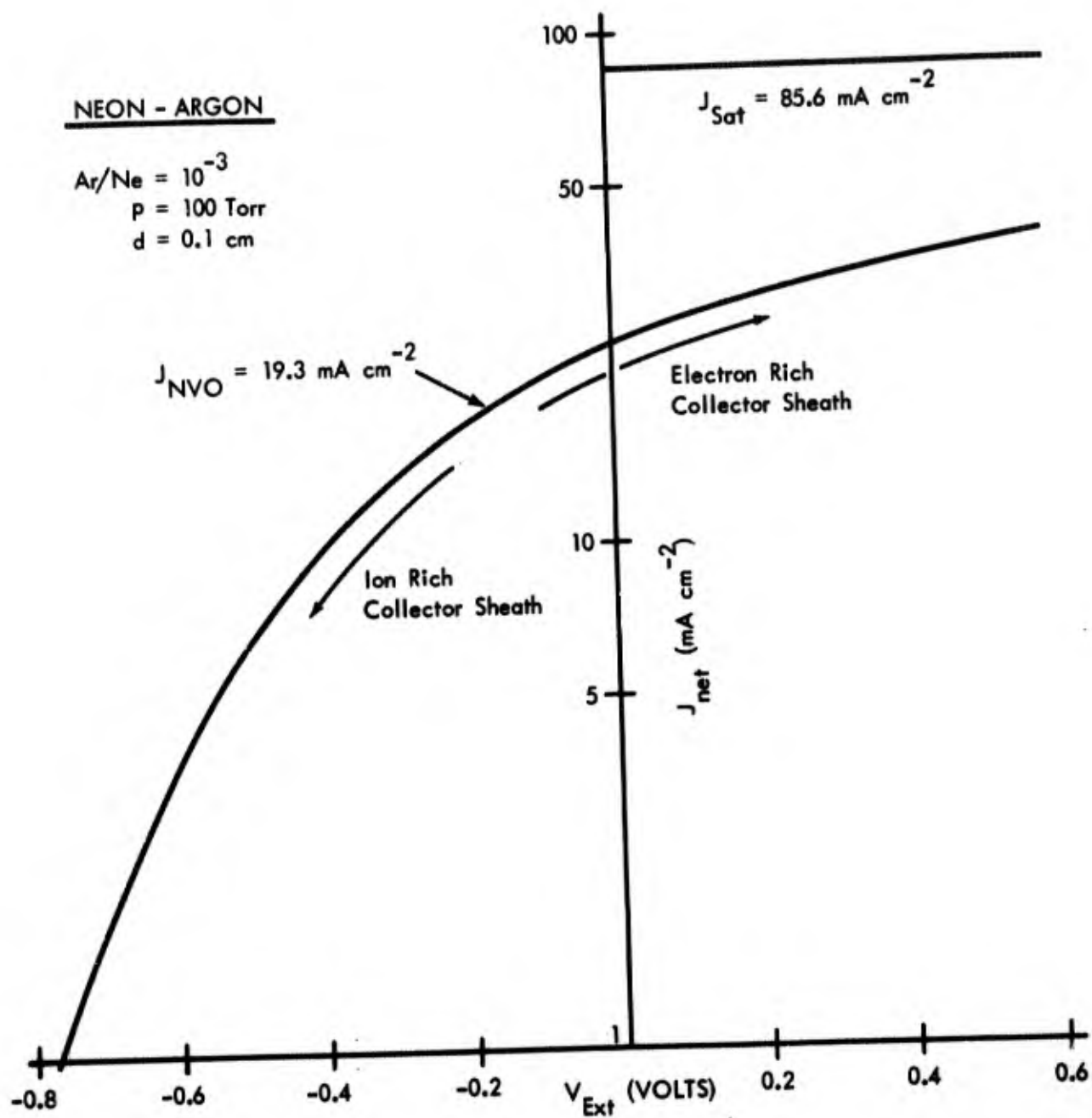
Fig. 2. Computed current-voltage characteristic for neon-argon mixture with electron-rich emitter sheath. The emitter work function is equal to the collector work function.

12

despite the fact that four ions (Ne^+, Ne_2^+, Ar^+, Ar_2^+) can exist in the Ne-Ar plasma. Reaction kinetic studies[6] show that at pressures $\gtrsim$ 100 torr, Ne^+ is rapidly converted into Ne_2^+, so that the mobility of Ne^+ does not play an important role under the present conditions. The mobilities of the remaining ions, Ne_2^+, Ar^+, Ar_2^+, in 100 torr of neon,[6] are all very similar ($\simeq$ 53 cm^2 $(V.sec)^{-1}$) because of the non-resonant character of their motion. We thus approximate with a single value of ion mobility.

With the solutions in the closed form presented in Section III, very little computational time is required to determine the I-V characteristics compared to models[2] requiring iterative solution of coupled equations. The curve discussed here (Fig.2) was, in fact, first obtained by hand calculations and these were consistent with the results later obtained using a computer code. The solutions were coded for a computer by C. B. Leffert.

The smooth curve shown in Fig. 2 rises asymptotically towards the saturation current density of 85.6 mA cm^{-2} which for practical purposes is attained at an applied potential $\simeq$ 1.5 V. In the earlier transport studies of Leffert[3] which considered n constant throughout the plasma, the computed current in general increased rapidly with increasing potential and saturated more rapidly than the curve in Fig. 2. The experimental I-V curves, however, did not exhibit this rapid saturation but approached the saturation current much more gradually. We are encouraged by the fact that these experimental curves, taken at low values of pressure and gap separation, are very similar in shape* to the curve shown in Fig. 2.

V. DISCUSSION

The present physical model of electron transport is considered a good first approximation for predicting current-voltage characteristics from gross plasma characteristics. The most serious objections against the theory concern the use of constant temperatures for ions and electrons in the plasma and the assumption of macroscopic charge-neutrality throughout the plasma. These are discussed very briefly below.

---

*We cannot compare the present theory directly with the earlier inpile experimental curves because the ion-generation rate in those experiments was not well known.

13

Evidently for the situation where the emitter is 800-1,000°K hotter than the collector, the ion, electron and neutral-atom temperatures cannot be constant but must vary across the plasma. Since the ions lose on the average one-half their energy per collision with an atom, then T_+ is probably close to T_g. This ion-atom temperature T_{+g} will vary between the emitter temperature T_E and the collector temperature T_c but no large error will be introduced in the transport equations if we assign to T_{+g} an average value $\overline{T}_{+g} = (T_E + T_c)/2$.

The average electrode temperature cannot be as readily assigned to the electrons. In general, the electrons are only slowly thermalized in collisions with atoms at moderate gas pressures so that the electron temperature is often higher than $\overline{T}_{+g}$. This is particularly the case when an ion-rich sheath exists at the emitter and thermionic electrons are injected into the plasma with temperatures $\sim$ 5,000-10,000°K. Even for a noble gas pressure of 100 torr and gap separation of 10^{-1} cm, these energetic electrons can reach the collector without attaining thermal equilibrium. In fact, the concept of electron temperature, arising from the supposed Maxwellian distribution of the electrons is questionable.

For the present study, however, where an electron-rich sheath exists at the emitter, the thermionic electrons are retarded before entering the plasma. It is assumed, therefore, that at the emitter sheath-plasma boundary, the electrons have a temperature approximately the same as the emitter temperature. Because these already-retarded electrons experience further frequent collisions with gas atoms at pressures $\sim$ 100 torr, we make the additional assumption that the electron temperature can be replaced by an average value $\overline{T}_-$ where $\overline{T}_- \approx \overline{T}_{+g}$. However, the theory does not require these two temperatures to be equal, but only that T_- and T_{+g} are constant throughout the plasma region.

Our basic assumption is that of approximate charge neutrality ($n^- \approx n^+$) in the plasma. Extreme deviations from charge neutrality can be determined by using Poisson's equation to investigate when the relationship $(n^- - n^+) \ll n$ is no longer true. However, this inequality becomes a somewhat arbitrary test for situations that are not extreme. A more rigorous transport study is then required which would differentiate at the start between the electron and ion distributions across the plasma.

The transport theory presented in this report breaks down when volume loss processes such as recombination become significant. The importance of

14

volume loss terms in comparison with ambipolar diffusion loss can be determined approximately by investigating the characteristic lifetime of ions due to these various loss processes. For example, for dissociative recombination loss in the plasma, the lifetime of ions is $\tau_R \approx \frac{1}{\alpha n^-}$; for diffusion $\tau_D \approx \frac{\Lambda^2}{D_a}$ where Λ is the characteristic diffusion length of the container. For the diffusion dominated mode $\tau_D \ll \tau_R$. If τ_R is reduced by increasing αn^-, or conversely if τ_D is increased (by operating at higher values of p or d) until $\tau_D \approx \tau_R$, then the present theory is no longer applicable.

REFERENCES

1. C. B. Leffert, D. B. Rees and F. E. Jamerson, ONR Annual Report No. 5, Contract Nonr-3109(00), AD 609 177, Oct. 1964; also Sections A, B, and C of this report.

2. L. K. Hansen and C. Warner, Proc. I.E.E,E. Thermionic Conversion Specialist Conference (Gatlinburg), p. 44, Oct. 1963.

3. C. B. Leffert, Adv. Energy Conv. 2, 417, 1962.

4. R. F. Hill and F. E. Gifford, Proc. I.E.E.E. Thermionic Conversion Specialist Conference (Gatlinburg), p. 279, Oct. 1963.

5. J. C. Bowe, Phys. Rev., 134, A355, 1964.

6. D. B. Rees, ONR Annual Report No. 5, Contract Nonr-3109(00), AD 609 177, Oct. 1964, Section D.

ELECTRON TRANSPORT TUBE - DEVELOPMENT

ABSTRACT

A diode has been developed for the inpile study of electron transport
through plasmas generated by fission fragment ionization. The design is
based on the following requirements:

1. Maximum emitter $(BaO-UO_2-W)$ temperature of $1400°C$.

2. Self contained electron gun that can be operated inpile.

3. Direct thermocouple measurement of emitter temperature.

4. Nitrogen gas cooling of tube structure and provision for control of
   cesium reservoir temperature.

5. The collector area should be well defined so that current density can
   be accurately measured.

CONTENTS

OBJECT

The object is to develop an argon-cesium diode which will be operated inpile to measure electron transport through the plasma generated by fission fragments from a $BaO-UO_2-W$ emitter.

SUMMARY

1. Component fabrication and heat transfer studies have been completed on a diode which meets the requirements of the electron transport study.
2. The input power to the electron gun for an emitter temperature of 1400°C was approximately 160 watts independent of gas pressure under 100 torr of argon.
3. Thermal expansion decreases the emitter-collector gap 0.023 in. at an emitter temperature of 1400°C.
4. The true emitter surface temperature was approximately 20°C lower than that measured by the thermocouples which will be used when the diode is inserted in the reactor.
5. The nitrogen coolant flow rate was determined for optimum temperature.
6. To generate 160 watts of nuclear heat to achieve 1400°C emitter temperature inpile, a neutron flux of $5.3 \times 10^{12} n/cm^2/sec$ at the emitter is needed.

1.0 Introduction

The noble gas plasma diode program involves independent investigations of the emitter, plasma and collector. A candidate emitter material, $BaO-UO_2-W$, has been developed.[1] Studies of ion generation rate are complete[2] and electron density measurements[3] and analysis[4] of plasmas generated in gas mixtures by fission fragments are in progress. These studies were necessary in order to find emitter compositions and plasma conditions that are useful for a noble gas thermionic converter. This phase of the program involves measurement of electron transport through a plasma. A metal-ceramic diode designed for operation inpile is required. In addition a theoretical study of the electron transport problem has been undertaken.[5]

A simple planar diode was selected. Means for measuring the emitter

temperature inpile were required. An electron gun was incorporated to provide additional heat to permit some variation of the emitter temperature inpile.

A prototype assembly of the electron gun-diode was used to obtain data on: (1) variation of emitter-collector spacing with emitter temperature, (2) calibration of true emitter surface temperature versus inpile reference thermocouple, (3) temperature of critical parts of the tube with various coolant-gas flows and (4) thermionic emission measurements of the $BaO-UO_2-W$ emitter. The details of the tube fabrication are presented in the appendix.

2.0 Design

2.1 Emitter - The emitter composition for the inpile tube is 76 v/o oxide (24 v/o tungsten) with the oxide portion containing 45 m/o BaO (55 m/o UO_2). This combination is designated 7645. This composition was selected to give a reasonably high fission fragment yield and good electron emission.

The emitter is a disc 0.75 in. diameter of thickness 0.060 in. and is shown in the electron transport tube drawing of Fig. 2. The core of the emitter is separated from the tantalum support tube by a 0.0012 in. tungsten foil which serves as a diffusion barrier. For these dimensions in a neutron flux of 10^{13} neutrons/cm^2-sec the nuclear heat generated will be 300 watts as given in Appendix A.

2.2 Electron Transport Tube - A photograph of the experimental prototype of the electron transport tube and a drawing of the tube are shown in Figs. 1 and 2.
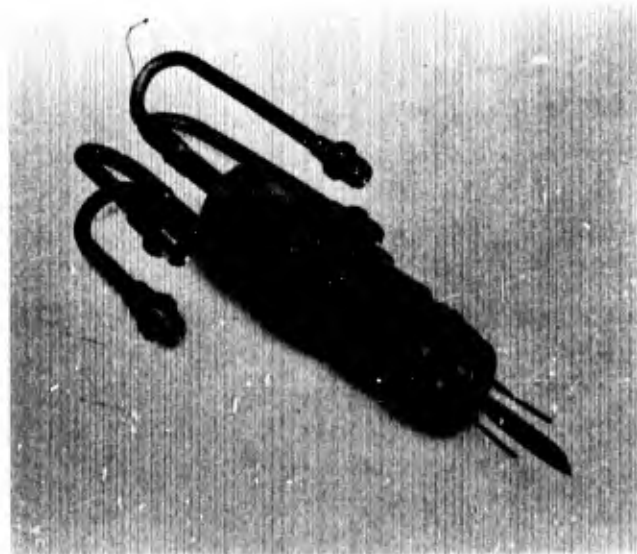
Fig. 1. Photograph of electron transport tube.

2
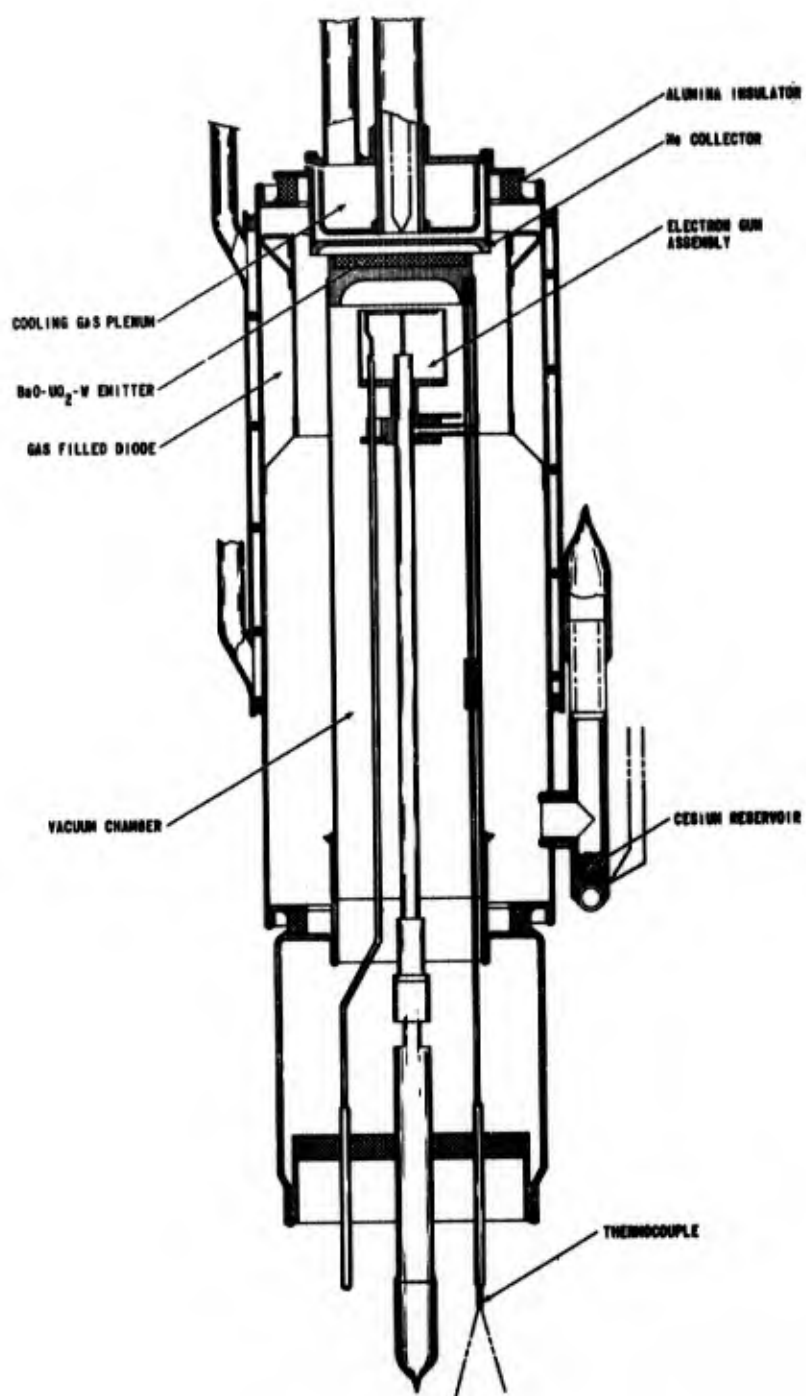
Fig. 2. Drawing of electron transport tube.

3

The three major components of the tube are (1) the diode, (2) the electron gun and (3) the heat transfer system.

The diode includes the BaO-UO$_2$-W emitter and a molybdenum collector with a 0.040 inch spacing. The emitter caps a tantalum tube which serves as a part of the electron gun envelope.

The electron gun consists of a thoriated tungsten pancake heater, 0.375 in. diameter, shielded by a small tantalum cup. The gun is mounted on two leads to a stem. This stem is sealed via a Kovar shell to the end of a tantalum tube. The emitter caps the other end of this tube. Two W-Re thermocouples (sheathed in a tantalum tube of 0.040 in.) imbedded into the back side of the emitter for inpile monitoring purposes are also enclosed in the gun assembly. The output of the thermocouples pass through the stem. The gun, with barium getters, is sealed off to be operated independently of the diode section for test purposes.

The heat transfer system consists of two independent components, (1) the jacket and (2) the collector exchanger. The jacket completes the diode envelope by connecting the electron gun to the collector assembly. The jacket, made of stainless steel, consists of two concentric cylinders separated by a spirally wound wire, which directs the gas flow from the collector end to the gun end of the transport tube. The prototype tube was provided with a sight hole (as shown in Fig. 1) for viewing the emitter-collector gap.

The collector-exchanger consists of a plenum located on the back of the collector body to control the collector temperature.

The electron gun has been included as a separate but integral part of the transport tube so that the tube may be processed and the emitter tested in the laboratory prior to entering the reactor. The gun used in the prototype experiment, to be reported here, has operated over 60 hours with the emitter at 1400°C and for half of this time it was operated as a sealed unit.

3.0 Component Tests

The tests were conducted by operating the prototype transport tube in a bell jar. The sealed-off gun served as a source of heat for the emitter and a closed circuit nitrogen gas system provided the means for cooling.

3.1 Diode Spacing - In order to space properly the emitter-collector, it is necessary to know the thermal expansion of the emitter support tube. This expansion was determined experimentally . The data are shown in Fig.3 in which the growth of the emitter support tube (or the decrease in the emitter-collector distance) is plotted against the emitter temperature. At 1400°C the elongation is 0.023 in.
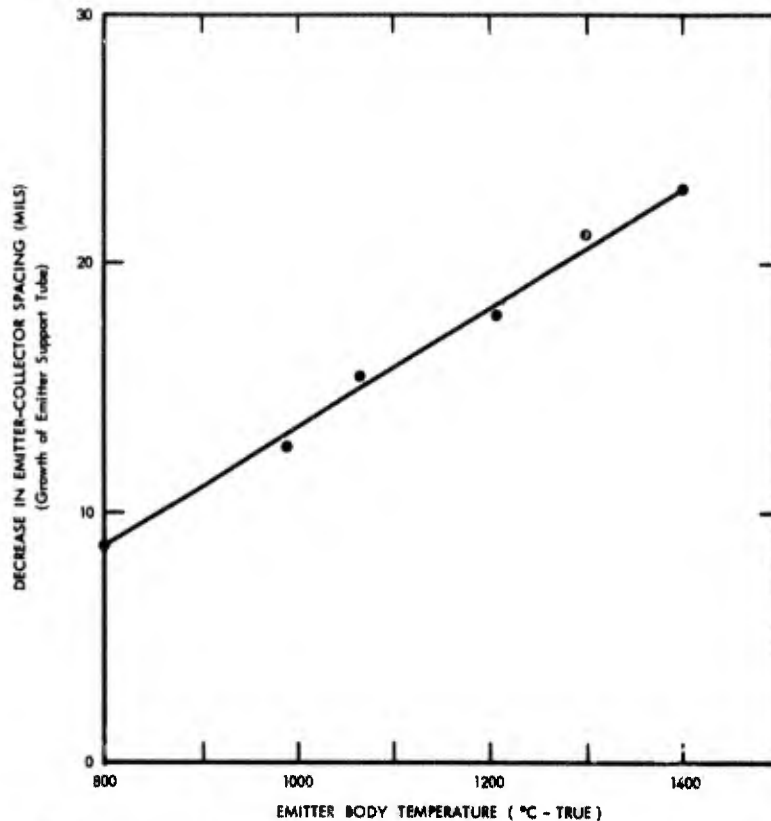
Fig. 3. Effect of temperature on emitter-collector spacing.

3.2 Emitter Temperature - As shown in Fig. 2, the temperature of the emitter surface is monitored by two thermocouples swaged into holes in the back side of the emitter body. Terminals for these W-Re thermocouples are located in the base of the electron gun. It was important to determine how these thermocouple data correlate with the emitter surface temperature itself.

Figure 4 represents data from four thermocouples randomly located and spot welded on the emitter surface. After a test, the thermocouples were moved to new locations on the surface and the experiment repeated. The points, therefore, indicate the spread that can be expected from different thermocouples in addition to the variation in temperature over the surface.

5
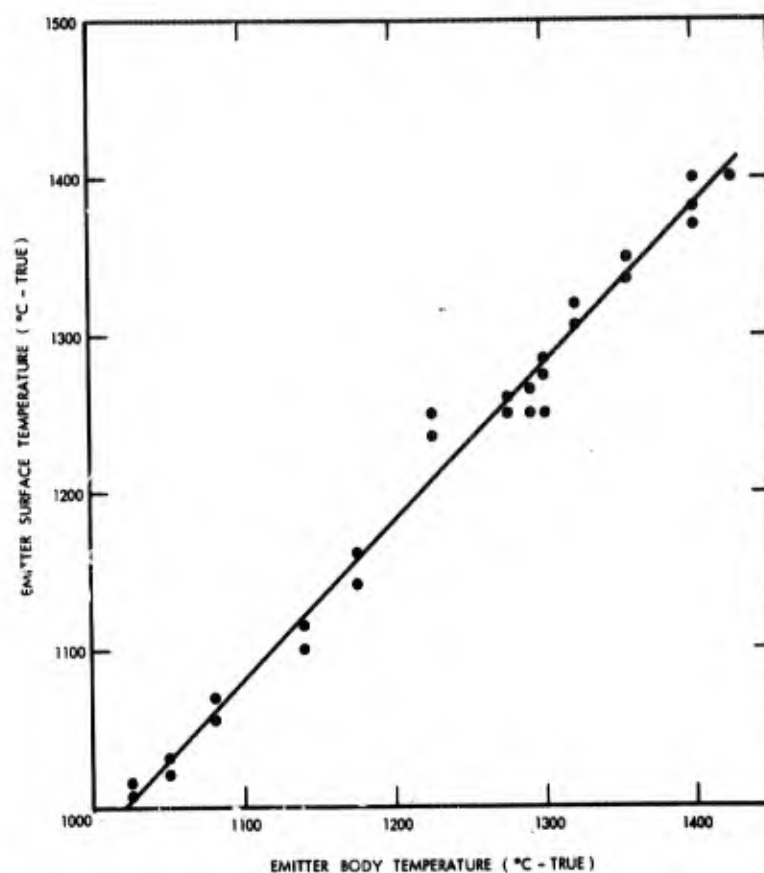
Fig. 4. Emitter body temperature versus emitter surface temperature.

The line drawn through the points indicates a possible difference in surface temperature (lower than body temperature) of approximately 20°C at 1400°C. Observations by an optical pyrometer also indicate temperatures varied over the surface approximately 20°C.

3.3 Power Requirements - A 5,000 volt dc power supply supplied the high voltage to the electron gun while a specially modified dc transistorized low voltage power supply furnished voltage for the gun heater. The emitter was run at positive ground potential to simplify the thermocouple instrumentation. A typical distribution of voltages and currents when the emitter is at 1400°C is

Electron beam	E = 600 volts
(current-voltage)	I = 0.1 amp
Gun heater	E = 8.9 volts
(current-voltage)	I = 9.7 amp.

6

The variation of temperature with input power is shown in Fig. 5 in which the three curves represent dc power, heater power and the total power.
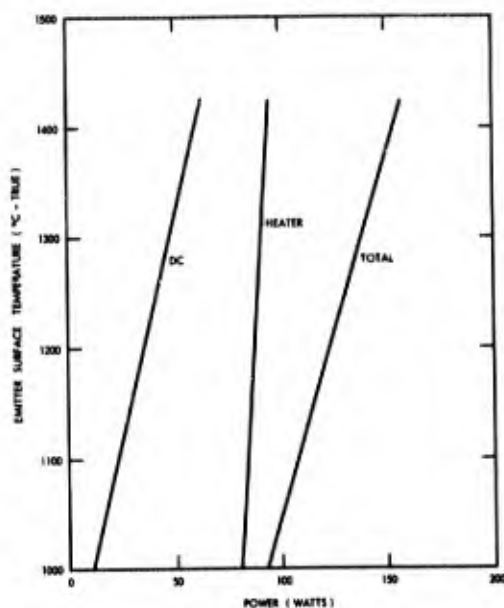
Fig. 5. Influence of input power on emitter temperature.

3.4 Heat Exchanger - The temperature of the collector assembly and the jacket versus the emitter temperature is plotted in Fig. 6.
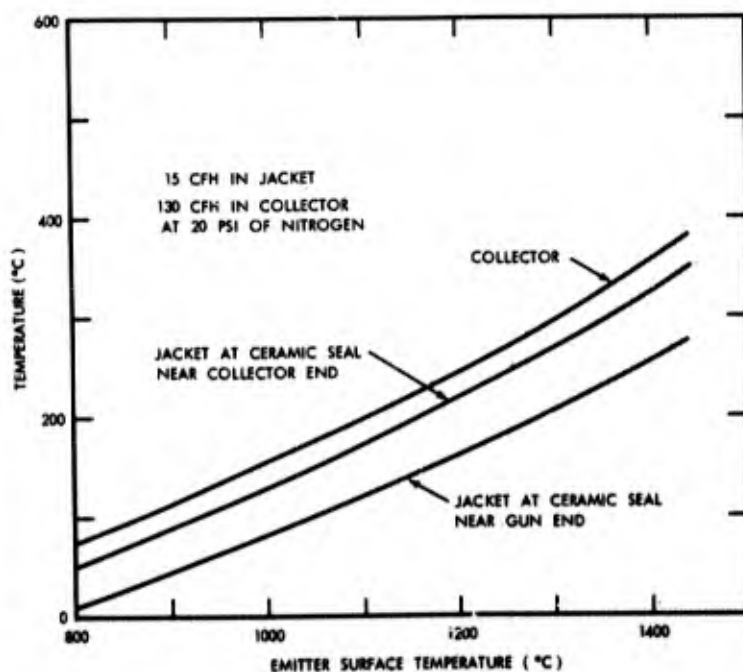
Fig. 6. Temperature profile of components.

7

A schematic of the closed gas flow system is shown in Fig. 7.
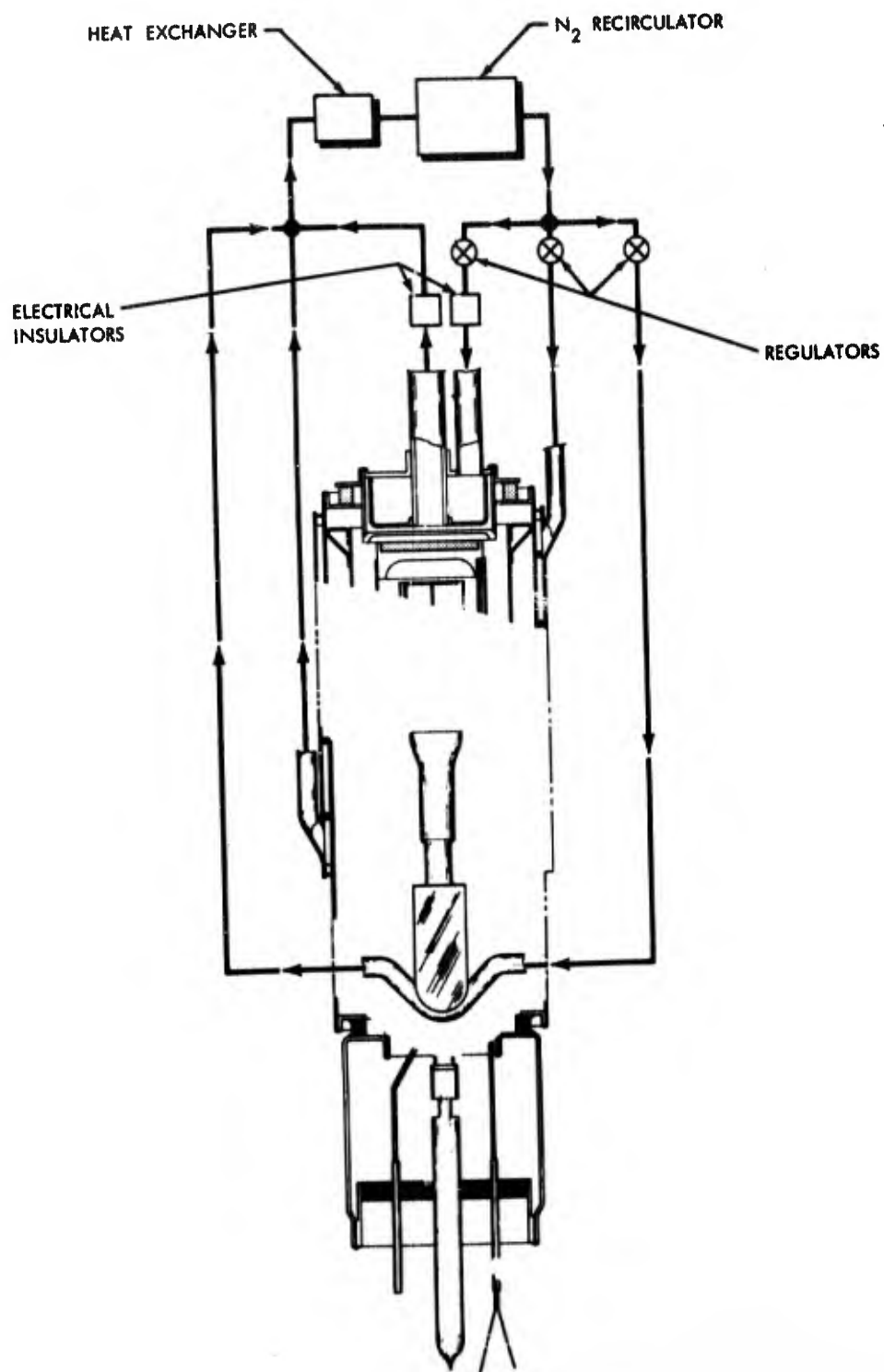
Fig. 7. Gas flow system.

A pressure of 20 psi was easily developed by a diaphragm type gas pump acting as a recirculator. Because the emitter was centrally located, it was not clear which direction the coolant gas should flow. It was found most desirable to flow into the collector end of the jacket. A water cooled heat extractor chamber simulates the reactor pool.

3.5 Thermionic Emission - The three compositions of emitters tested are 7638, 7645 and 7552. The latter two types used enriched uranium. The 7638 (natural uranium) sample served as the emitter in the prototype transport tube. Figure 8 shows the emission versus temperature characteristics of this one emitter. Emission was observed using the high-field pulsed method.[1]
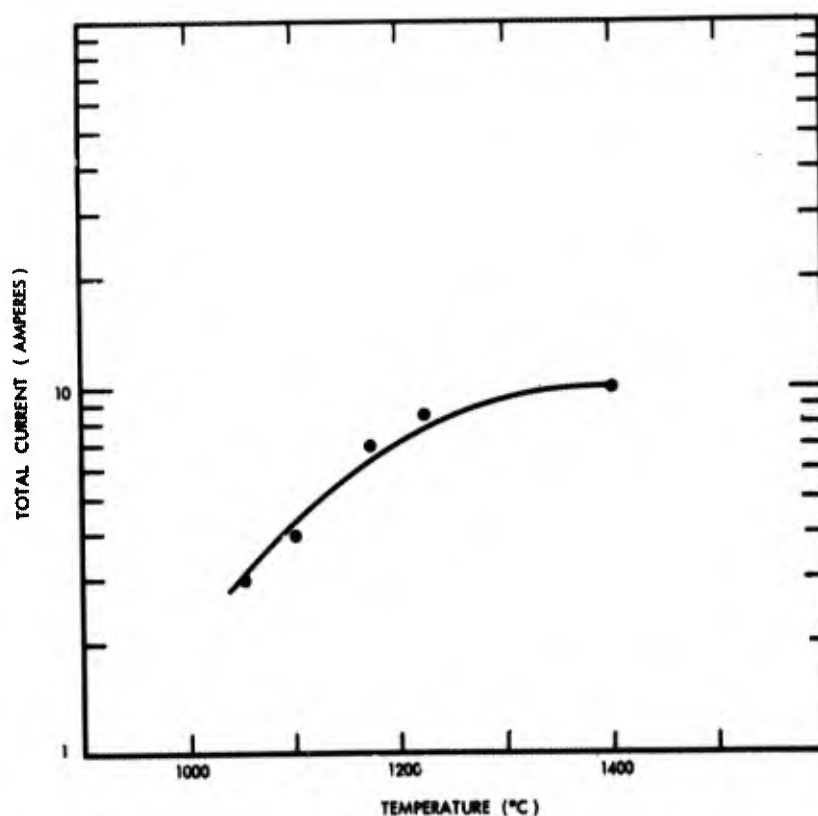
Fig. 8. Thermionic emission versus temperature for type 7638 emitter.

It may be noticed that the current leveled off at approximately 10 amperes. This occurred after about 30 hours of ageing some of which was at 1550°C. Only at this temperature did the emitter show good activation. Arcing at high voltage between the emitter and collector prevented higher current measurements.

9

The other emitters with enriched uranium also required long processing times. In one case the emission was comparable to that in the prototype tube. The others were lower. One feature, as yet unexplained, is that a liquid appeared on the emitter surface at about 1250°C. Also, a large deposit of residue condensed onto the collector. Additional work is being done to investigate these emitter problems which are thought to involve materials purity and/or processing prior to electron emission tests.

4. Acknowledgments

Appreciation is expressed to: D. M. Lee for technical assistance in fabrication and test problems; R. F. Hill for the emitter development, and F. E. Jamerson for guidance and consultation services. Thanks also to Mr. R. Dusman for the design and fabrication of the transport tube, and R. Aikin for accomplishing special welds.

5. References

1. F. E. Gifford and R. F. Hill, "Development of Barium Oxide-Uranium Oxide-Tungsten Emitters for use in Nuclear Heated Thermionic Converters, Part I," Final report for Nonr-3870(00), July 1, 1964 (AD 447212).

2. C. B. Leffert, D. B. Rees, F. E. Jamerson, "Noble Gas Plasmas Produced by Fission Fragments", GMR-451, to be published in JAP, Dec. 1965.

3. C. B. Leffert, "Theory and Experimental Results for the First Inpile Microwave Measurement of Electron Density", Section C of this report.

4. C. B. Leffert, D. B. Rees, F. E. Jamerson, "Investigations on the Direct Conversion of Nuclear Fission Energy to Electrical Energy in a Plasma Diode", Report No. 5, ONR Contract Nonr-3109(00), October 31, 1964.

5. D. B. Rees, "Theory for Thermionic Electron Transport Through a Plasma with Uniform Volume Production and Ambipolar Diffusion Loss", Section D of this report.

A-1. Fabrication

Figure 9 shows, in detail, the joints used in fabricating the electron transport tube.

① HELI-ARC
② OFHC COPPER
③ NI, Au, Cu 925°C
④ Ni-Cu 1225°C
⑤ SILVER SOLDER
⑥ DIRECT SS-Cu SEAL
⑦ SPOT WELD
⑧ CRIMPED
⑨ STAKED
⑩ ELECTRON BEAM WELDED
⑪ PINCH-OFF PRESSURE WELDED
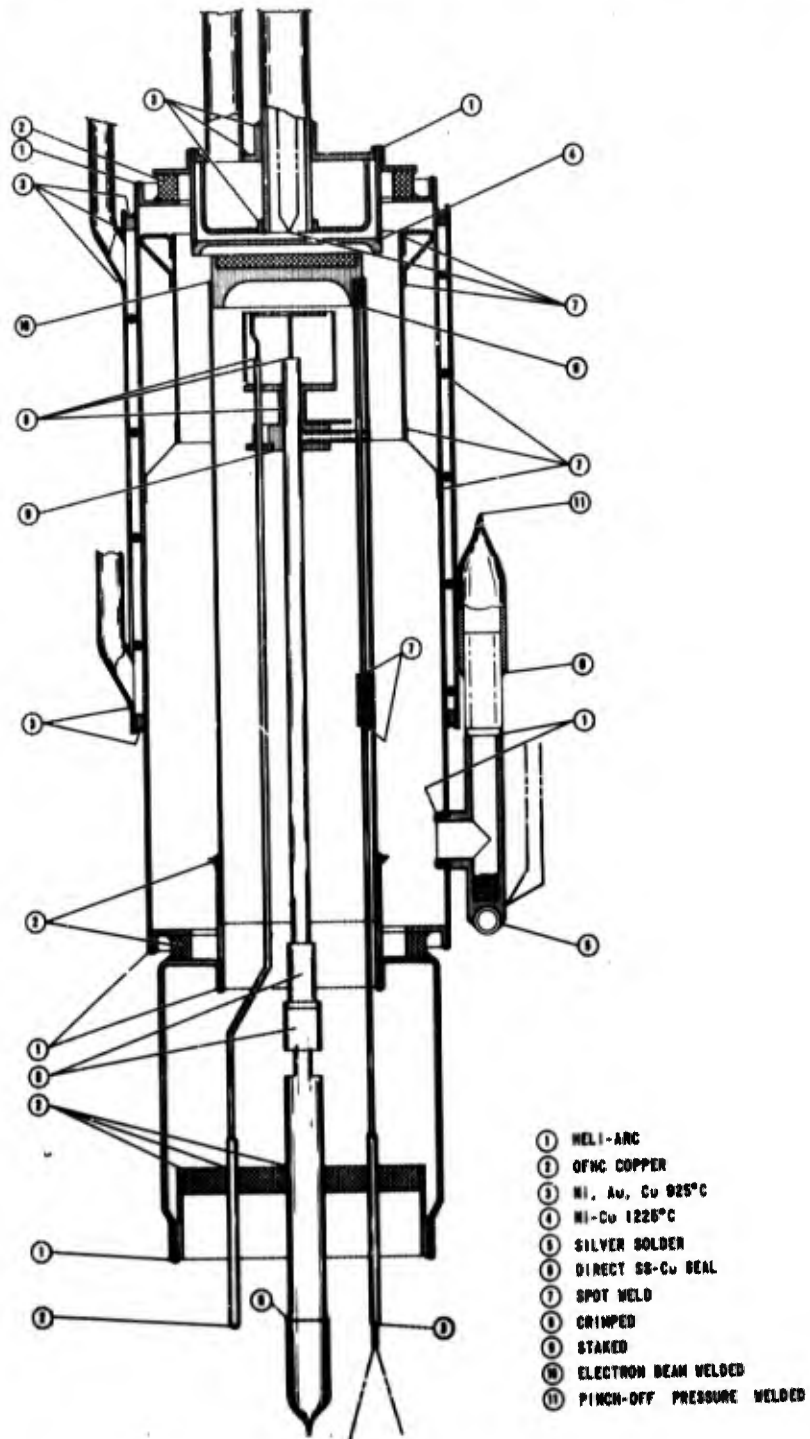
Fig. 9. Detailed drawing of electron transport tube.

A-1.1. Diode

Emitter - The emitter used in the prototype tube contains natural uranium with a composition of 76 v/o oxide (24 v/o tungsten) with the oxide portion containing 38 m/o BaO (62 m/o UO_2). This combination is designated 7638. The fabrication and processing procedure for making this type of emitter has been described.[1] The emitter for the first inpile test will be 7645 with enriched uranium.

The two holes in the tantalum section of the emitter body receive a sheathed tungsten-rhenium thermocouple. The thermocouples are held in place by swaging the tantalum emitter body onto the sheath. This emitter body is electron beam welded in the end of the tantalum support tube which serves as a portion of the electron gun envelope.

Collector - The collector, a molybdenum disc, has a lip on the periphery of the surface facing the emitter for the purpose of defining the volume of plasma generated by fission fragment ionization. The wires of a sheathed chromel-alumel thermocouple are spot welded to the center of the back side of the 0.020 in. thick collector. The thermocouple is fed through a centrally located outlet cooling tube and allowed to protrude through the wall of this tube at a bend external to the collector assembly. A hard solder joint completes the seal between the cooling tube and the thermocouple sheath.

A-1.2 Electron Gun - The electron gun assembly is shown in Fig. 10A. A 0.015 in. diameter (1% thoriated tungsten) filament is wound in a 4 turn pancake of 0.375 in. diameter. A tantalum cup surrounds the filament and serves as a heat shield. A 0.060 in. diameter tantalum support rod is inserted through the center of the cup and held in place by mechanical pressure. One end of the filament is inserted into a hole drilled in the end of this rod and held there by mechanical pressure. The other end of the filament is inserted in a hole of a 0.040 in. diameter support wire and held by mechanical pressure. This smaller support wire is insulated from the tantalum cup by a sapphire bushing.

Three 0.062 in. diameter sapphire rods center the electron gun inside the tantalum emitter tube. The spacing between the heater and back side of the emitter body is approximately 0.140 in. A thin tantalum disc, spot

12
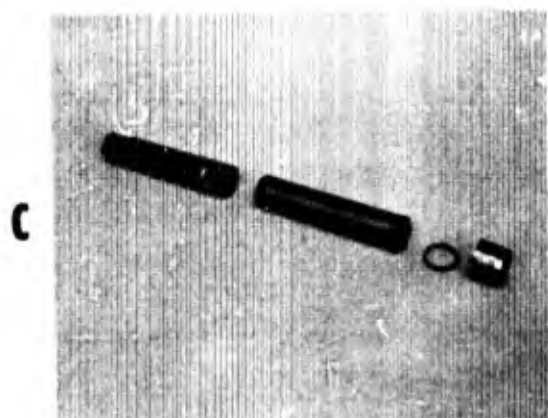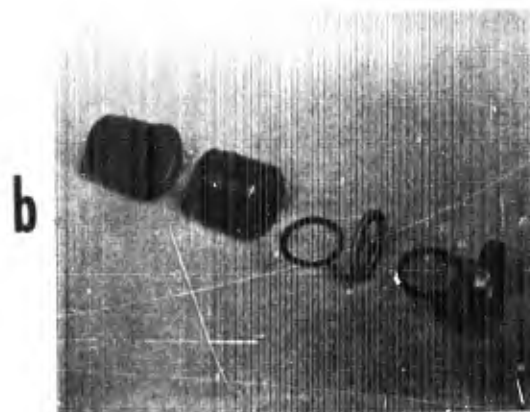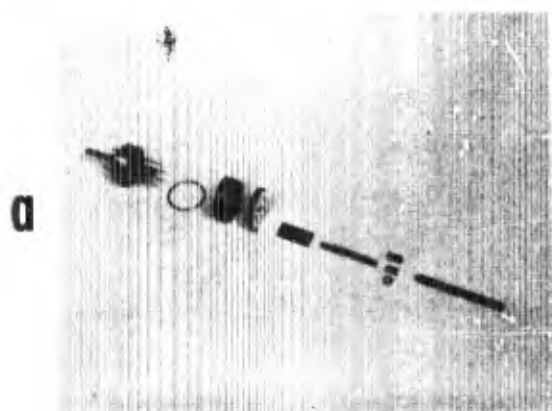
Fig. 10.   Electron gun assembly.

13

welded to one section of the tantalum cup and cut out for the thermocouples to pass through, shields the sapphire rods and ceramic base from evaporants.

The other ends of the two gun support members terminate at an 8 pin ceramic-metal base as shown in the photograph (Fig. 10B). The center tube serves as a pump-out for the electron gun as well as the main support for the gun. The base was constructed by copper brazing eight 0.040 in. inside diameter, one 0.187 in. diameter and one 1.187 in. diameter Kovar tubes to a molybdenum-manganese metallized SC98D ceramic wafer.

Two barium getters are connected in parallel and shielded from the ceramic base by a nickel foil. Two 5.5 in. long - 0.040 in. sheath diameter (W-5 Re/W-26Re) thermocouples supplied by Continental Sensing, Inc. were copper brazed into two of the base tubes. The grounded sealed ends of each thermocouple were swaged into holes in the rim on the back side of the emitter assembly.

A 0.075 in. long quartz tube, held in place by small nickel wires spot welded to the sheath, surrounds each thermocouple and is located at the heliarc weld near the end of the tantalum emitter tube. This tube serves as an electrical insulator so that the potential at the emitter body itself may be known.

The envelope for the gun consists of the tantalum tube, a thimble, the Kovar shell and the base. The stainless steel thimble, initially spot welded to the tantalum tube, is copper brazed. The addition of the thimble as seen in Fig. 10C results in a successful brazed joint between tantalum and steel. The thimble is heliarced to the Kovar shell.

This shell, with a diameter larger than the tantalum tube provides a shoulder to braze a ceramic insulating assembly. This ceramic assembly consists of a ceramic ring and S.S. flange as shown in Fig. 10D which is copper brazed to the Kovar shell before the tantalum tube-thimble assembly is welded in place.

The final heliarc weld occurs between the Kovar shell and the Kovar skirt on the electron gun base as shown in Fig. 10E.

A-1.3 Heat Transfer System - The two components of the transfer system are the jacket and the collector exchanger. The jacket completes the diode envelope by connecting the electron gun assembly to the collector assembly

14

while the collector exchanger includes a plenum arrangement on the back side of the collector to transfer heat. Nitrogen gas is used as the heat transfer medium.

Jacket - The jacket consists of two concentric cylinders separated by a 0.040 in. diameter stainless steel wire spirally wound to uniformly cool the jacket area. A ring soldered at each end, in addition to an inlet gas line at one end and an outlet gas line at the other, completes the assembly. Mounted inside and toward one end is a tantalum heat shield. Figure 11 shows the parts that make up the jacket and end views of the completed assembly.
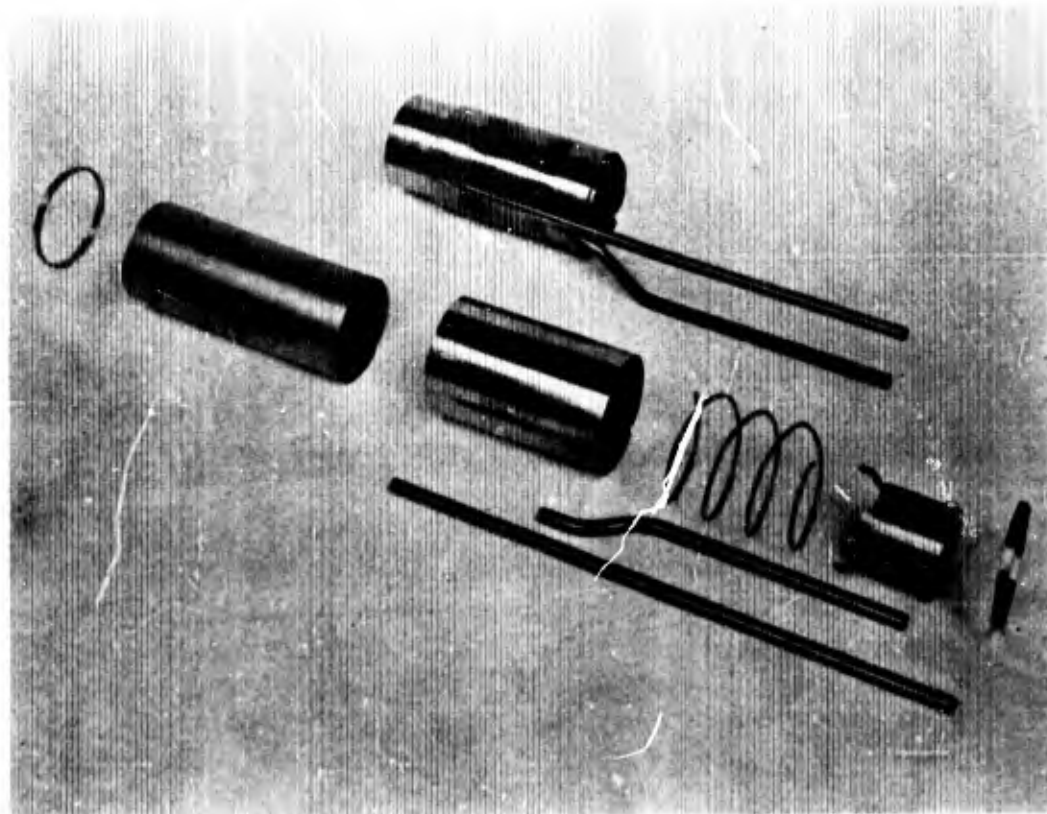
Fig. 11. Jacket components and assembly.

It may be noticed that two holes appear in the side of the jacket. The one through both walls is used only in the prototype tube to observe the emitter-collector gap. The hole which is located near the electron gun end is for the cesium reservoir appendage.

Cesium Reservoir - This reservoir as shown in Fig. 12 is attached to the jacket by a heliarc weld. The vial was crushed and the area slightly heated to cause the cesium to drop into the reservoir itself.

(a) TRANSFER SYSTEM

1 GRAM CESIUM VIAL

NICKEL MESH

COPPER TUBING

FIRST PINCH-OFF

(b) RESERVOIR

FINAL PINCH-OFF

TRANSPORT TUBE
ASSIMILATION
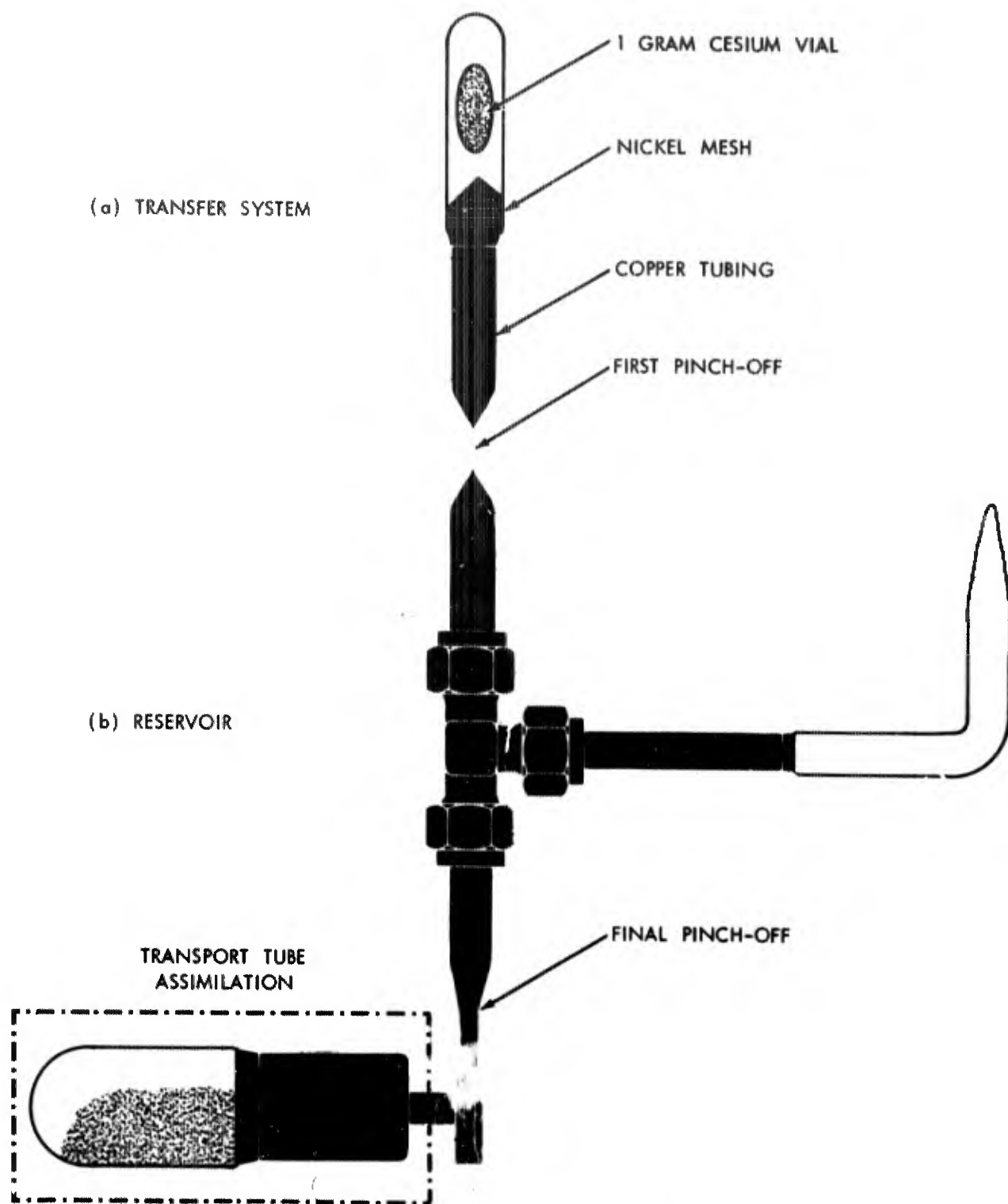
Fig. 12.   Cesium reservoir system.

Fig. 12A shows the arrangement that best accomplished the transfer task
and Fig. 12B shows the reservoir attached to a glass tube. The tee
served only to expedite the experiment as the final reservoir will have
a tee with brazed joints.

Collector Heat Exchanger - The back side of the collector serves as a section of the exchanger as may be observed in Fig. 9. The nitrogen gas enters the tube nearest the outer extremity of the collector exchanger, fills the central plenum and passes out along the outer wall to maintain that region cool for protection of the ceramic ring assembly (not shown). The gas then passes radially inward on the back side of the collector and out through the central tube, which also contains a thermocouple.

A photograph of the collector assembly and its components for the collector heat exchanger is shown in Fig. 13A. A pre-copper brazed ceramic ring-metal flange assembly, shown in Fig. 13B is heliarced to the collector heat exchanger assembly seen in Fig. 13C. As a final operation the electron gun assembly and the collector assembly are heliarced to the jacket.
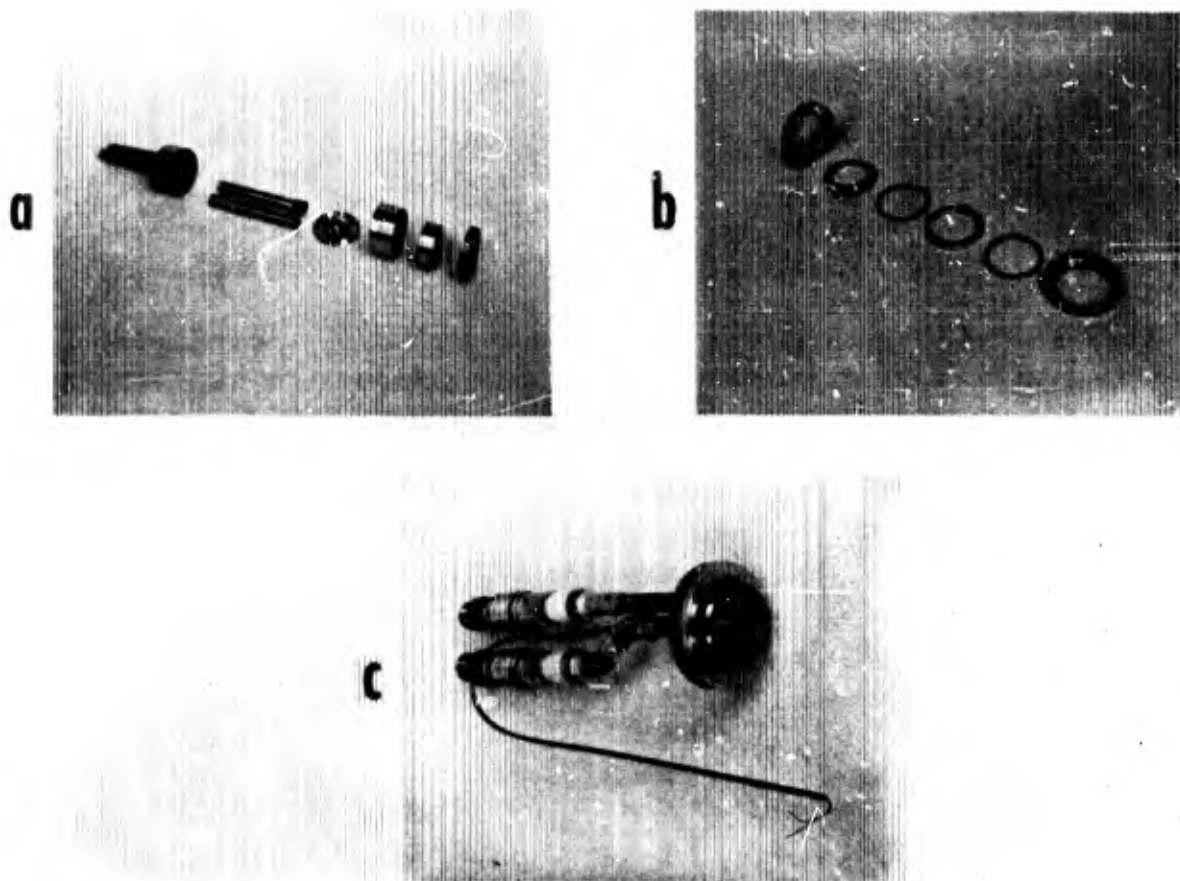
Fig. 13. Insulator and collector heat exchanger assembly.

17

A-2. Nuclear Data

Two different compositions containing enriched uranium (7645 and 7552 samples) have been tested. In the calculations below a composition 7550 is considered and should represent some average of the two compositions of interest.

v/o Oxide	75
v/o Tungsten	25
m/o Barium Oxide	50
m/o Uranium Oxide	50

Density (g/cm^3)

Barium	2.04
Uranium	3.50
Oxygen	0.71
Tungsten	4.82
Total -	11.07

Macroscopic cross sections, cm^{-1}

$\sum_f$(U-235)	$(\sigma_f = 580 \text{ b})$	5.20
$\sum_a$(U-235)	$(\sigma_a = 687 \text{ b})$	6.18
$\sum_a(B_a)$	$(\sigma_a = 1.17 \text{ b})$	0.01
$\sum_a$(W)	$(\sigma_a = 19.2 \text{ b})$	0.30
$\sum_a(O_2)$	$(\sigma_a = 2\times10^{-4} \text{ b})$	-----
$\sum_t \text{ cm}^{-1}$		
		6.49

The self-shielding effect of the emitter material must be considered to determine the fission rate in the various emitter cores. The equation below represents the fission rate in a lumped absorber.

$$F = \sum_f t \, A \, \phi \, f$$

where F is the fission rate (fissions-sec^{-1})

$\sum_f$ is the fission cross section (cm^{-1})

t is the thickness of the emitter core (cm)

A is the surface area of the emitter core(cm^2)

ϕ is the unperturbed neutron flux (neutrons-$cm^{-2}sec^{-1}$)

f is the self-shielding factor.

18

Values for the various parameters for this equation are:

$$\Sigma_f = 5.2 \quad \text{(calculated)}$$
$$t = 0.15$$
$$A = 2.85$$
$$\phi = 10^{13}$$
$$f = 0.4 \quad \text{(calculated)}$$
$$1 \text{ watt} = 3 \times 10^{10} \text{ fissions-sec}^{-1}$$

Under these conditions the total nuclear heat input would be 200 watts for a flux of 10^{13} n-sec^{-1}-cm^{-2} at the emitter.

PUBLICATIONS

1. F. E. Jamerson, C. B. Leffert, and D. B. Rees, "Secondary Electron Yield from Fission Fragments", J. Appl. Phys. **36**, 355 (1965).

2. D. B. Rees, C. B. Leffert, and F. E. Jamerson, "Electron Density in Mixed Gas Plasmas", Proceedings of the IEEE Thermionic Converter Specialists Conference at San Diego, Calif., October 25-27, 1965.

3. C. B. Leffert, D. B. Rees, and F. E. Jamerson, "Noble Gas Plasma Produced by Fission Fragments", A.P.S. Bulletin **10**, 239 (Nov. 2, 1965).

General Motors Research Laboratories
12 Mile and Mound Roads, Warren, Michigan

INVESTIGATIONS ON THE DIRECT CONVERSION OF NUCLEAR
FISSION ENERGY TO ELECTRICAL ENERGY IN A PLASMA
DIODE, by C. B. Leffert, D. B. Rees and F. E. Gifford

126 pp. incl. figs.

Annual Technical Summary Report, November 1, 1964
to October 31, 1965 (Report No. 6)

Contract Nonr-3109(00)

Reaction kinetics and electron transport were
studied in noble gas plasmas generated by fission
fragment ionization in order to evaluate these
plasmas for a nuclear thermionic energy converter.
The electron density that would result from fis-
sion fragment ionization of Ar-Cs and Ne-Ar gas
mixtures was predicted from the computed ion gen-
eration rate and ion loss processes in the plasma.
The first experimental verification of the elec-
tron density was made with a resonant microwave
cavity operated inpile. For typical conditions in
a research reactor, i.e. a neutron flux of 10^{13}cm-2

1. Direct energy conversion
2. Thermionics
3. Gaseous electronics
4. Plasma physics

I. C. B. Leffert
II. D. B. Rees
III. F. E. Gifford
IV. General Motors Corporation
Research Laboratories
V. Nonr-3109(00)

sec^{-1} and an electron temperature of 1300°K, the computed maximum electron density for
neon-argon, viz., 2.4x10^{12}cm-3 occurs at Ar/Ne=3.4x10^{-4} and 94 torr while for argon-
cesium, the maximum electron density is 3.6x10^{12}cm-3 and occurs at Cs/Ar=1.7x10^{-4} and
94 torr. The favorably-high electron density in argon seeded with cesium and the fact
that argon has the lowest electron-neutral scattering cross section (Ramsauer) minimum
at energies typical of an operating converter, indicate that this gas mixture is par-
ticularly well-suited for the noble gas converter.

The electron transport properties of these plasmas are being investigated theore-
tically and a ceramic-metal diode with a nuclear thermionic emitter (BaO-UO2-W) has
been developed for inpile measurement of the electron transport properties. Analyti-
cal solutions have been obtained for the current-voltage characteristic of a therm-
ionic diode in which the plasma is generated by uniform fission-fragment ionization
and the electron density is controlled by ambipolar diffusion loss.

General Motors Research Laboratories
12 Mile and Mound Roads, Warren, Michigan

INVESTIGATIONS ON THE DIRECT CONVERSION OF NUCLEAR FISSION ENERGY TO ELECTRICAL ENERGY IN A PLASMA DIODE, by C. B. Leffert, D. B. Rees and F. E. Gifford

126 pp. incl. figs.

Annual Technical Summary Report, November 1, 1964 to October 31, 1965 (Report No. 6)

Contract Nonr-3109(00)

Reaction kinetics and electron transport were studied in noble gas plasmas generated by fission fragment ionization in order to evaluate these plasmas for a nuclear thermionic energy converter. The electron density that would result from fission fragment ionization of Ar-Cs and Ne-Ar gas mixtures was predicted from the computed ion generation rate and ion loss processes in the plasma. The first experimental verification of the electron density was made with a resonant microwave cavity operated impile. For typical conditions in a research reactor, i.e. a neutron flux of 10^{13} cm^{-2}

1. Direct energy conversion
2. Thermionics
3. Gaseous electronics
4. Plasma physics

I. C. B. Leffert
II. D. B. Rees
III. F. E. Gifford
IV. General Motors Corporation Research Laboratories
V. Nonr-3109(00)

sec^{-1} and an electron temperature of 1300°K, the computed maximum electron density for neon-argon, viz., 2.4×10^{12} cm^{-3} occurs at Ar/Ne=3.4×10^{-4} and 94 torr while for argon-cesium, the maximum electron density is 3.6×10^{12} cm^{-3} and occurs at Cs/Ar=1.7×10^{-4} and 94 torr. The favorably-high electron density in argon seeded with cesium and the fact that argon has the lowest electron-neutral scattering cross section (Ramsauer) minimum at energies typical of an operating converter, indicate that this gas mixture is particularly well-suited for the noble gas converter.

The electron transport properties of these plasmas are being investigated theoretically and a ceramic-metal diode with a nuclear thermionic emitter (BaO-UO$_2$-W) has been developed for inpile measurement of the electron transport properties. Analytical solutions have been obtained for the current-voltage characteristic of a thermionic diode in which the plasma is generated by uniform fission-fragment ionization and the electron density is controlled by ambipolar diffusion loss.

DOCUMENT CONTROL DATA · R&D

(Security classification of title, body of abstract and indexing annotation must be entered when the overall report is classified)

1. ORIGINATING ACTIVITY *(Corporate author)*	2a. REPORT SECURITY CLASSIFICATION
Research Laboratories, General Motors Corporation 12 Mile and Mound Roads, Warren, Michigan 48090	UNCLASSIFIED
	2b. GROUP N A

3. REPORT TITLE

INVESTIGATIONS ON THE DIRECT CONVERSION OF NUCLEAR FISSION ENERGY TO ELECTRICAL ENERGY IN A PLASMA DIODE.

4. DESCRIPTIVE NOTES *(Type of report and inclusive dates)*

Annual Report No. 6 - November 1, 1964 to October 31, 1965

5. AUTHOR(S) *(Last name, first name, initial)*

Leffert, Charles B.
Rees, David B.
Gifford, Fay E.

6. REPORT DATE	7a. TOTAL NO. OF PAGES	7b. NO. OF REFS
October 31, 1965	126	75

8a. CONTRACT OR GRANT NO.	9a. ORIGINATOR'S REPORT NUMBER(S)
Nonr-3109(00)	None
b. PROJECT NO. 099-345	
c.	9b. OTHER REPORT NO(S) *(Any other numbers that may be assigned this report)*
d.	None

10. AVAILABILITY/LIMITATION NOTICES

Qualified requesters may obtain copies of this report from DDC.

11. SUPPLEMENTARY NOTES	12. SPONSORING MILITARY ACTIVITY
None	Office of Naval Research (Zip Code: 20360) Power Branch (Code 429) Department of the Navy, Washington, D. C.

13. ABSTRACT

Reaction kinetics and electron transport were studied in noble gas plasmas generated by fission fragment ionization in order to evaluate these plasmas for a nuclear thermionic energy converter. The electron density that would result from fission fragment ionization of Ar-Cs and Ne-Ar gas mixtures was predicted from the computed ion generation rate and ion loss processes in the plasma. The first experimental verification of the electron density was made with a resonant microwave cavity operated inpile. For typical conditions in a research reactor, i.e. a neutron flux of $10^{13}cm^{-2}sec^{-1}$ and an electron temperature of 1300°K, the computed maximum electron density for neon-argon, viz., $2.4\times10^{12}cm^{-3}$ and occurs at Ar/Ne=3.4×10^{-4} and 94 torr while for argon-cesium, the maximum electron density is $3.6\times10^{12}cm^{-3}$ and occurs at Cs/Ar=1.7×10^{-4} and 94 torr. The favorably-high electron density in argon seeded with cesium and the fact that argon has the lowest electron-neutral scattering cross section (Ramsauer) minimum at energies typical of an operating converter, indicate that this gas mixture is particularly well-suited for the noble gas converter.

The electron transport properties of these plasmas are being investigated theoretically and a ceramic-metal diode with a nuclear thermionic emitter ($BaO-UO_2-W$) has been developed for inpile measurement of the electron transport properties. Analytical solutions have been obtained for the current-voltage characteristic of a thermionic diode in which the plasma is generated by uniform fission-fragment ionization and the electron density is controlled by ambipolar diffusion loss.

DD FORM 1 JAN 64 **1473**

14. KEY WORDS	LINK A		LINK B		LINK C	
	ROLE	WT	ROLE	WT	ROLE	WT
1. Direct energy conversion 2. Thermionics 3. Gaseous electronics 4. Plasma physics						

INSTRUCTIONS

1. **ORIGINATING ACTIVITY:** Enter the name and address of the contractor, subcontractor, grantee, Department of Defense activity or other organization *(corporate author)* issuing the report.

2a. **REPORT SECURITY CLASSIFICATION:** Enter the overall security classification of the report. Indicate whether "Restricted Data" is included. Marking is to be in accordance with appropriate security regulations.

2b. **GROUP:** Automatic downgrading is specified in DoD Directive 5200.10 and Armed Forces Industrial Manual. Enter the group number. Also, when applicable, show that optional markings have been used for Group 3 and Group 4 as authorized.

3. **REPORT TITLE:** Enter the complete report title in all capital letters. Titles in all cases should be unclassified. If a meaningful title cannot be selected without classification, show title classification in all capitals in parenthesis immediately following the title.

4. **DESCRIPTIVE NOTES:** If appropriate, enter the type of report, e.g., interim, progress, summary, annual, or final. Give the inclusive dates when a specific reporting period is covered.

5. **AUTHOR(S):** Enter the name(s) of author(s) as shown on or in the report. Enter last name, first name, middle initial. If military, show rank and branch of service. The name of the principal author is an absolute minimum requirement.

6. **REPORT DATE:** Enter the date of the report as day, month, year; or month, year. If more than one date appears on the report, use date of publication.

7a. **TOTAL NUMBER OF PAGES:** The total page count should follow normal pagination procedures, i.e., enter the number of pages containing information.

7b. **NUMBER OF REFERENCES:** Enter the total number of references cited in the report.

8a. **CONTRACT OR GRANT NUMBER:** If appropriate, enter the applicable number of the contract or grant under which the report was written.

8b, 8c, & 8d. **PROJECT NUMBER:** Enter the appropriate military department identification, such as project number, subproject number, system numbers, task number, etc.

9a. **ORIGINATOR'S REPORT NUMBER(S):** Enter the official report number by which the document will be identified and controlled by the originating activity. This number must be unique to this report.

9b. **OTHER REPORT NUMBER(S):** If the report has been assigned any other report numbers *(either by the originator or by the sponsor)*, also enter this number(s).

10. **AVAILABILITY/LIMITATION NOTICES:** Enter any limitations on further dissemination of the report, other than those imposed by security classification, using standard statements such as:

  (1) "Qualified requesters may obtain copies of this report from DDC."

  (2) "Foreign announcement and dissemination of this report by DDC is not authorized."

  (3) "U. S. Government agencies may obtain copies of this report directly from DDC. Other qualified DDC users shall request through

    _____ ."

  (4) "U. S. military agencies may obtain copies of this report directly from DDC. Other qualified users shall request through

    _____ ."

  (5) "All distribution of this report is controlled. Qualified DDC users shall request through

    _____ ."

If the report has been furnished to the Office of Technical Services, Department of Commerce, for sale to the public, indicate this fact and enter the price, if known.

11. **SUPPLEMENTARY NOTES:** Use for additional explanatory notes.

12. **SPONSORING MILITARY ACTIVITY:** Enter the name of the departmental project office or laboratory sponsoring *(paying for)* the research and development. Include address.

13. **ABSTRACT:** Enter an abstract giving a brief and factual summary of the document indicative of the report, even though it may also appear elsewhere in the body of the technical report. If additional space is required, a continuation sheet shall be attached.

It is highly desirable that the abstract of classified reports be unclassified. Each paragraph of the abstract shall end with an indication of the military security classification of the information in the paragraph, represented as *(TS), (S), (C),* or *(U).*

There is no limitation on the length of the abstract. However, the suggested length is from 150 to 225 words.

14. **KEY WORDS:** Key words are technically meaningful terms or short phrases that characterize a report and may be used as index entries for cataloging the report. Key words must be selected so that no security classification is required. Identifiers, such as equipment model designation, trade name, military project code name, geographic location, may be used as key words but will be followed by an indication of technical context. The assignment of links, rules, and weights is optional.